Travail de fin d'études et stage[BR]- Travail de fin d'études : Simulation and Adaptation of a Biomass Combined Heat and Power Plant with CO2 Capture[BR]- Stage d'insertion professionnelle

Auteur : Beguin, Brieuc
Promoteur(s) : Léonard, Grégoire
Faculté : Faculté des Sciences appliquées
Diplôme : Master en ingénieur civil électromécanicien, à finalité spécialisée en énergétique
Année académique : 2021-2022
URI/URL : http://hdl.handle.net/2268.2/14396

University of Liège

Faculty of Applied Sciences

Simulation and Adaptation of a Biomass Combined Heat and Power Plant with CO_2 Capture

Beguin Brieuc

Thesis presented for obtaining the Master's degree in
Electromechanical Engineering

Supervisor:
Léonard Grégoire

Academic year 2021-2022

Abstract

This master's thesis addresses the preliminary design of an amine-based, post-combustion CO_2 capture pilot integrated into a biomass-fired CHP plant. Simulation models of the different subsystems (*i.e.* the biomass furnace, the thermodynamic cycle and the carbon capture unit) are developed with the software Aspen Plus. In particular, the performance of the capture unit is assessed and optimised. The submodels are then merged into a single model. This combined model offers an overview of the system as a whole and enables the prediction of interactions between the different subsystems. The repercussions of a localised change in operating conditions can therefore be measured. In addition to the modelling work, the capture unit is sized according to the identified nominal conditions. Energy integration within the existing plant is also investigated and the best compromise is identified. Finally, an order-of-magnitude cost estimation is calculated to support the decision making of the project.

Résumé

Ce travail de fin d'études porte sur la conception préliminaire d'une installation pilote de captage de CO_2 en post-combustion avec un solvent aminé intégrée à une centrale à cogénération alimentée par de la biomasse. Les différents composants du système (c'est-à-dire la chaudière, le cycle thermodynamique et l'unité de captage de CO_2) sont modélisés à l'aide du logiciel Aspen Plus. En particulier, les performances de l'unité de captage sont évaluées et optimisées. Les sous-modèles sont ensuite fusionnés en un seul modèle. Ce modèle combiné offre une vue du système dans sa globalité et permet de prédire les interactions entre les différents sous-systèmes. Les répercussions d'un changement localisé des conditions opératoires peuvent ainsi être mesurées. En complément du travail de modélisation, l'unité de captage est également dimensionnée en fonction des conditions nominales identifiées. L'intégration énergétique au sein de la centrale existante est également étudiée et le meilleur compromis est identifié. Enfin, une estimation des coûts est calculée pour soutenir la prise de décision du projet.

Acknowledgements

First of all, I would like to thank heartily Prof. Grégoire Léonard, who offered me the opportunity to do my master's thesis in his research unit and guided me throughout the entire semester.

I also address a special thanks to Mr Muhammad Salman, who met with me on a weekly basis, providing relevant pieces of advice, and who was always available to address my problems, especially with Aspen Plus.

Prof. Pierre Dewallef, by agreeing to share his model with me, also helped me considerably to understand and to model the Sart Tilman CHP plant.

And finally, I am also very grateful to Mr Kevin Sartor, who provided a lot of useful data on the functioning of the CHP plant. In addition, he dedicated time on several occasions to answer my questions and fill my knowledge gaps.

Contents

List of Figures

List of Tables

CHAPTER 1

Introduction

1.1 Context

Earth's climate depends on the radiant energy emitted by the Sun. Radiation strikes the surface of the planet and increases its temperature. However, this direct contribution alone is insufficient to explain the average temperature (15 °C).

The atmosphere is a major contributor that ought to be taken into account when describing the climatic system. Like any other body with a non-zero temperature, the Earth's surface emits radiation (mainly infrared). The composition of the atmosphere includes radiatively active gases that absorb this infrared radiation, leading to an increase in atmosphere temperature. Heated by this absorption, the atmosphere in turn emits infrared radiation back towards the Earth, increasing de facto its temperature. It is illustrated on the left side of Figure 1.1, in which the arrows represent radiative heat transfers.

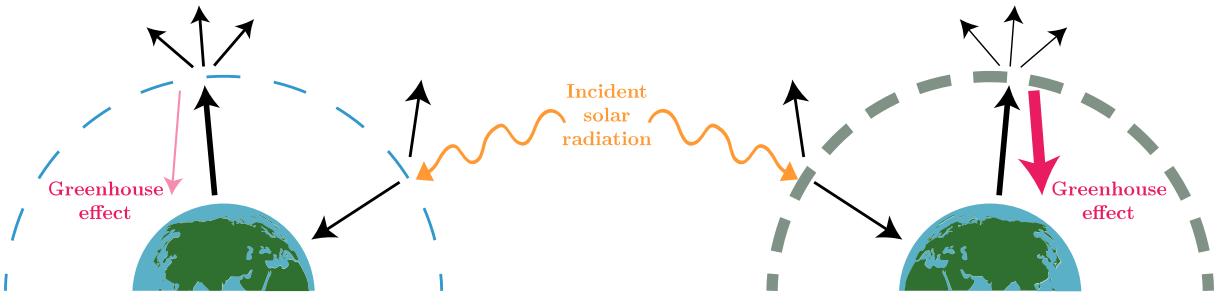

(a) Natural situation

(b) With anthropogenic emissions

Figure 1.1: Illustration of the greenhouse effect

This mechanism is called the *greenhouse effect* and, as explained, is a naturally-occurring atmospheric phenomenon. It contributes to an increase in the average temperature of

around 30 K, which makes life on Earth sustainable. However, this essential equilibrium is being disrupted by human activities.

The Industrial Revolution (19^{th} century) has profoundly transformed the world from communities organized around agriculture and craftsmanship into societies of manufacturing and consumption.

Fossil fuels such as coal, oil and natural gas (with increasing historical usage in that order) have been used since then to produce electricity, to power industrial processes and to fuel means of transportation. Alongside other anthropogenic activities such as deforestation, agriculture and industrial processes, burning fossil fuels lead to atmospheric emissions of large quantities of long-lived gases (mainly carbon dioxide CO_2, methane CH_4 and nitrous oxide N_2O). They are usually called greenhouse gases (GHG) as they contribute to the intensification of the greenhouse effect, described here above. These gases are indeed radiatively active and amplify the naturally-occurring warming. This is naively illustrated on the right-hand side of Figure 1.1 by the thicker dotted line representing the atmosphere with a larger concentration of GHG. Collectively, the consequences of this anthropogenic contribution are referred to as *climate change*.

Climate change is the source of great public concern. The scientific community has been studying these phenomena extensively. In particular, the United Nations have established in 1988 the International Panel on Climate Change (IPCC). This group of experts has been compiling the relevant literature into Assessment Reports, which reflect the current knowledge on climate change. In their reports, the IPCC addresses the evidence of climate change, the necessary adaptations to the established changes and the mitigation strategies to further limit the phenomenon.

Figure 1.2 shows the change in global surface temperature from the pre-industrial levels[1] to nowadays. At the time of writing, anthropogenic emissions have already contributed to a global warming of around 1 °C [IPCC 2018; NASA 2022]. It may seem negligible with respect to the contribution of the naturally-occurring greenhouse effect, yet this change to the equilibrium is predicted to cause calamitous consequences, as forecasted by the IPCC's projections. Among many others, the identified repercussions include global increase in mean temperatures, sea level rise, disastrous impacts on biodiversity, and more frequent natural disasters such as droughts, wildfires and even tropical cyclones. Generally speaking, a concerning increase in weather extremes is expected. At human scale, global warming is also likely to provoke water and food scarcity, health hazards and economical and geopolitical conflicts. [IPCC 2018]

Evolving in a carbon-constrained world requires coordinated international action. The most recent, striking treaty is the 2015 Paris Agreement. The international community has committed to addressing this global issue by "limiting global warming to well below 2 °C and pursuing efforts to limit it to 1.5 °C" [European Commission 2022b]. To assess the feasibility of this ambitious plan, the IPCC published in 2018 the *Special Report on Global Warming of 1.5 °C* [IPCC 2018].

[1] When studying climate change, the pre-industrial levels, *i.e.* averaged over the period 1850-1900, are often used as a comparison standard.

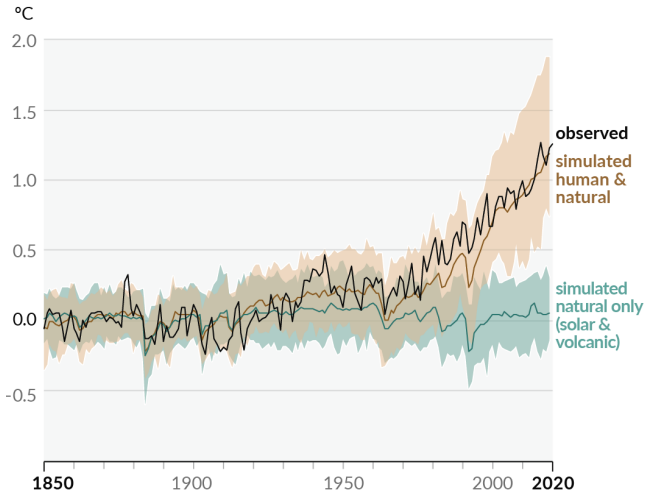

Figure 1.2: Change in global surface temperature (annual average) as observed and simulated using human & natural and only natural factors (both 1850-2020) [IPCC 2021]

In 2019, in the continuity of the aforementioned commitment, the European Commission has unveiled the *European Green Deal*, which is a set of policy measures that aims at achieving climate neutrality by 2050. The intermediate target is the 55% reduction of GHG emissions by 2030 as defined by the *Fit-for-55* package. [IEA 2020a]

The emission trading system of the European Union (EU ETS) is one of the tools that support the previously-described ambitions by targeting the CO_2 emissions of key sectors (*e.g.* power and heat production, energy-intensive industrial processes, commercial aviation within the European Economic Area and so on). The EU ETS is a cap and trade system organised around the EU allowances (EUA). With each EUA representing the emission of $1\,t_{CO_2}$, involved companies are expected to surrender annually the corresponding amount of allowances. These EUA can be traded in an internal market. With an annual decrease in the number of EUA, the unit price of an EUA is expected to rise continuously, effectively encouraging involved companies to strive for carbon-neutral processes. Figure 1.3 illustrates the recent evolution of the EUA price. [European Commission 2022a]

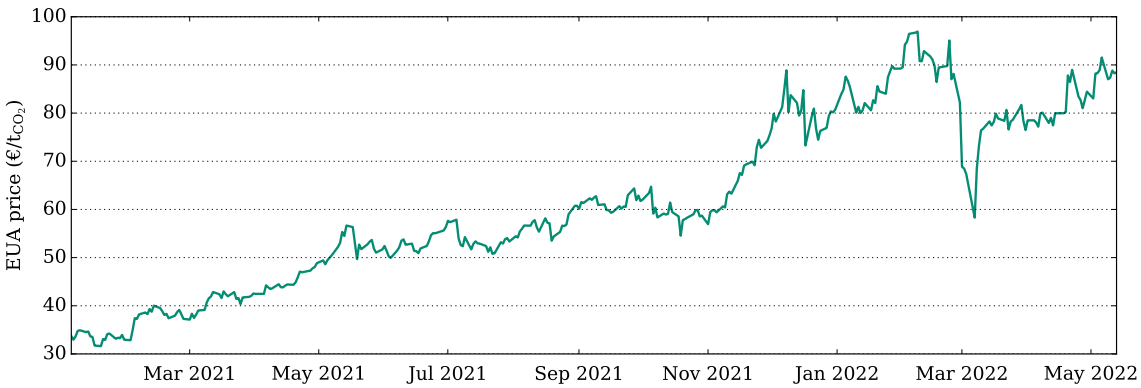

Figure 1.3: Recent evolution of the EUA price. Data from [Ember 2022]

In addition to economic intensives and legislative constraints, climate change mitigation strategies include the development of sustainable technologies. As the top priority, the global energy demand must be reduced. In existing processes, the losses ought to be cut

down or, in other words, the efficiencies have to increase. The deployment of renewable energy sources is also a major effort that should be encouraged. At last, the use of fossil fuels must be limited to the bare minimum and technologies should be developed to further limit their emissions. In this work, the focus is placed upon one of them: Carbon Capture, Utilisation and Storage.

1.2 Carbon Capture, Utilisation and Storage

Carbon Capture, Utilisation and Storage (CCUS) refers to a series of technologies that aim at preventing CO_2 emissions into the atmosphere by capturing them, either at concentrated point sources or directly from the atmosphere. The captured CO_2 is then reused as a resource or stored for long-term disposal.

The power and industry sectors dominate the emissions of anthropogenic CO_2, with the majority of carbon dioxide originating from combustion applications [Metz et al. 2005]. In these sectors, most of the sources have developed or are developing emission-free alternatives. Examples include nuclear and renewable energies for power and heat generation, electric motors for individual vehicles, novel energy storage opportunities and so on. Facing the urgency of action, CCUS is however recognised as an effective short-term strategy to reduce emissions pending the massive deployment of the alternatives.

In the context of limiting global warming to less than 2 °C (Paris Agreement), most mitigation scenarios cannot find a solution without CCUS. It is therefore an essential solution intrinsically. [Bui et al. 2018; IPCC 2018]

Moreover, CCUS is considered to be a serious long-term strategy to mitigate hard-to-abate emissions from crucial industrial processes such as steel, pulp and paper, petrochemical processing and cement.

The following sections describe the different steps of CCUS and the range of existing technologies.

1.2.1 Capture from point sources

Capturing CO_2 is most feasible from large-scale, stationary, concentrated sources (*e.g.* fossil fuel-fired power generators, industrial production systems and chemical plants) at which fossil fuels are combusted.

There are three major capture routes within combustion systems:

1. post-combustion capture
2. pre-combustion capture
3. oxyfuel combustion

As CO_2 is almost always found in gas mixtures, all capture routes involve a gas separation unit at some point. Beyond this similarity, the different approaches require application-specific considerations and adaptations. The three routes are individually described in the following sections and are collectively summarised in Figure 1.4.

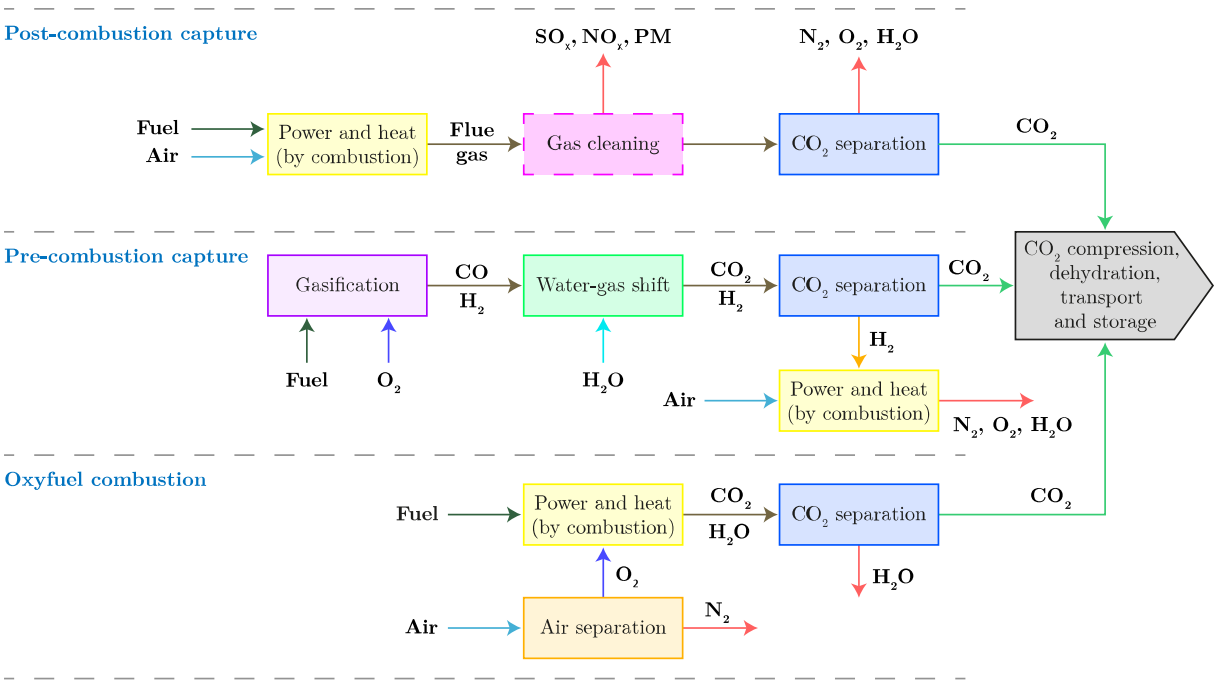

Figure 1.4: Capture routes. Adapted from [Madejski et al. 2022; Metz et al. 2005]

1.2.1.1 Post-combustion capture

As its name suggests, post-combustion capture (PCC) occurs after the combustion process. It relies on the selective separation of exhaust gases. Indeed, in the dedicated post-combustion capture unit, CO_2 is removed from the gaseous mixture while the other gases are vented into the atmosphere. Depending on the fuel and on local legislation, the PCC unit can be preceded by filters or by gas cleaning units that aim at removing other pollutants: sulphur oxides (SO_x), nitrogen oxides (NO_x) and particulate matter (PM).

The decisive advantage of this capture route is the possibility to retrofit a PCC unit to an existing power plant, therefore facilitating the rapid deployment of CCUS without the need for an extensive overhaul of the existing facility. [Cousins et al. 2016]

Within the considered route, a variety of PCC technologies exist, although not all of them are equally mature [Bui et al. 2018]. Because of the relevance of PCC within this work, some technologies are further described in Section 1.3.

1.2.1.2 Pre-combustion capture

Pre-combustion capture refers to combustion processes in which the fuel is treated beforehand. The solid fuel (coal or biomass) is first converted to a synthetic gas, or syngas, mainly composed of CO and H_2. This step is called *gasification*. The water-gas shift reaction, described by Equation (1.1), further converts the CO into CO_2. [Madejski et al. 2022]

$$CO + H_2O \longrightarrow CO_2 + H_2 \tag{1.1}$$

The carbon dioxide is then captured by separation from the mixed stream. The syngas is rich in CO_2, which allows for easier removal compared to PCC. Finally, the purified

hydrogen stream supplies a gas turbine. As only H_2 is burned, the combustion chamber produces water, and it does not emit any carbon dioxide.

This capture route is implemented in Integrated Gasification Combined Cycles (IGCC).

1.2.1.3 Oxyfuel combustion

In oxyfuel combustion, fuel is burned in an oxygen-enriched atmosphere. As a consequence, the flue gas of this combustion only contains a mixture of CO_2 and H_2O. Dehydrating this flue gas (*i.e.* condensing the water content) yields a nearly pure stream of CO_2.

The absence of N_2 as a thermal ballast motivates the need for flue gas recirculation (FGR) to maintain the temperature within material limits.

The difficulty lies in obtaining a nearly-pure O_2 stream to supply the combustion chamber. This is done in an air separation unit (ASU), which most often involves cryogenics. [Bui et al. 2018]

1.2.1.4 Capture from industrial processes

Albeit they represent the largest share of emissions, combustion processes are not the singular sources of CO_2. Some carbon-intensive industrial processes, such as steelmaking, cement production and petrochemical refining, are also contributors. CCUS is particularly relevant for these applications as the emissions are inherent to the process and abatement would require the development of alternatives.

Cement production, for instance, involves the calcination of limestone (Equation (1.2)). This processing step occurs at around 1400 °C and supplying the required heat can already emit carbon dioxide (depending on the source). In addition, CO_2 is a product of the chemical reaction itself. For these reasons, it is estimated that $880\,\mathrm{kg_{CO_2}}$ is emitted for each tonne of cement. [Bui et al. 2018; Kuramochi et al. 2012]

$$\mathrm{CaCO_3} \longrightarrow \mathrm{CaO} + \mathrm{CO_2} \tag{1.2}$$

Similarly to cement production, steelmaking is also a major industrial source of CO_2 because of both its energy insensitivity and its process. Be it the coke pyrolysis or the blast furnace use, most production steps are responsible for carbon dioxide emissions. In total, they amount to $1.8\,\mathrm{t_{CO_2}}$ per tonne of crude steel. [Bui et al. 2018; Kuramochi et al. 2012]

Those examples motivate the potential of carbon capture when applied to industrial processes, beyond the decarbonisation of energy sources. Other examples include the use of fuels as feedstock in petrochemical processes and biomass fermentation for ethanol production. [Metz et al. 2005]

1.2.2 Transport

If the captured carbon cannot find a purpose on site, it has to be transported either to a storage site (Section 1.2.3) or to a utilisation facility (Section 1.2.4).

CO_2 can either be transported by pipeline, ship, rail or road.

Pipeline transport is the most cost-effective method and also the most developed one, as there exists an extensive pipeline network in North America. Strong of 8000 km, this dedicated network is used to transport CO_2 to Enhanced Oil Recovery (EOR) sites. Large-scale transportation of CO_2 by ships has yet to be implemented, but it has a lot of potential for very large distances. On the contrary, rail and road transport appear to be only viable over small distances and for small volumes. [Boot-Handford et al. 2014; Bui et al. 2018; IEA 2021]

Prior to transport, the captured stream of CO_2 must be compressed. In some cases, it is even advantageous to aim for dense phases such as a supercritical fluid or a liquefied cryogenic state. The compression step represents a significant energy consumption that is translated into efficiency losses or increased expenditures, depending on the capture configuration. [Bui et al. 2018]

1.2.3 Storage

Storage, or sequestration, refers to the permanent disposal of CO_2 in stable geologic sinks. The CO_2 is injected into porous rock formations overlaid by impermeable cap rocks, effectively sealing the reservoir. Once injected, the CO_2 diffuses within the reservoir, dissolves and, over a long period of time, mineralizes.

The potential storage sites can be located onshore or offshore and include saline aquifers, former coal deposits and depleted oil and gas fields. They are estimated to be in excess of expected future requirements. However, their location can be remote from capture sites, hence the need for transport. [IEA 2021]

1.2.4 Utilisation

CO_2 can also be seen as a commodity. It can be used as a reagent for the production of synthetic fuels, plastics or chemicals. As of today, 230 Mt_{CO_2} are already used annually as feedstock, mainly for urea production and enhanced oil recovery (EOR) but also in the food industry. Utilisation is interesting as it attributes an end value to a captured volume of CO_2, hence reducing the price of capture. [Boot-Handford et al. 2014; IEA 2019]

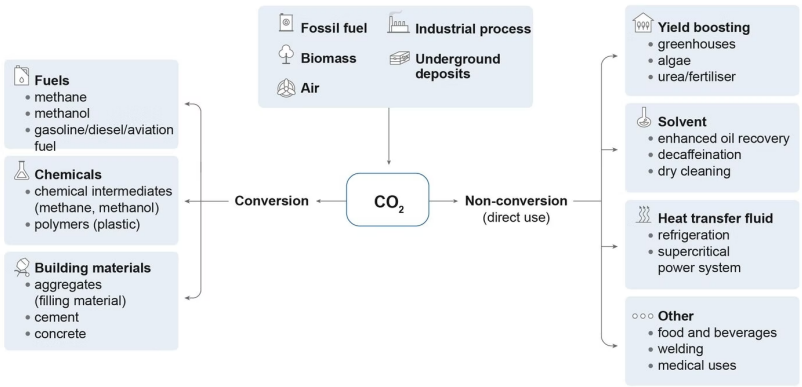

Figure 1.5: Overview of CO_2 utilisation pathways [IEA 2021]

1.2.5 Carbon Capture and Negative Emissions Technologies

Negative Emissions Technologies (NET) or Carbon Dioxide Removal (CDR) refer to the removal of CO_2 directly *from the atmosphere*. They allow for the compensation of hard-to-abate sources and, in the long term, they could presumably revert some changes by reducing the atmospheric CO_2 concentration.

In this section, two CDR technologies are introduced: Direct Air Capture (DAC) and Bio-Energy with Carbon Capture and Storage (BECCS). Other candidates include afforestation, reforestation, biochar and ocean alkalinisation. [IEA 2022]

1.2.5.1 Direct Air Capture

Direct Air Capture (DAC) technologies filtrate the ambient air and extract the CO_2 from it. The two majors technologies are liquid DAC, which captures carbon dioxide in liquid chemical solutions, and solid DAC, which involves a solid adsorption/desorption cycle. [IEA 2022]

Because of the low CO_2 concentration in the air (around 417 ppm [NASA 2022]), DAC facilities must ingest massive volumes of air. This complicates the capture process with respect to large point sources. DAC has yet to be demonstrated on a large scale and costs are currently much higher than other CCUS alternatives (Figure 1.6).

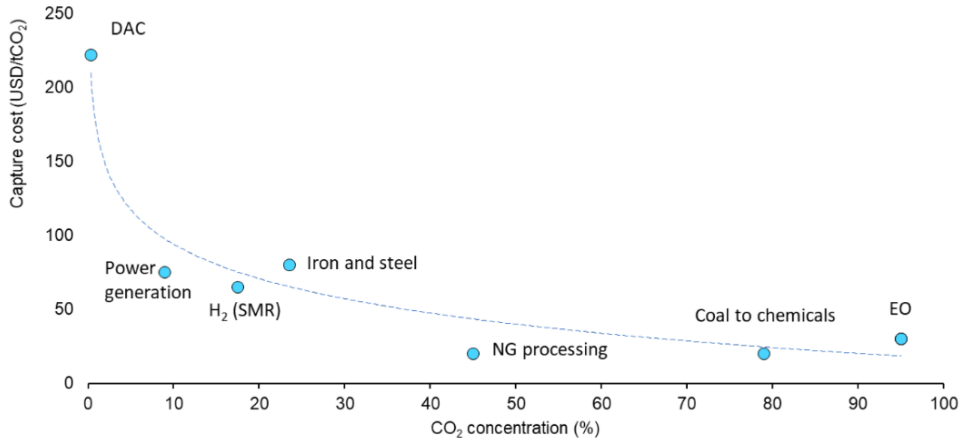

Figure 1.6: Costs of the different CO_2 capture technologies when put in perspective with the CO_2 concentration in the source [IEA 2022]

1.2.5.2 Bio-Energy with Carbon Capture and Storage

Bio-Energy with Carbon Capture and Storage (BECCS) is an extension of CCS that includes biomass combustion for energy generation (called bio-energy).

Biomass fuels take in CO_2 from the atmosphere as they grow and release it when they decompose or when they are combusted. Using biomass feedstock in a power plant equipped with a CCS unit adds a supplementary layer of capture while reclaiming valuable energy through the combustion process. A net amount of CO_2 is therefore extracted from the atmosphere. In other words, carbon dioxide is removed from the atmosphere through the biosphere. It is illustrated in Figure 1.7.

All mitigation scenarios that limit global warming to 1.5 °C involve BECCS to some extent [IPCC 2018]. However, it should be noted that the potential of BECCS within the mitigation scenarios has received some criticism regarding its limitations, mainly because of the competition for land with food production and biodiversity conservation but also because of knowledge gaps regarding side-effects. [Fuss et al. 2014; Minx et al. 2018]

Moreover, sustainable biomass management is key to permitting the potential of BECCS. Life cycle analyses highlight the importance of many factors, such as the supply chain emissions. [Pour 2019]

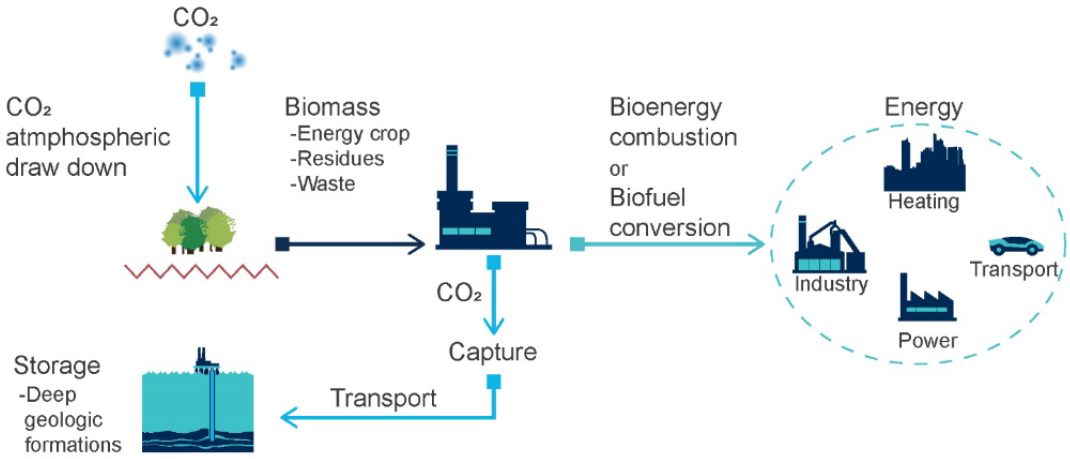

Figure 1.7: Concept illustration of BECCS [Global CCS Institute 2019]

1.3 Overview of post-combustion capture technologies

As post-combustion capture boils down to selective gas separation from exhaust gases, the PCC technologies take advantage of different properties or reactions. A high-level overview of the existing technologies is provided in this section.

1.3.1 Chemical absorption

In chemical absorption, a liquid solvent preferentially reacts with the CO_2 contained in the flue gas. The reaction is reversible and the solvent can be regenerated with the application of heat. This results in a cyclic process. As it involves a chemical reaction, chemical absorption is also referred to as reactive absorption. Its main drawback resides in its extensive heat consumption and most studies focus on reducing it. [Boot-Handford et al. 2014; M. Wang et al. 2011]

Most of the available solvents are amines (or amine blends). More details about the commonly-used solvents and their alternatives are discussed in Chapter 2.

Chemical absorption is currently the most mature PCC technology. It is deployed in many pilot plants but also in the few commercial applications of CCS. [Bui et al. 2018]

1.3.2 Adsorption

Adsorption refers to the attachment of CO_2 to a solid surface of an adsorbent. In this configuration, the loaded flue gas is circulated in presence of porous materials that trap carbon dioxide. From there, several regeneration routes exist: regeneration by applying heat (temperature swing adsorption), by reducing the pressure (pressure swing adsorption) or by applying a vacuum (vacuum swing adsorption). [M. Wang et al. 2011]

Candidates for adsorption include zeolites, activated carbon and alumina, among many others. The reader can refer to [Sai Bhargava Reddy et al. 2021] for a recent overview of the options.

One of the main advantages of adsorption is the tolerance to a wide range of temperature and pressure conditions. [Bui et al. 2018]

1.3.3 Cryogenics separation

The different gases from which CO_2 has to be separated have different temperatures of condensation. For instance, at atmospheric pressure, CO_2 condenses around $-57\,°C$. This property can be used to selectively condensate CO_2 by supplying refrigeration to the gas mixture. The simplicity of this technique comes at the expense of a large operational cost that makes it more suitable for capture from highly-concentrated streams, such as oxyfuel combustion flue gas. [Madejski et al. 2022; M. Wang et al. 2011]

1.3.4 Membrane separation

Two distinct separation technologies involve membranes. First, membranes can be used as contact areas between the flue gas and a liquid solvent (gas absorption membrane). And second, membranes can be used to take advantage of their own selectivity (gas separation membranes). In this case, the separation relies on the difference in permeability of the gases. The partial pressure at either side of the membrane dictates the permeation. [Madejski et al. 2022; M. Wang et al. 2011]

It can be noted that the application of this technology to the present case study (described in Section 1.5) has been assessed in a previous master's thesis. [Bonanno 2020]

1.4 Scope and objectives of this thesis

The main objective of this master's thesis is to lay the basis for the deployment of an amine-based post-combustion CO_2 capture pilot to treat the flue gas of the existing Sart Tilman combined heat and power (CHP) plant (described in Section 1.5).

The choice of post-combustion capture is motivated by the retrofitting potential of the case study. As the plant for which flue gases have to be decarbonised is already operating, a major overhaul of the facility would be required to allow for the implementation of an oxyfuel boiler or a pre-combustion capture unit. Therefore, retrofitting a post-combustion CO_2 capture unit is a coherent choice.

Chemical absorption is chosen because it is a mature technology and because it suits well the low CO_2 partial pressure in the considered flue gas.

Alongside this process selection, design choices, sizing calculations and economic evaluation based on the case study must be performed to help support the decision.

A better understanding of the selected process is to be gained by reading Chapter 2. In the continuity of this description, existing CCS projects are reviewed.

Simulating the PCC unit is essential to determine its operating conditions. Moreover, it has been decided to model the existing CHP plant coupled with the future, adjacent CO_2 capture unit in order to understand the interactions between the different systems. Chapter 3 addresses the combined modelling of the facility. Assumptions, design choices and parametric optimization are also detailed.

The simulation results are translated into equipment sizing and requirements in Chapter 4.

The possible heat integration strategies of the CO_2 capture unit into the existing CHP plant are investigated and the results are reported in Chapter 5. With this study, the chapter delineates the potential impact of the capture unit onto the CHP plant.

Finally, a preliminary economic evaluation of the pilot is provided in Chapter 6. It does not have the pretension to evaluate the exact cost of the facility but can serve as a first basis to support the implementation of this project.

1.5 Description of the case study

1.5.1 Combined Heat and Power

Prior to the description of the aforementioned Sart Tilman plant, a short introduction to combined heat and power (CHP) is given, as it is the driving technology of this plant.

Combined heat and power (CHP), also known as cogeneration, is the concurrent production of heat and electricity by a single energetic system and therefore from a single source of primary energy. Many CHP configurations exist, and a variety of fuels can be used. Qualifying for being such a system only requires combining electricity production and heat recovery in an effective manner. It can be noted that, in some industrial applications, the cogeneration system produces heat and mechanical power, as the alternator is replaced by another process.

The interest versed in this technology arises from the observation that power plants often reject high-temperature waste heat that could be valued. On average, the efficiency at which traditional fossil-fuelled power plants operate reaches 30 % - 50 % [EEA 2016; EIA 2020], wasting a staggering share of primary energy. CHP is about using this wasted heat, driving efficiencies up to 80 % - 90 % [Salomón et al. 2011; J. Wang et al. 2019].

As the second energy product is produced from the losses of the generation of the first one, the overall losses of such systems are much lower than the accumulated losses from

equivalent standalone productions. This is illustrated in Figure 1.8.

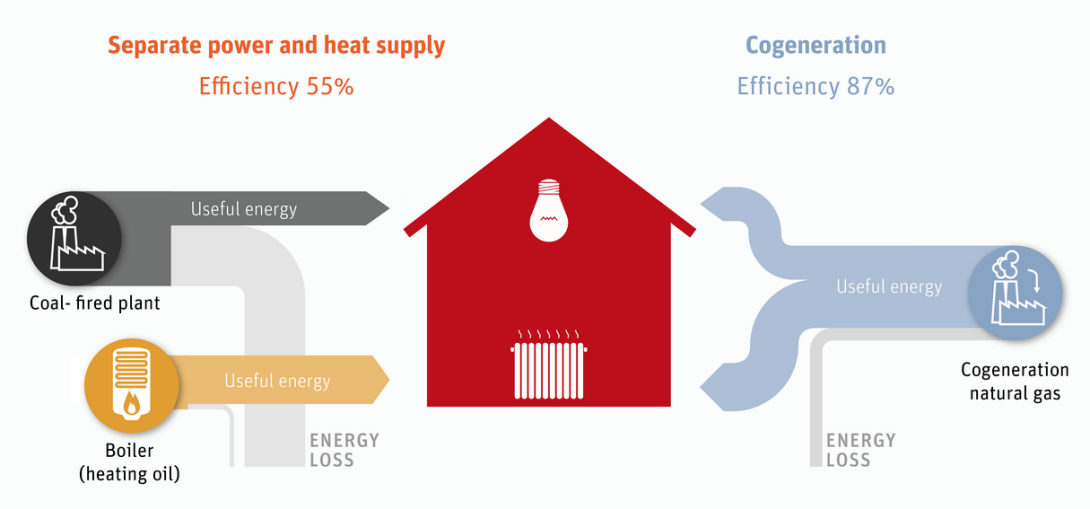

Figure 1.8: Comparison of combined production versus standalone productions [Wikipedia 2022a]

Higher fuel conversion efficiency translates into lower primary energy consumption and therefore leads to a reduction in CO_2 emissions (and in other combustion pollutants as well). This alone is a motivation for the use of such systems.

Between the two products (heat and electricity in most cases), one can be identified as the principal one while the other is a by-product. In large-scale CHP facilities, heat production is usually the by-product using the excess energy from electricity generation (operation with electricity priority). In small-scale CHP plants, the roles can be inverted: the focus can be placed on heat generation to supply a district heating network or an industrial process (operation with heat priority). The constraining factor is the presence of sufficient heat demand in the vicinity of the plant because heat is difficult to carry over large distances. [Sartor 2018]

1.5.2 Sart Tilman CHP plant

1.5.2.1 General information

The Sart Tilman campus and the hospital of the University of Liège are heated by a 10 km-long district heating network (DHN) that supplies approximately 70 buildings, amounting to a total heated area of 470 000 m^2. Amongst the connected buildings, the hospital stands out not only because it represents 25 % of the heated area but also because it requires heat and steam 24 h per day for its internal processes. [Sartor and Dewallef 2018]

Since 2012, an industrial biomass-fired CHP plant is in operation to supply the base load of this DHN. The 12 MW, moving grid biomass boiler is stoked by wood pellets (around 2.5 t/h) and generates steam (around 13 t/h) in a conventional Rankine cycle. The cogeneration unit has a nominal thermal power of 7 MW_{th} and a nominal electric power of 2.4 MW_e, from which around 400 kW_e of self consumption must be subtracted.

This includes pumping work, lighting and other ancillary consumption. [Sartor 2018]

To prevent material degradation, acceptable temperatures are maintained inside the furnace by recirculating a fraction of the flue gas. The threshold temperature is set at 950 °C.

The CHP plant has not been designed to meet 100 % of the heat demand. In fact, the techno-economic optimum of such systems is reached when the operation is constant over long periods of time, as a decrease in the heat demand harms the overall efficiency of the process. In this case, the CHP plant can supply approximately 60 % of the heat demand. Supplementary (and backup) power is provided by four conventional gas boilers. These secondary boilers are not considered in this modelling work. [Sartor 2018]

1.5.2.2 Description of the thermodynamic cycle

Figure 1.9 shows the layout of the plant and the cycle is described hereafter. The reader should note that the chosen convention in this master's thesis is to express the pressure levels in absolute terms.

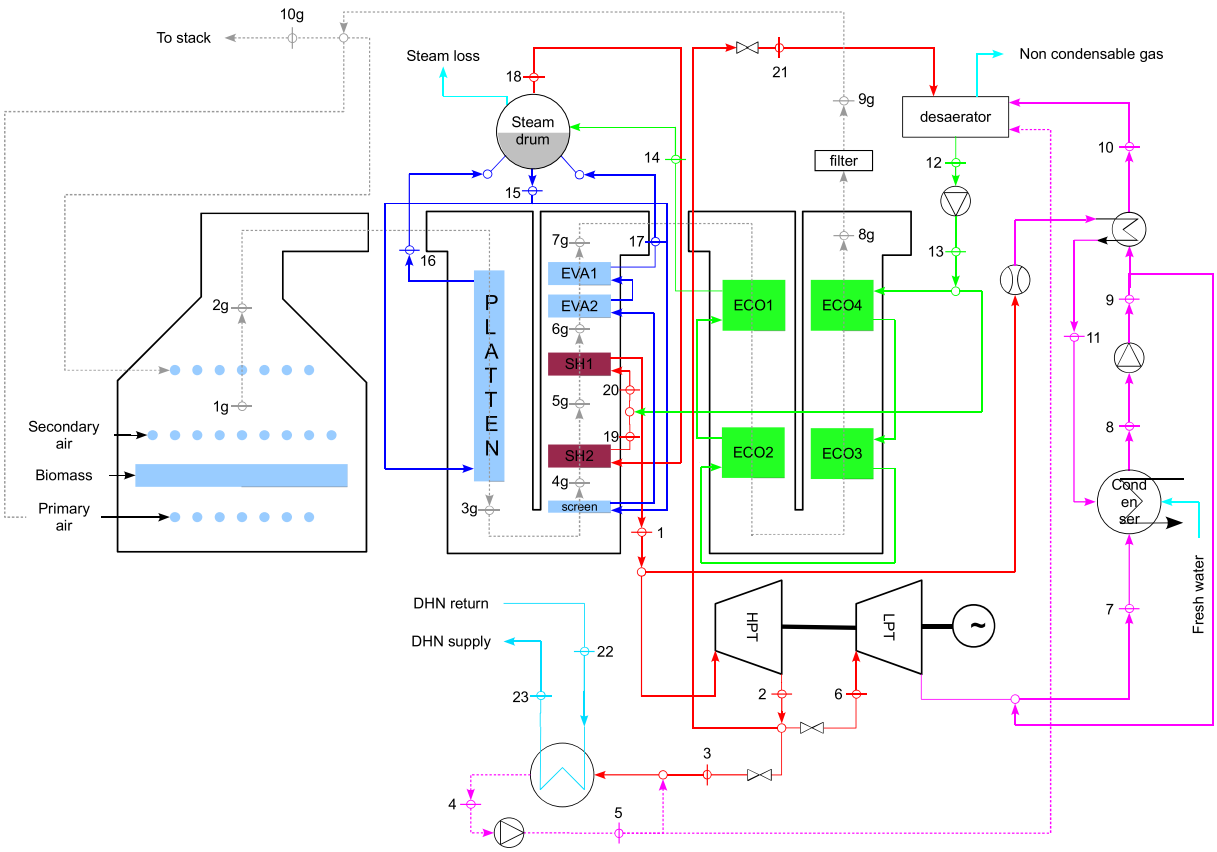

Figure 1.9: Schematic of the Sart Tilman CHP plant [Sartor 2018]

The boiler generates around 13 t/h of superheated steam at 420 °C and 4200 kPa. A first, high-pressure turbine (HPT) expands it down to 550 kPa and generates electricity at the same time.

At the HPT outlet, the steam flow is divided into three contributions:

- a first, major fraction is condensed in two consecutive heat exchangers feeding the DHN (bottom left in Figure 1.9). The condensed water is pumped, a fraction is recirculated at the inlet of the DHN heat exchangers for temperature regulation and the rest is sent to the deaerator (top right in Figure 1.9).
- a second fraction is expanded in a second, low-pressure steam turbine (LPT) down to approximately 10 kPa. The steam is then tempered and condensed at 40 °C in the main condenser (on the right in Figure 1.9) before being pumped and injected into the deaerator.
- a third fraction is directly fed to the deaerator.

The separated streams are therefore reconciled in the deaerator. This piece of equipment aims at removing the non-condensable gas, such as O_2 dissolved in water, thanks to steam injection.

The boiler feedwater exits the deaerator at 115 °C and 200 kPa. The water is then vaporized back to superheated steam in a network of heat exchangers, including economizers, evaporators and superheaters (centre in Figure Figure 1.9).

The boiler operates continuously at full capacity. However, the Rankine cycle distributes the contributions to the DHN and to the LPT depending on the DHN demand.

CHAPTER 2

Process description and literature review

The present chapter brings details on the functioning of the selected CO_2 capture technology, *i.e.* the amine-based post-combustion capture. The reasons for this choice were motivated in Section 1.4.

The chapter is split into two parts: Section 2.1 is dedicated to the description of the selected process while examples from the literature are reported in Section 2.2.

2.1 Process description

2.1.1 Typical process flowsheet

The amine-based PCC CO_2 capture process itself can be decomposed into two steps: absorption of CO_2 in the absorption column (or absorber) and desorption in the stripping column (or stripper) to regenerate the solvent. The regenerated solvent can then be reused in the first step. This circular principle is shown in Figure 2.1.

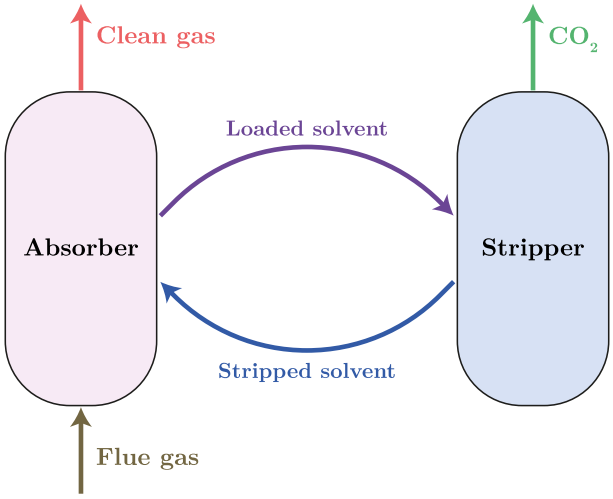

Figure 2.1: Simplified schematic of the process

The detailed process is illustrated in Figure 2.2 and is explained hereafter (adapted from [Léonard 2013; Metz et al. 2005; Peeters 2021]).

First of all, a fraction of the flue gas (or the entire volume, depending on the ambition of the capture unit) goes through a direct contact precooler, *i.e.* a heat exchanger that is intended to bring the flue gas temperature down to 40 °C. The pre-cooling section includes a flash separator, from the top of which the cooled flue gas exits while condensates (mainly water) are recuperated at the bottom.

The cooled gas is then blown by a fan in order to compensate for the pressure drop in the next equipment: the absorber. The blown gas is injected at its bottom.

A solvent is also injected as a liquid solution at the top of this column and flows downwards as the flue gas rises. The solvent preferentially reacts with the CO_2 in the gas phase, effectively disposing the flue gas of its CO_2 content (up to a certain percentage, called the *capture rate* or the *capture efficiency*). Discussion over the nature of the solvent is provided in Section 2.1.2. The chemical absorption of CO_2 into the solvent is an exothermic reaction, which justifies the need for a pre-cooling section as lower temperatures favour exothermic reactions.

The flue gas continues to rise through the column and enters the washing section (or washer), located just above the absorption section (at the top of which the solvent is injected). The washer is a cleaning section in which liquid water is injected to recuperate solvent droplets that have been entrained with the flue gas, hence reducing the solvent losses. The washer also helps regulate the water balance in the system by varying the temperature of the saturated flue gas. Finally, the latter is vented to the atmosphere.

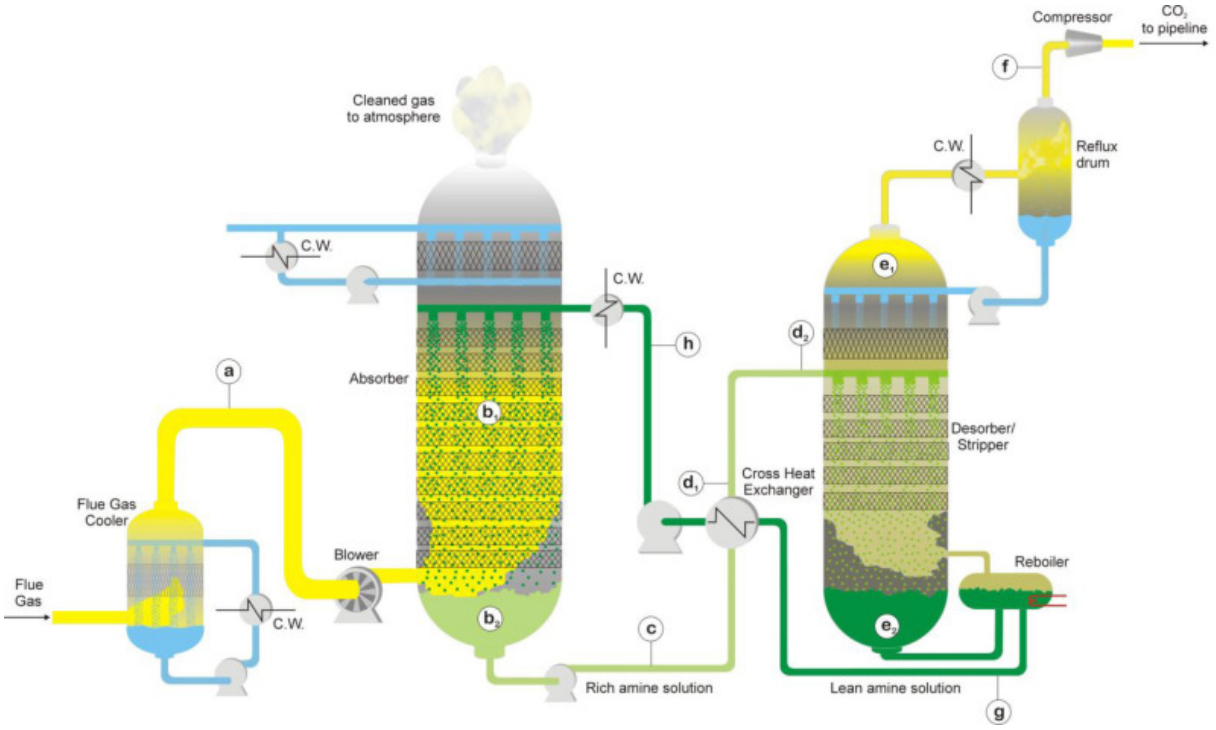

Figure 2.2: Detailed schematic of the process [Krzemień et al. 2013]

The liquid solvent is recuperated at the bottom of the absorber. At this point, it is loaded with CO_2 and is referred to as the *rich solvent solution*. As mentioned, absorption of CO_2 is an exothermic process and the released heat increases the solvent temperature up to around 50 °C.

The rich solution is then brought to a higher pressure level by a pump, before going through a heat exchanger that heats the solvent up to 100 °C - 140 °C. At this temperature, the absorption reaction is reversed and the captured CO_2 can be released from the solvent in the stripping column. This step is called *solvent regeneration*.

At the bottom of this column, the liquid solvent is partially vaporised by a reboiler in order to supply the necessary thermal energy for solvent regeneration. The higher pressure level of the stripper (with respect to the absorber) allows for a smaller reaction heat of solvent stripping, and therefore for a lower reboiler heat duty.

The liquid solvent, now stripped of its captured CO_2, exits at the bottom of the stripper and is called the *lean solvent solution*. It is fed back and cooled down into the previously-mentioned heat exchanger, called the *lean-rich heat exchanger*, as it heats up the rich solution by depleting the sensible heat of the lean solution.

The lean solution is brought back to the inlet of the absorption column, after flowing through a final heat exchanger providing the remaining cooling duty to reach the target temperature of 40 °C.

At the top of the stripper, the separated CO_2 first goes through a washing section, which is also dedicated to the recovery of solvent droplets. It is then cooled down to 40 °C in a condenser to recuperate the water, which is, in turn, injected back at the top of the washing section.

The gaseous product of the stripper is, therefore, a highly-concentrated CO_2 flow, which finally undergoes a series of compression steps to reach the required conditions for pipeline transport (see Section 1.2.2).

The capture rate can be mathematically defined as follows [Cousins et al. 2016]:

$$\text{Capture efficiency} = \frac{\dot{m}_{CO_2,in} - \dot{m}_{CO_2,out}}{\dot{m}_{CO_2,in}} \cdot 100 = \frac{\dot{m}_{CO_2,capt}}{\dot{m}_{CO_2,in}} \cdot 100 \tag{2.1}$$

This elementary process description corresponds to the configuration considered for the case study. More details on the design choices and specifications of each component will be discussed in Chapter 3.

2.1.2 Solvent

As mentioned in Chapter 1, most chemical solvents used in CO_2 capture applications are aqueous amines.

Amines are derivatives of ammonia wherein at least one hydrogen atom has been supplanted by a group. The distinction can be made between primary, secondary and tertiary amines, having respectively one, two and three replaced hydrogen atoms.

2.1.2.1 Selected solvent

The solvent studied in this work is a solution with 30 wt-% of monoethanolamine (MEA).

Monoethanolamine is a primary alkanolamine, *i.e.* one of its hydrogen atoms has been replaced by an alkyl group. Its chemical formula is C_2H_7NO and its structure is shown in Figure 2.3.

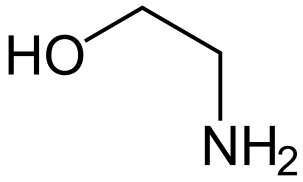

Figure 2.3: Chemical structure of MEA [Wikipedia 2022b]

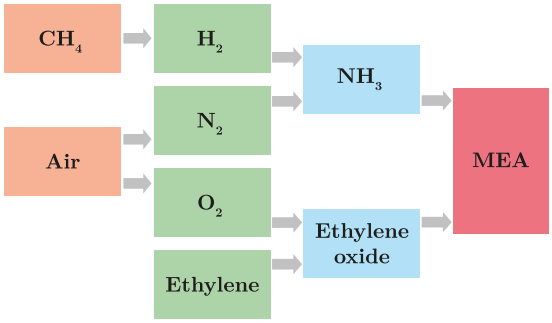

Figure 2.4: MEA production pathway [Luis 2016]

Monoethanolamine is produced from the reaction between aqueous ammonia (NH_3) and ethylene oxide (EO). A single NH_3 molecule can either form a primary, a secondary or a tertiary ethanolamine, depending on how many EO molecules it reacts with. The respective products are named monoethanolamine (MEA), diethanolamine (DEA) and triethanolamine (TEA), respectively. Ammonia itself is produced by combining nitrogen and hydrogen. Although the former is abundant in the air, the latter is usually produced by steam reforming, which involves fossil fuels as reagents (typically methane CH_4) and as combusted fuels to supply the necessary heat of reaction. Ammonia production is therefore a source of CO_2 emissions. [Luis 2016]

Figure 2.4 illustrates the different components involved in MEA production.

Regarding carbon capture, MEA is the most mature solvent and the most widely used. On the one hand, its main strength resides in its fast reaction kinetic with CO_2 [Reynolds et al. 2016]. On the other hand, its main drawbacks include equipment corrosion, substantial energy consumption associated with its regeneration and its proneness to degradation. The latter is discussed in the next section.

Increasing the MEA concentration up to 40 wt-% leads to desirable energy savings but it comes with an increased risk of corrosion [Abu Zahra 2009]. For this reason, sticking with the conventional 30 wt-% solution is a reasonable choice.

More details about the chemical interactions between MEA and CO_2 are provided in Chapter 3.

2.1.2.2 Solvent losses

Solvent losses can disrupt the operation of an MEA-based PCC unit by depleting the reactive compound.

The two major mechanisms that dictate losses are solvent emissions and solvent degradation.

The former boils down to gaseous solvent and liquid droplets being entrained within the gas phase that is vented to the atmosphere. The washing section of the absorber prevents most of these emissions.

Solvent degradation refers to the decomposition of MEA into other chemical species or to chemical reactions that involve MEA, also transforming it into other compounds. As most degradation products do not fulfil the absorption role of MEA, carbon capture systems must include a solvent make-up stream to compensate for the losses.

Four main degradation routes have been identified [Léonard 2013]:

- thermal decomposition: aqueous MEA decomposes spontaneously from 200 °C.
- thermal degradation with CO_2: irreversible reactions with CO_2 start consuming the MEA above 120 °C.
- oxidative degradation: the O_2 content in the flue gas oxidises the solvent.
- degradation due to flue gas contaminants: depending on the type of fuel, impurities (such as SO_x and NO_x) can degrade the solvent. This type of degradation can even motivate the deployment of a pretreatment unit aimed at reducing the concentration of these pollutants.

The flue gas composition therefore has a major influence on the operating conditions for several reasons. First of all, the absorption efficiency is proportional to the CO_2 concentration. Secondly, the O_2 concentration promotes oxidative degradation. And finally, SO_x and NO_x also contribute increasingly to MEA degradation as their concentration rises. This is mainly a concern for coal-fired and biomass-fired power plants.

Similarly to pure MEA, degradation products can also exit the system with the flue gas, which is undesirable. The washing section helps reduce the emission of degradation products. [Léonard 2013]

Degradation assessment is not within the scope of this work. It is nonetheless a non-negligible phenomenon and it is taken into account whenever it is possible.

2.1.2.3 Alternative solvents

Albeit the most mature solvent, the performance of MEA is getting overshadowed by novel alternatives. Among others, ammonia (NH_3), methyl-diethanolamine (MDEA), piperazine (PZ) and ionic liquids (IL) are considered. [Luis 2016]

In particular, a new benchmark has been proposed to better reflect the state of the art of chemical absorption, ousting MEA from this role. The aforementioned benchmark is a 40-wt% solution of piperazine (PZ) and amino-methyl-propanol (AMP) in a 1:2 molar ratio. [Feron et al. 2020; IEAGHG 2019]

Nevertheless, the maturity of MEA-based capture surpasses the theoretical benefits of alternative solvents when it comes to short-term deployment.

2.2 Literature review of existing CCUS projects

Before diving into the modelling work, it is relevant to have a look at current efforts to implement CO_2 capture units, with emphasis on amine-based post-combustion capture and on BECCS.

2.2.1 Commercial-scale facilities

At the time of writing, only two commercial-scale CCUS facilities have been deployed so far in the power sector [IEA 2020b]:

- the Boundary Dam plant in Saskatchewan, Canada. Retrofitted to a coal-fired power plant, it is capable of capturing $1\,Mt_{CO_2}$/year. It uses a proprietary amine solvent developed by Shell.
- the Petra Nova plant in Texas, United States. It is also retrofitted to a coal-fired power plant. Its capture rate amounts to $1.4\,Mt_{CO_2}$/year. The involved solvent is the KS-1 amine solvent that is developed by Mitsubishi Heavy Industries (MHI). The operation of the CO_2 capture unit has been suspended in May 2020 because of cost competition with oil during the pandemic.

In other industrial sectors, commercial-scale CCUS plants are already operating in various countries. Most of them are located in the USA, Canada, China and Australia. The facilities are mainly linked to the petrochemical industry (oil refining, natural gas processing and so on) of the aforementioned countries. Other sectors are also involved, such as fertiliser production. Other countries hosting a commercial-scale CCUS plant include Algeria, Norway, Hungary, Brazil and the UAE. In Belgium, for instance, a consortium of petrochemical corporations has launched a plan to deploy, by 2030, pilot plants on their production sites, located around the Port of Antwerp. [Global CCS Institute 2022]

2.2.2 Pilot-scale facilities

The objective of the deployment of pilot plants is to study the operation of a carbon dioxide capture unit from a scaled-down installation. In particular, anticipating challenges that arise during sustained operation is crucial, as is tackling current issues that penalise the technology. Moreover, novel contributions (such as alternative solvents or innovative process configurations) can be tested to reconcile simulation results with experimental data.

Numerous pilot plants are currently in operation around the world. A database compiling the existing projects is maintained by the Global CCS Institute. [Global CCS Institute 2022]

In Belgium, the only operating CCUS project is the LEILAC pilot plant at the Heidelberg cement plant in Lixhe. The capture technology is process-specific and is called *direct separation*. The raw limestone is calcined and decarbonated indirectly by an external reactor. This allows for the emission of a pure CO_2 stream as the combustion products are not mixed with the raw materials. In addition, PCC technologies that were introduced in the previous chapter could also be applied to mitigate the emissions from the source of heat. [LEILAC 2020]

Regarding amine-based pilot plants, comparative papers have been published [Cousins et al. 2016; Idem et al. 2015]. What emerges from the literature is that most operating PCC pilot plants are within a capture range of 10 kg_{CO_2}/h to 1000 kg_{CO_2}/h [Cousins et al. 2016]. This observation can serve as a basis for the design point of the case study considered in this work. Indeed, the upper bound of the range (1 t_{CO_2}/h) is picked as a target for the case study. This decision brings the studied project from the edge of the definition of a pilot plant into the realm of demonstration units.

Amongst the existing (or decommissioned) pilot plants, projects can be selected as a reference to validate the future simulation results. A notable example is the Esbjerg pilot plant. Between 2004 and 2008, the EU funded the CASTOR project that aimed at developing post-combustion capture technologies in addition to CO_2 sequestration case studies [CORDIS 2011]. As part of this project, the Esbjerg coal-fired power plant in Denmark hosted a 1 t_{CO_2}/h pilot plant. Several experimental campaigns have been conducted, both with the reference solvent (30 wt-% of MEA) and with novel blended amine solvents (CASTOR1 and CASTOR 2). Among other investigations, the absorber liquid-to-gas ratio (*i.e.* the ratio of solvent flow rate to flue gas flow rate) was optimised and the MEA degradation rate was measured. The pilot achieved sustained operation at a 90% capture rate. The heat consumption of the reboiler amounted to 3.7 GJ/t_{CO_2}. [Knudsen et al. 2009]

It is also relevant to note that, with the aid of different solvents and process modifications, the performance of a capture unit can be improved. For instance, between 2010 and 2014, Alstom Power and The Dow Chemical Company developed and operated a 1 t_{CO_2}/h pilot at the coal-fired power plant in Le Havre, France. They used a proprietary, advanced amine solvent (UCARSOL FGC 3000) and managed to reach a stable heat duty of 2.3-2.4 GJ/t_{CO_2} with a 90% capture rate thanks to equipment improvements. [Baburao et al. 2014]

2.2.3 BECCS facilities

Deployment of Bio-Energy with Carbon Capture and Storage, be it commercial-scale applications or pilot plants, is more confined.

Currently, only five BECSS facilities are in operation, reaching an annual captured amount of 1.5 Mt_{CO_2}/year. They capture CO_2 from North American bioethanol production factories and reuse it in Enhanced Oil Recovery (EOR) applications. [Global CCS Institute 2019]

In biomass-fired power plants, the deployment of CCS started in the recent past. The first BECCS pilot coupled to a power station debuted operation in 2019 at the Drax power station in North Yorkshire, United Kingdom. This is the first pilot capturing carbon from the combustion of a 100%-biomass feedstock. In 2020, it was extended by a second pilot, increasing the capture capacity to 1.3 t_{CO_2}/d. [Drax 2020; IEA 2020b]

2.2.4 BECCS facilities integrated into CHP plants

Although estimations of the potential have been performed for specific regions [Beiron et al. 2021], it seems that there is no operating pilot plant combining carbon capture with a biomass-fired cogeneration plant. Researchers have even pointed to the lack of research on BECCS applied specifically to CHP plants [Levihn et al. 2019].

CHAPTER 3

Combined modelling of the facility

As a reminder, the scope of this master's thesis is to lay the basis for the construction of an MEA-based PCC CO_2 capture pilot dedicated to the treatment of the flue gas emitted by the Sart Tilman CHP plant.

Prior to the actual materialization of the pilot plant, it is necessary to predict its future operating point. This knowledge allows for the sizing of the unit, which in turn paves the way for an economic evaluation of the project. For this purpose, the pilot must be modelled and simulated beforehand.

On top of this, it is also important to be able to study how to integrate the retrofitted capture unit into the existing CHP plant. Understanding how it would react to any change in operating conditions is crucial, as is measuring the impact it would have on the CHP plant. To meet these objectives, it has been decided to model the entire facility, effectively encapsulating both the existing plant and the planned pilot into a single model.

The aforementioned combined model is developed in the present chapter.

3.1 Modelling approach

The studied facility can be broken down into the following elements:

- the CHP plant, which can be further decomposed into the following parts:
  - the biomass furnace, in which biomass is combusted and transformed into a hot flue gas
  - the heat exchanger network, that generates steam for the thermodynamic cycle by consuming the thermal energy of the flue gas
  - the thermodynamic cycle, that converts the generated steam into electricity and hot water for the district heating network (DHN)
- the CO_2 capture unit, that depletes the CO_2 from a fraction of the flue gas

The chosen approach is to model each of these components separately. From the global point of view, the submodels are only interconnected by heat and mass transfers and they do not share equipment. They can therefore be validated independently, before being combined into a single model. This approach is illustrated in Figure 3.1. Another advantage of this approach is that it allows for a more in-depth study of certain aspects without the heaviness of a complete model.

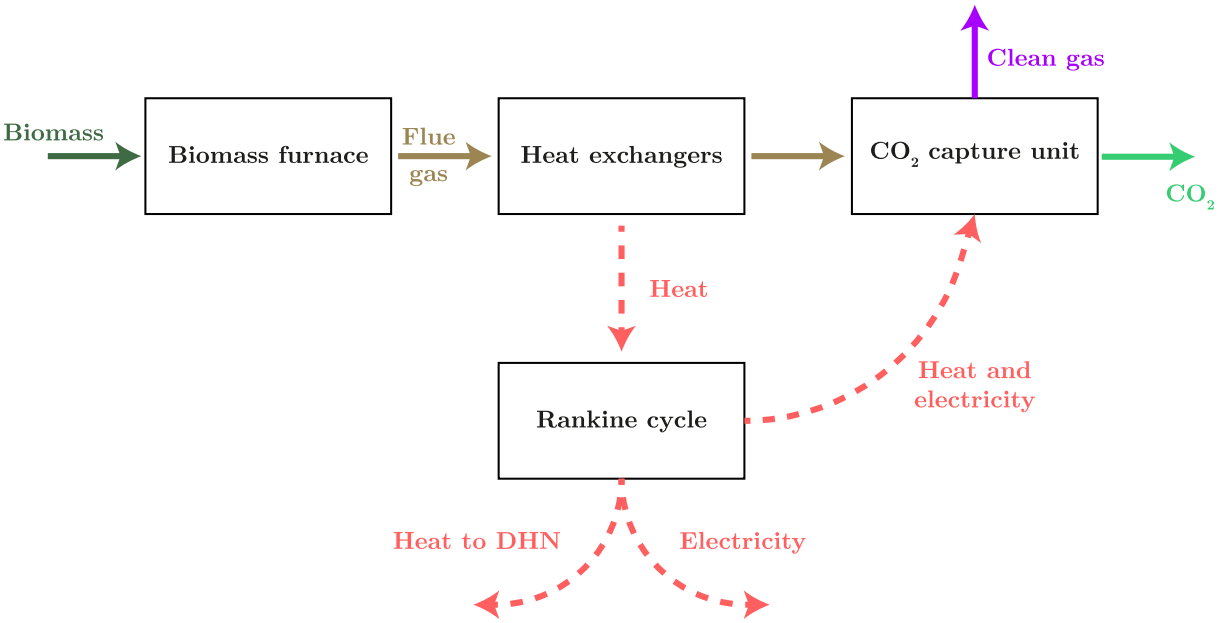

Figure 3.1: Schematic of the submodels and their interactions

The targeted level of detail of each submodel is dictated by its respective purpose within the modelling work. In particular, the heat exchanger network has been simplified as no change in operating conditions is expected. It is therefore not considered as a standalone submodel. In consequence, the combined model is composed of three submodels: the biomass furnace (Section 3.3), the CO_2 capture unit (Section 3.4) and the thermodynamic cycle (Section 3.5).

The Sart Tilman CHP plant has been previously modelled by P. Dewallef and K. Sartor, using the software EES [Sartor, Quoilin, et al. 2014]. This previous work serves as a validation basis for the relevant submodels developed in this work (*i.e.* the biomass furnace and the thermodynamic cycle).

3.2 Description of the modelling environment

The present work was performed using version 11 of Aspen Plus. Aspen Plus is a chemical process simulation software developed by AspenTech.

Aspen Plus relies on its large databanks of chemical species that come with their corresponding chemical properties. Combined with the appropriate selection of a thermodynamic model suited for the application, the software is able to simulate chemical systems using complex calculations. Aspen Plus is capable of handling complex chemical processes, such as distillation or electrolyte solutions, both of these examples being relevant in the

modelling of an amine-based CO_2 capture unit. [Ortega 2019]

In Aspen Plus, unit operation models represent actual pieces of equipment such as reactors, pumps, distillation columns, heat exchangers and so on. These models can be connected together with streams of different types (material, heat and work) in order to form a complete process flowsheet. The modelled process can then be simulated and analysed, thanks to the different available tools.

In the following sections, more features of Aspen Plus will be explained as they are used in this modelling work.

3.3 Submodel 1: biomass furnace

The biomass furnace is the starting point of the modelling work. It is meant to predict the behaviour of the rest of the system if its own initial conditions were to change. Indeed, its outputs (*i.e.* the flue gas and heat) are inputs to the other two submodels. In other words, the submodel serves two purposes:

1. predict the amount of heat that is supplied to the thermodynamic cycle
2. predict the composition of the flue gas that is supplied to the CO_2 capture unit

3.3.1 Thermodynamic properties model

Selecting an adequate thermodynamic model is essential in any simulation. In this first submodel, the selected model is the Peng-Robinson equation of state because it is recommended for combustion processes. [AspenTech 2019]

3.3.2 Inputs and assumptions

The furnace receives two inputs: a stream of solid biomass together with a volume of ambient air to sustain the combustion.

Aspen Plus is not intended for the simulation of biomass combustion. Moreover, as biomass engulfs a large range of organic solids with different compositions, there is no corresponding generic component in Aspen Plus databases. However, biomass can be manipulated through the *non-conventional* component type, which is dedicated to heterogeneous solids with unknown chemical formulas.

The exhaustive definition of such a non-conventional component requires the following mass distributions:

1. the ultimate analysis: mass distribution in carbon, hydrogen, oxygen, nitrogen, sulphur and ash
2. the proximate analysis: mass distribution in water, ash, volatile matter and fixed carbon
3. the sulphur analysis: mass distribution in pyritic sulphur, organic sulphur and sulphates

Non-conventional components do not participate in phase or chemical equilibrium. However, some physical properties are still needed for the simulation and Aspen Plus comes with embedded models to calculate them from the aforementioned mass distributions. [AspenTech 2013]

In the present work, the selected models are the HCOALGEN enthalpy model and the DCOALIGT density model as their relevance has been confirmed in previous works. [AspenTech 2013; Jana and De 2014]

The use of these two models is however not total. In fact, the heat of combustion is not predicted by built-in models. Instead, it is supplied directly to the software, in order to take advantage of an analysis conducted in June 2021 on a wood pellet sample. The moisture content was also measured on this occasion. These experimental results are presented in Table 3.1.

Moisture (wt-%)	7.20
Lower Heating Value ($MJ\,kg^{-1}$)	17.258
Higher Heating Value ($MJ\,kg^{-1}$)	20.034

Table 3.1: Results of the sample analysis conducted in June 2021

The sample analysis also yielded the following ultimate analysis, which can also be referred to as the *elemental analysis*.

Component	Wet basis (wt-%)	Dry basis (wt-%)	Dry ash-free basis (wt-%)
C	46.96	50.60	50.70
H	5.66	6.10	6.11
O	39.90	43.00	43.08
N	0.09	0.10	0.10
S	0.01	0.01	0.01
Ash	0.18	0.19	–
Water	7.20	–	–

Table 3.2: Ultimate analysis of the wood pellets, as measured in June 2021

The proximate analysis was not performed on the sample. This data (Table 3.3) is therefore deduced from the analysis of another sample, found in the *Phyllis2* database [sample #3251, ECN 2022], which is a database for the physico-chemical composition of many biomass samples. The chosen sample is a wood pellet of which the water content and heating values are as close as possible to the studied sample. A comparison is available in the Appendix (Table A1).

Finally, regarding the sulphur analysis, it is assumed that there is no pyritic sulphur (FeS_2) and the sulphate content is set equal to the ash content in the biomass, *i.e.* 0.18%.

Moisture (wt-%)	7.20
Fixed carbon (wt-%)	14.12
Volatile matter (wt-%)	78.50
Ash content (wt-%)	0.18

Table 3.3: Chosen values for the proximate analysis of the wood pellets

These three mass distributions are sufficient to define the biomass fuel in the Aspen Plus model.

The furnace is operating in atmospheric conditions as biomass is oxidised by ambient air. Wood pellets being stored on-site in silos, their thermodynamic state also corresponds to the ambient conditions. In the simulation model, ambient conditions are set following the values listed in Table 3.4. Attention must be paid to the influence of the relative humidity, as it governs the amount of water injected into the furnace. A variation of this parameter can alter the flue gas composition.

Temperature (°C)	25
Pressure (Pa)	101 325
Relative humidity (%)	50

Table 3.4: Assumed ambient conditions

3.3.3 Modelling

The Aspen Plus flowsheet of the developed model is depicted in Figure 3.2.

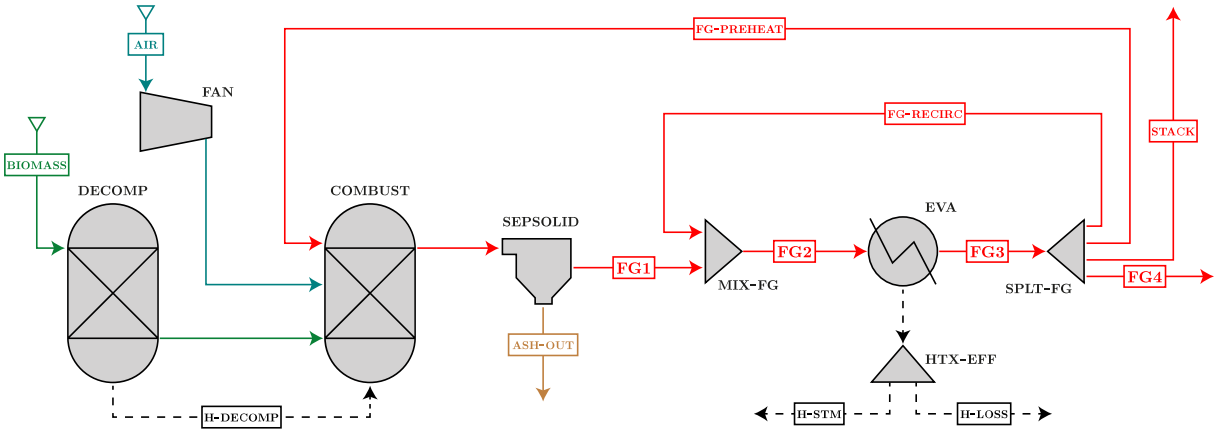

Figure 3.2: Flowsheet of the biomass furnace submodel

The aforementioned inputs of the model enter the flowsheet on the left side: the biomass stream is drawn in green and the ambient air stream is coloured in teal. Material streams are depicted with solid strokes while dotted lines represent heat or work streams. This convention is kept as such throughout the entire master's thesis.

As suggested for the combustion of solid fuels [AspenTech 2013], the combustion of biomass is divided into two steps, each of them being modelled by a unit block model:

1. the decomposition of the non-conventional biomass into conventional components in the block DECOMP

2. the formation of gaseous products in the block COMBUST

The DECOMP block is an RYIELD reactor, which is a built-in reactor model. It is used when the composition of the output is known, but when the reaction stoichiometry and kinetics are unknown [AspenTech 2019]. In fact, this reactor converts any input into the specified output distribution. In this case, biomass is converted into conventional components (C, H_2, O_2, N_2, S and H_2O) and into another non-conventional component representing the ash content that does not burn.

The output distribution corresponds to the wet-basis ultimate analysis. To enable simulations with different biomass compositions, it is convenient to spare the user from manipulating the block directly. Specifying the yield from the input stream is an automated process performed by a Calculator block, which is an operation block that accepts Fortran declarations or Excel macros to manipulate variables within the flowsheet.

The RYIELD block is set to operate at ambient conditions (*i.e.* 1 atm and 25 °C, see Table 3.4). The decomposition heat is generated during the process and it is carried over to the second reactor (COMBUST).

COMBUST is modelled by another built-in reactor model, namely the RGIBBS model. This reactor does not require the reaction stoichiometry either and is used for unknown reactions or for systems with many reactions. Moreover, although the expected output chemical species must be specified, the distribution of the products is calculated by the block. It works by minimizing the Gibbs free energy of the system. This ensures the most plausible combination of products. [AspenTech 2019]

As these successive reactor blocks model biomass combustion, the expected gas composition is a blend of CO_2, H_2O, N_2, O_2, SO_x (SO_2 and SO_3), NO_x (NO, NO_2 and N_2O) and CO.

In addition to the decomposed biomass, COMBUST also takes in ambient air (which is first blown through a fan) and a fraction of the flue gas to preheat this combustion air. The preheating fraction of the flue gas is inserted at the level of the primary air injection, as illustrated in Figure 1.9. Preheating introduces a first recycling loop in the model. The simulation is therefore not straightforward and requires a certain number of iterations as the input must be updated for each new value of the output until convergence is reached. In this first submodel, the limited weight of this recirculation with respect to the total volume of the flue gas limits the complexity of the iterative process.

The product of COMBUST is a material stream containing flue gas and ashes. The latter are separated from the gaseous phase by the SEPSOLID block. Physically, this block represents the precipitation of ashes to the bottom of the furnace.

The ash-free gas stream is then mixed with another fraction of the flue gas. It models the flue gas recirculation introduced in Chapter 1. The injection is what distinguishes the states *1g* and *2g* in Figure 1.9. Its flow rate is varied by a *Design Spec* until the flue gas temperature reaches the threshold value of 950 °C. A *Design Spec* is an embedded tool in

Aspen Plus that manipulates a designated variable during the simulation process until the target set on another variable is achieved.

Figure 3.3 illustrates the modelling approach conceptually: DECOMP models the decomposition of the wood pellets (in green) while COMBUST combines the decomposed biomass, the ambient air injection and the air preheating to model the combustion process itself. The flue gas recirculation is injected afterwards in order to cool down the combustion gases below material limits. Together, these components model the combustion chamber.

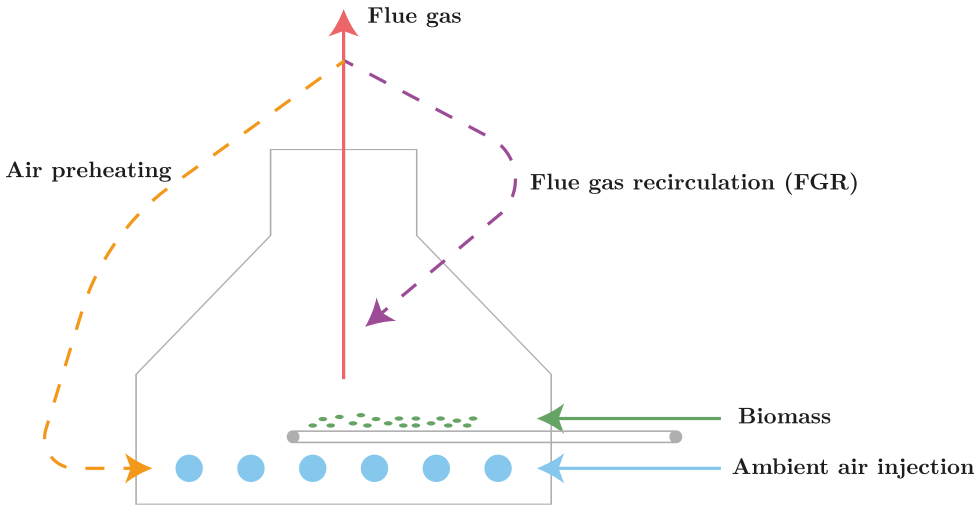

Figure 3.3: Concept illustration of the furnace submodel

The simplified model of the heat exchanger network is placed in series. The heat exchangers are modelled by a single HEATER block, which removes an amount of heat from the inlet stream in order to reach the outlet temperature of 170 °C. A heat stream is available to make the connection with the submodel of the Rankine cycle.

To account for non-idealities and losses, an arbitrary efficiency is implemented by the HTX-EFF block. It splits the heat stream H-BOIL in a usable fraction H-STM (connected to the Rankine cycle) and a lost fraction H-LOSS (emitted to the atmosphere). As a first guess, the efficiency is set at 98%, which is the combustion efficiency defined in the reference EES model introduced in Chapter 1. With this initial value, any loss in the heat exchanger network is presumably ignored. The value should therefore be updated during the validation process.

Finally, aside from the recirculated volumes, the exhaust of the furnace is split into two streams. The first is destined for the capture unit while the second is sent to the stack.

3.3.4 Validation

The model is validated by comparing the simulation results with the aforementioned EES model. The latter used a different biomass composition and the inputs of the present model are therefore adapted for this validation step. The comparison of the flue gas composition is available in Table 3.5.

	EES model (vol-%)	Aspen Plus model (vol-%)
CO_2	11.54	11.67
H_2O	11.19	11.15
N_2	70.51	70.73
O_2	6.75	6.33
SO_2	7.75×10^{-4}	7.79×10^{-4}
CO	–	1.36×10^{-3}
SO_3	–	3.93×10^{-6}
NO_2	–	2.38×10^{-4}
NO	–	0.12
N_2O	–	6.17×10^{-6}

Table 3.5: Flue gas composition according to the two models

The predicted composition is in accordance with the EES model. Nonetheless, the NO concentration stands out as a surprisingly high value. To reflect on this observation, the formation mechanisms of NO_x during the combustion of biomass can be discussed.

First, prompt NO_x formation can be neglected as it usually occurs in fuel-rich environments, which is not the case with biomass combustion. Second, the fuel NO_x can also be discarded as the reason for the excessive NO concentration. Indeed, in both the parent model and the Aspen Plus model, the nitrogen content of the biomass is entirely oxidised. What remains to explain the outlier is the thermal NO_x formation, which depends on the temperature.

As explained in the previous section, the injection of flue gas into the combustion chamber is implemented by a double structure (*i.e.* the air preheating and the flue gas recirculation). The parent model differentiates the states *1g* and *2g* (Figure 1.9) and this approach is imitated to use the intermediate temperature as a validation point. Indeed, the Aspen Plus model predicts a temperature of 1358 °C versus 1376 °C in the reference model.

The drawback of this decision is that the calculation of the flue gas composition is made at this higher temperature level because it becomes the operating temperature of the COMBUST block. Thermodynamically, the formation of thermal NO_x is therefore favoured and this could explain the unexpected NO concentration. To support this claim, both recirculation streams are reconnected at the inlet of the COMBUST block in the submodel and the recirculated flow rate is varied. The NO concentration is plotted against the operating temperature of COMBUST in Figure A1, which is available in the Appendix. It emerges that the predicted NO concentration falls sharply when the temperature decreases.

Thus, to adjust the model, it appears that the flue gas recirculation should indeed be injected into the COMBUST block, or even merged with the preheating stream.

Because this flaw was spotted near the end of the master's thesis, this change was not implemented and the flue gas composition was not updated in the subsequent developments. However, this choice does not discredit the results because the respective proportion of

the other gases is almost identical. In particular, the most important ones (*e.g.* CO_2 and H_2O) have the same weight in the composition. In addition, the dependent models have been run and no difference was spotted in the results.

The focus is brought back to the validation of the furnace submodel. The required flue gas recirculation flow rate, which is calculated by the aforementioned *Design Spec* to reach the temperature of 950 °C, is equal to 15 061 kg/h, which is similar to 15 766 kg/h as predicted by the EES model.

The artificial heat exchanger efficiency can be updated based on this validation run. The expected thermal transfer amounts to 10 444 kW_{th} and the Aspen Plus model yields 10 686 kW_{th}. As an updated guess, the efficiency can therefore be set at 97.74%. It is merely a band-aid applied to the model because the heat transfer depends on the flue gas composition (which is not totally accurate) and on the flue gas flow rate. Indeed, the temperatures before and after the heat exchanger network are set.

It is thus important to keep in mind that it is a simplistic model that neglects real-life interactions and equipment characteristics. However, it succeeds at predicting both the heat transfer and the flue gas composition with satisfying accuracy, effectively meeting the defined objectives.

3.3.5 Results

Setting the biomass flow rate to 2404 kg/h and using the composition identified in the sample analysis, the biomass furnace can be simulated. The results, summarised in Table 3.6 and Table 3.7, are used as a basis for the rest of the modelling work.

	Volume fractions (vol-%)	Mass fractions (wt-%)
CO_2	11.80	17.89
H_2O	11.12	6.90
N_2	70.77	68.27
O_2	6.17	6.80
SO_2	8.70×10^{-4}	1.92×10^{-3}
CO	1.69×10^{-3}	1.63×10^{-3}
SO_3	4.07×10^{-6}	1.12×10^{-5}
NO_2	2.38×10^{-4}	3.74×10^{-4}
NO	0.13	0.13
N_2O	6.47×10^{-6}	9.81×10^{-6}

Table 3.6: Flue gas composition from the biomass furnace model

Under the assumption of an ideal gas, the mole fraction is identical to the volume fraction because the molar volume of an ideal gas is constant (22.414 $m^3\,L^{-1}$ in normal conditions).

As explained in Chapter 2, the pilot plant must be sized to capture approximately 1 t_{CO_2}/h. The corresponding flue gas flow rate can be calculated based on the previous results.

Flue gas flow rate (kg/h)	23 117
Ash flow rate (kg/h)	4.24
Thermal power transferred from the flue gas (kW)	10 607.79
Thermal power received by the cycle (kW)	10 368.05

Table 3.7: Main results of the biomass furnace model

As the capture rate (*i.e.* the ratio of captured CO_2 to inlet CO_2) is set at 90%, there must be 1.11 tons of CO_2 at the inlet of the capture unit. CO_2 representing 17.89 wt-% of the flue gas, the required flue gas flow rate amounts to 6210.8 kg/h (rounded up to 6211 kg/h). This represents a treated fraction of 27%, hence a reduction of 24% in CO_2 emissions.

Flow rate (kg/h)	6211
Temperature (°C)	170
Pressure (Pa)	101 325

Table 3.8: Specifications of the flue gas sent to the capture unit

3.4 Submodel 2: CO_2 capture unit

The cornerstone of the modelling work is the second submodel: the CO_2 capture unit. Contrary to the other submodels, the corresponding installation is not already existing. Instead, it has to be designed and its future performance ought to be predicted.

The simulation model considered in the present work originates from a parent model developed by Prof. Grégoire Léonard [Léonard 2013]. It corresponds to the process description detailed in Chapter 2. Adapted with case-specific considerations, it becomes an efficient tool to support the implementation of the pilot plant.

The inlet conditions, *i.e.* the gas flow rate and composition, are those calculated by the biomass furnace submodel (Table 3.6 and Table 3.8). Moreover, the plant utilities (heat and electricity) are allegedly supplied by the Rankine cycle, described in the third submodel (Section 3.5). As this integration is further discussed in Chapter 5, the utilities are assumed directly available and up to any amount.

3.4.1 Chemical equations

The studied CO_2 capture system is based on chemical absorption. Before being an efficient numeric tool, it must be a faithful representation of the real process. The relevant sets of chemical equations are thus defined in this section.

3.4.1.1 Equilibrium equations

In water, MEA behaves like an electrolyte. By definition, electrolytic species are substances that dissolve into ions, of which the movement allows for the conduction of electricity.

In the present model, it is assumed that dissociation occurs so rapidly that the system reaches chemical equilibrium. The dissociation of monoethanolamine in water is therefore modelled by the following equilibrium reactions (Table 3.9).

Equation	Name
$MEA^+ + H_2O \longleftrightarrow MEA + H_3O^+$	Amine protonation
$CO_2 + 2\,H_2O \longleftrightarrow H_3O^+ + {HCO_3}^-$	Bicarbonate formation
${HCO_3}^- + H_2O \longleftrightarrow H_3O^+ + {CO_3}^{2-}$	Carbonate formation
$MEACOO^- + H_2O \longleftrightarrow MEA + {HCO_3}^-$	Carbamate formation
$2\,H_2O \longleftrightarrow H_3O^+ + OH^-$	Water hydrolysis

Table 3.9: Equilibrium reactions [Abu Zahra 2009; B.-H. Li et al. 2016]

3.4.1.2 Kinetic equations

In addition to MEA dissolution, two sets of chemical equations are defined to represent the absorption and, equivalently, the desorption of CO_2 by the solvent (Table 3.10 and Table 3.11 respectively).

In the Aspen Plus simulation, these reactions are limited to the absorber and the stripper, as they are not expected to occur elsewhere.

Unlike the modelling of the dissolution reactions, the kinetics of these reactions are governed by the temperature-dependent Arrhenius equation:

$$k = A\, e^{-\frac{E}{RT}} \tag{3.1}$$

This power law expresses the reaction rate constant k (in $\mathrm{mol\,L^{-1}\,s^{-1}}$) as a function of the absolute temperature T (in K). R is the universal gas constant ($8.314\,\mathrm{J\,K^{-1}\,mol^{-1}}$). The parameters A and E, respectively the pre-exponential factor (in $\mathrm{mol\,L^{-1}\,s^{-1}}$) and the activation energy (in $\mathrm{J\,mol^{-1}}$), are reaction-specific. Their value is given for each reaction in Table 3.10 and in Table 3.11.

Equation	A $[\mathrm{mol\,L^{-1}\,s^{-1}}]$	E $[\mathrm{J\,kmol^{-1}}]$
$OH^- + CO_2 \longrightarrow {HCO_3}^-$	1.33×10^{17}	5.55×10^{7}
${HCO_3}^- \longrightarrow OH^- + CO_2$	6.63×10^{16}	1.07×10^{8}
$MEA + CO_2 + H_2O \longrightarrow MEACOO^- + H_3O^+$	3.02×10^{14}	4.13×10^{7}
$MEACOO^- + H_3O^+ \longrightarrow MEA + CO_2 + H_2O$	5.52×10^{23}	6.92×10^{7}

Table 3.10: Absorber reactions

Equation	A [mol L^{-1} s^{-1}]	E [J kmol^{-1}]
$OH^- + CO_2 \longrightarrow HCO_3^-$	1.33×10^{17}	5.55×10^7
$HCO_3^- \longrightarrow OH^- + CO_2$	6.63×10^{16}	1.07×10^8
$MEA + CO_2 + H_2O \longrightarrow MEACOO^- + H_3O^+$	3.02×10^{14}	4.13×10^7
$MEACOO^- + H_3O^+ \longrightarrow MEA + CO_2 + H_2O$	6.50×10^{27}	9.54×10^7

Table 3.11: Stripper reactions

A more in-depth explanation of the chemical reactions can be found in [Lv et al. 2015].

3.4.1.3 Degradation equations

Two additional kinetic equations can be added to model the degradation of MEA, described in Section 2.1.2:

$$MEA + 1{,}3\,O_2 \longrightarrow 0{,}6\,H_3N + 0{,}1\,HEI + 0{,}1\,HEPO + 0{,}1\,HCOOH + 0{,}8\,CO_2 + 1{,}5\,H_2O \quad (3.2)$$

$$MEA + 0{,}5\,CO_2 \longrightarrow 0{,}5\,HEIA + H_2O \quad (3.3)$$

The degradation products that have not been defined previously are ammonia (H_3N) and other components resulting from the degradation of MEA (HEI, HEPO, HCOOH and HEIA). More details about the degradation mechanisms that yield those products are available in [Léonard 2013].

Equation	A [mol L^{-1} s^{-1}]	E [J mol^{-1}]
3.2	1.36×10^6	55 111
3.3	8×10^{11}	144 210

Table 3.12: Kinetic constants for the degradation reactions

Degradation is not within the scope of this work and these equations are not integrated into the model. However, the harmful effect of the O_2 concentration within the flue gas (introduced in Section 2.1.2) is obvious from Equation (3.2).

3.4.1.4 Derived metrics

Monitoring the performance of the capture unit is done by measuring the solvent loading.

The loading of the solvent is the ratio of the number of moles of CO_2 over the number of moles of MEA. As explained previously, ions are formed in the CO_2-MEA-H_2O system. They can be taken into account by calculating the loading as follows [Duan et al. 2012]:

$$\alpha = \frac{[CO_2] + [MEACOO^-] + [HCO_3^-] + [CO_3^{2-}]}{[MEA] + [MEACOO^-] + [MEA^+]} = \frac{[CO_2]_{app}}{[MEA]_{app}} \quad (3.4)$$

Aspen Plus automatically calculates the *apparent* fraction of the main substances, *i.e.* the sum of the fractions of a chemical compound and its related ions.

The loading takes two values: the rich loading α_{rich} (at the outlet of the absorber) and the lean loading α_{lean} (at the outlet of the stripper). The former is an image of the capture efficiency of the absorber: the larger the rich loading, the larger the amount of CO_2 absorbed into the solvent and therefore the more efficient the absorber is. Similarly, the lean loading is an image of the regeneration efficiency: a low value indicates efficient desorption as only a limited fraction of CO_2 is still bound to the solvent.

The capture rate (or capture efficiency) that was defined previously can be rewritten to include the loadings ($\dot{n}$ refers to molar flow rates):

$$\text{Capture efficiency} = \frac{(\alpha_{rich} - \alpha_{lean})\dot{n}_{MEA,app}}{\dot{n}_{\text{CO}_2,in}} \cdot 100 \tag{3.5}$$

3.4.2 Thermodynamic properties model

As explained before, one of the most crucial steps when simulating complex chemical systems is the choice of an adequate thermodynamic model. Indeed, it is essential to calculate correctly the properties of the different chemical species. An unsuitable model would seriously harm the reliability of the simulation as it would yield imprecise values.

In the case of CO_2 capture, the most demanding element is the amine solvent. Indeed, due to strong intermolecular interactions, ideality cannot be assumed. Instead, the asymmetric electrolyte nonrandom two-liquid model with the Redlich-Kwong equation of state (ENRTL-RK) is the best alternative. [AspenTech 2019; Léonard 2013]

3.4.3 Relevant Aspen Plus features

Before diving into the modelling of the capture unit, it is relevant to introduce some features as they are used in the model.

First of all, the *Design spec* is a constraining tool that manipulates a specified variable in order to reach a target that is set on an output variable. For example, the hot stream flow rate of a heat exchanger could be varied until the desired cold stream outlet temperature is attained. This tool was already employed in the furnace submodel (Section 3.3).

Secondly, the simulation is run in *Sequential mode*. This means that the Aspen Plus solver does not treat the whole flowsheet as a single system of equations. Instead, it follows a path composed of unit block models, solving them one after the other. However, due to closed loops in the sequence, it is not always possible to find a path for which all inputs are either known or computed from previous blocks. In this case, *tear streams* are used. Those are defined with initial conditions to allow for a first run. The solver updates the guesses iteratively based on the results of the previous run until the system converges, *i.e.* the calculated values are within the tolerance of the last guesses. Sufficient knowledge of the system is required to make an educated guess: the solver may not converge at all if the initial values are too distant from the real solution. Between two simulations, it is relevant to *reconcile* the tear streams. During reconciliation, the results of the previous run are pasted as initial guesses for the next simulation, effectively supporting the convergence of the system.

And finally, *mass balances* can be defined. The flow rate of a specified stream is calculated to respect a defined mass balance equation of n streams:

$$\sum_{i=1}^{n} \dot{m}_i = 0 \tag{3.6}$$

The balance equation can either pertain to the whole stream or to a specified chemical component within the stream.

3.4.4 Model description

The MEA-based capture process has been extensively described in Chapter 2. This section details how it is translated into an Aspen Plus model. The flowsheet of the model is available in Figure 3.4. To ease their distinction, streams are colour-coded:

- The red streams represent the flue gas (FG).
- The cyan streams form the solvent loop, circling between the absorber and the stripper. In their designation, 'R' indicates that it is the rich solution and 'L' stands for the lean solution.
- The blue streams are near-pure liquid water streams.
- The pink streams are near-pure CO_2 streams.
- The purple stream is the MEA make-up (MU) stream.

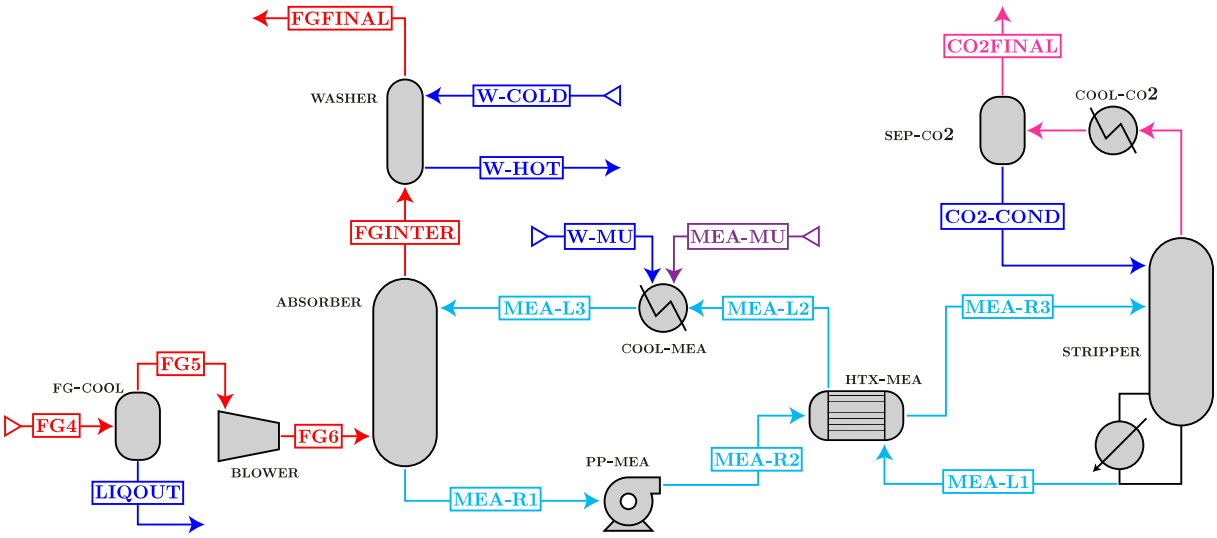

Figure 3.4: Flowsheet of the CO_2 capture unit

The flue gas, starting from the bottom left stream (FG3), is cooled down in the precooler (COOL-FG block). This block is a two-product flash separator that represents the direct contact cooler (DCC) that reduces the temperature of the flue gas down to 40 °C and recuperates the condensate at the bottom (LIQOUT). The remaining gaseous phase goes through the block BLOWER. Its operating parameters are displayed in Table 3.13.

Isentropic efficiency (%)	85
Mechanical efficiency (%)	95
Pressure increase (kPa)	1

Table 3.13: Blower parameters

Efficiency (%)	55
Pressure increase (kPa)	250

Table 3.14: Pump parameters

The blown flue gas enters the block ABSORBER by the bottom and exits at the top. More details about the absorber are provided in the following sections. The solvent injection point is located at the top (MEA-L3). Although it is physically located in the same tower, the washing section of the absorber is modelled as a standalone column (WASHER) in order to isolate the water loop, effectively decoupling it from the rest of the model and helping the convergence process. This loop is supplied by W-COLD and the liquid output is W-HOT.

The loaded solvent exits the absorber through the stream MEA-R1. The PP-MEA block models the pump that brings it to the higher pressure level (of which the value is discussed later). Its parameters are shown in Table 3.14.

The HTX-MEA represents the lean-rich heat exchanger. It is modelled after a counter-current shortcut exchanger, meaning that the calculations are limited to heat and mass balances, regardless of the real geometry. It is also discussed later.

The STRIPPER block includes its own washing section, so the rich solvent stream does not enter the block at the very top. The block model also includes the reboiler, from the bottom of which the regenerated solvent is transmitted to the block HTX-MEA. The lean solvent then goes through the heater COOL-MEA to be cooled down to 40 °C before finally closing the loop by entering the absorber. At the top of the stripper, the gaseous phase is entrained into the condensing section, which includes a heater (COOL-CO2) to cool the product down to 40 °C. Then, the flash separator (SEP-CO2) recuperates the condensed water and recirculates it at the top of the washing section of the stripper.

At the vapour outlet of SEP-CO2, dedicated models for the compression and purification steps could be added. As the fate of the captured CO_2 is still undefined, this equipment chain is not integrated into the model.

The tear streams mentioned in the previous section are the following: MEA-L3, MEA-R3 and CO2-LIQ. Initiating those with educated guesses allows for the convergence of the solver. They are chosen as tear streams because they are the inputs to the two columns, effectively forcing the algorithm to start by solving these critical structures.

In addition, a *Design Spec* is defined to reach the targeted capture rate of 90 %. The manipulated variable is the reboiler heat duty. In practice, during the flowsheet resolution, the captured CO_2 flow rate is measured (in the stream CO2FINAL) and compared with the CO_2 flow rate at the inlet of the capture unit (in the stream FG5). If the capture rate is less than 90 %, the reboiler heat duty is increased to regenerate more solvent and vice versa.

At last, two balances are also defined on the solvent loop (*i.e.* all blocks but the precooler,

the blower and the washer) according to the following equation:

$$\dot{m}_{\text{FG6}} + \dot{m}_{\text{MU}} = \dot{m}_{\text{FGINTER}} + \dot{m}_{\text{CO2FINAL}} \tag{3.7}$$

This mass balance is not applied to whole mixed streams but to specific components within the streams:

- MEA: the flow rate in the MEA-MU stream is calculated to match the degradation and emission rates of MEA.
- H_2O: the water balance is the most critical control loop of the simulation. Water can exit the system within the flue gas or within the CO_2 product stream. Neglecting this balance can provoke challenging convergence issues.

3.4.5 Assumptions and design choices

The complexity of real-life processes can be overwhelming and approximations are inevitable in simulations. However, cutting corners ought to be restrained and assumptions must be justified.

Moreover, designing a plant is about making decisions and setting values for a multitude of parameters. Most of them can be chosen so as to minimize some cost function (usually the price or the energy consumption). Considering the time limitation inherent to a master's thesis, a complete optimisation of the process is not feasible. Some design choices are made upfront.

In this section, the assumptions and design choices are motivated.

3.4.5.1 Steady-state operation

As the biomass boiler operates continuously at nominal capacity, the flue gas stream is expected to be of constant composition. Steady-state simulations are therefore sufficient to determine the optimal operating conditions.

Dynamic simulations are particularly relevant to study the effect of perturbations or expected changes in operating conditions. It is inevitable if one wants to assess the flexibility of the capture unit. However, these transitory regimes are out of the scope of this master's thesis and the simulations are limited to steady state.

3.4.5.2 Neglected degradation

The solvent degradation is also out of the scope of this work and is thus neglected. This phenomenon must nonetheless be kept in mind when designing the plant more precisely as it imposes the implementation of a make-up stream to compensate for the losses due to degradation.

3.4.5.3 Neglected losses

In accordance with the overall precision of the simulation, heat losses to the environment are neglected, and so are pressure drops in piping.

3.4.5.4 Stripper pressure

Desorption is more efficient at high temperature [Duan et al. 2012; Léonard 2013]. Moreover, operation at a higher pressure level results in a lower reboiler duty as the reaction heat of MEA stripping is inversely proportional to the pressure. However, raising the pressure provokes an increase in pumping work. It is therefore a trade-off between the reboiler heat duty and the electricity consumption of the unit, as decreasing the former leads to an increase in the latter. In addition, higher pressure levels come with increased safety issues.

In this work, the stripper pressure is set at 2 bar. This choice is justified by the large availability of on-site electricity but remains reasonable with respect to safety.

3.4.5.5 Minimum approach temperature in the lean-rich heat exchanger

During the operation of the capture unit, the rich solvent must be heated to the stripper temperature while the lean solvent must be cooled down to the absorber temperature. The lean-rich heat exchanger transfers heat from one fluid to the other.

The minimum approach temperature is a design choice that reflects the size of the heat exchanger. It is the minimum temperature difference between the hot fluid and the cold one. The smaller the approach temperature, the larger the heat exchanger needs to be, even going towards infinity if the approach equals zero.

In this model, it is set at 5 K, which is an ambitious value. A larger temperature approach would ensure a smaller heat exchanger but it would increase the reboiler heat duty and the lean solvent cooling duty as the less efficient heat transfer has to be compensated. This discussion is extended in Chapter 4.

3.4.5.6 Calculation mode

In Aspen Plus, there are two available calculation modes for columns: equilibrium and rate-based.

Equilibrium models assume that the gas phase reaches thermodynamic equilibrium with the liquid phase at each stage. The corresponding set of equations are the MESH equations, which include the Material balance equations, the Equilibrium equations, the mole fractions Summation equations and the Heat balance equations. [Perry and Green 2008]

This idealistic approach is chosen as it is easier to converge with respect to rate-based models, which integrate mass transfer limitations amongst others in its rigorous approach. The implications of this choice are discussed in Chapter 4.

3.4.5.7 Number of equilibrium stages

It is also necessary to select an appropriate number of stages so as to reach a satisfying CO_2 absorption. Indeed, a larger number of stages ensures a better separation, at the expense of an increased computational load and an increased column height if the pilot is sized directly from the equilibrium model.

Regarding the absorber, the inherited model used 4 equilibrium stages. To assess whether this number is sufficient for the present case study or not, several simulations are conducted and the rich loading is monitored, as it is an image of the separation efficiency.

As the operating conditions of the solvent entering the absorber are unknown at this point, several lean loadings are tested and the flow rate is controlled by a *Design Spec* to obtain a capture rate of 90 %. Figure 3.5 illustrates the results.

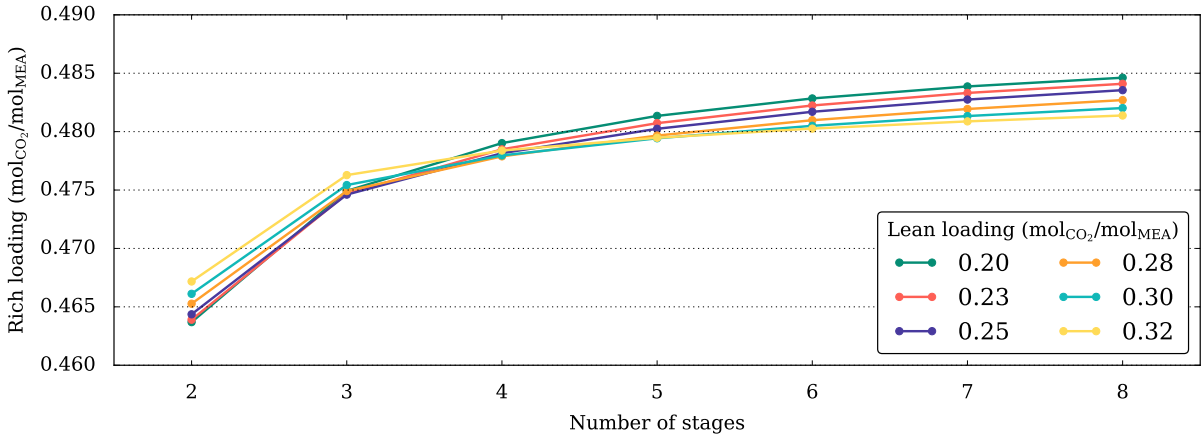

Figure 3.5: Rich loading as a function of the number of equilibrium stages for different lean loadings

In addition to the expected increase in separation efficiency, what emerges from this figure is the decreasing marginal efficiency gain as the number of stages increases. Because of this, and in conjunction with the increasing convergence issues, it is preferable to set the number of equilibrium stages in the absorber at 6.

In the parent model, the stripper was made up of 8 equilibrium stages (including one reboiler stage and 2 stages for the washing section). It appears that, with the exception of low values, the number of stripper stages has limited influence on the lean loading and on the reboiler heat duty. Indeed, both figures stabilise from 8 stages onwards. This discussion is supported by Figure A2, which is available in the Appendix. In this work, the number of equilibrium stages is therefore set to 10, which is within the stable range.

3.4.5.8 Solvent operating conditions

The final design choice is the operating point of the solvent, for which two choices are made upfront:

- the solvent concentration: 30 wt-% of MEA
- the solvent temperature at the inlet of the absorber: 40 °C

What remains to determine is the lean loading and the flow rate. As both the solvent concentration and the capture rate are set, these two parameters are actually equivalent: for a given lean loading, there is only one flow rate that leads to the targeted capture rate. However, there exist a plethora of valid lean loading/flow rate combinations. To choose the optimal pair, it is interesting to find the one that minimises the reboiler heat duty.

In fact, a minimum is expected because the supplied heat contributes to three processes that vary with the flow rate in opposite directions [Léonard 2013] as reported in Table 3.15. The reboiler heat duty can be expressed as a function of these contributions (Equation (3.8)). In this equation, $\dot{Q}_{\text{reboiler}}$ is the reboiler heat duty (kW), ΔH_{CO_2} is the desorption heat of CO_2 ($\text{kJ}\,\text{kg}^{-1}$), $c_{p,i}$ indicates a specific heat capacity ($\text{kJ}\,\text{kg}^{-1}\,\text{K}^{-1}$), the temperatures T_i are given in K, $H_{H_2O,vap}$ is the heat of vaporisation of water ($\text{kJ}\,\text{kg}^{-1}$) and $\dot{n}$ is the notation for a molar flow rate ($\text{mol}\,\text{s}^{-1}$) by opposition to the mass flow rate $\dot{m}$ ($\text{kg}\,\text{s}^{-1}$). [K. Li et al. 2016]

$$\dot{Q}_{\text{reboiler}} = \underbrace{\dot{n}_{CO_2}\,\Delta H_{CO_2}}_{\text{Heat of desorption}} + \underbrace{\dot{m}_{\text{solvent}}\,c_{p,\text{solvent}}\,(T_{in} - T_{out})}_{\text{Sensible heat}} + \underbrace{\dot{n}_{H_2O,vap}\,H_{H_2O,vap}}_{\text{Heat of vaporisation}} \tag{3.8}$$

Contribution	Evolution with the solvent flow rate
Heat of desorption	Independent
Sensible heat	Increases with the flow rate
Heat of vaporisation	Decreases with the flow rate

Table 3.15: Contributions to the reboiler heat duty

The optimisation process is done by running numerous simulations with different lean loadings. The capture rate is kept at 90% thanks to a *Design Spec* that adapts the solvent flow rate. The results of this parametric study are depicted in Figure 3.6. An optimal lean loading of $0.31\,\text{mol}_{CO_2}/\text{mol}_{MEA}$ can be identified. It corresponds to a mass flow rate of 7.75 kg/s. Similar values are reported in literature: $0.30\,\text{mol}_{CO_2}/\text{mol}_{MEA}$ [Duan et al. 2012] and $0.32\,\text{mol}_{CO_2}/\text{mol}_{MEA}$ [Abu Zahra 2009; Jana and De 2014; Luo et al. 2015].

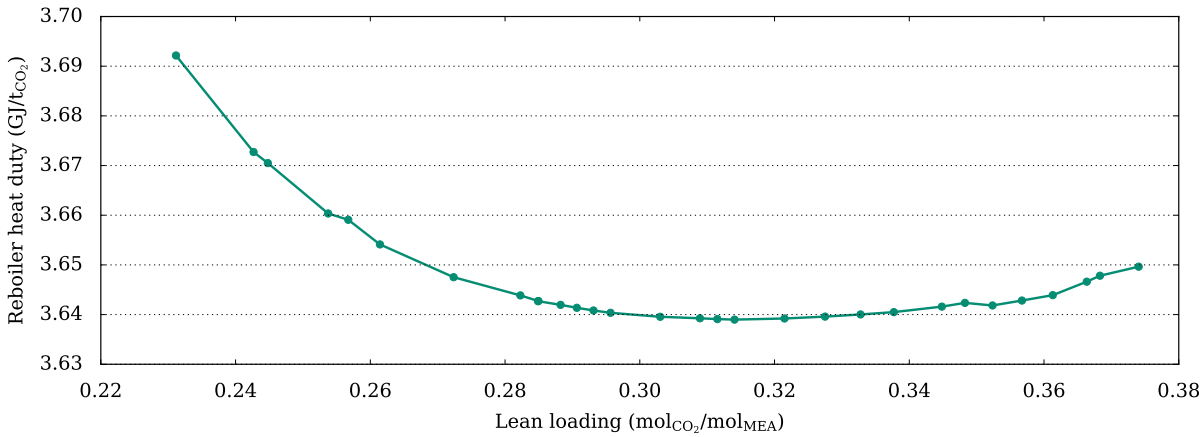

Figure 3.6: Reboiler heat duty as a function of the lean solvent loading

Although the model was simulated using a simplified calculation approach for the columns, the identified optimal operating point is likely to be almost identical in reality. Indeed, [Léonard 2013] compared the two methods and pointed out the common minimum.

3.4.6 Results

The model, described in Section 3.4.4, together with the parameters defined in Section 3.4.5, is simulated to evaluate the performance of the capture unit. The results are reported in Table 3.16.

Captured CO_2 (kg/h)	1000.11
CO_2 purity (wt-%)	98.28
Reboiler heat duty (kW)	1011.12
Reboiler heat duty (GJ/t_{CO_2})	3.6396
Capture rate (%)	90.02
Solvent flow rate (kg/s)	7.75
MEA concentration (wt-%)	29.99
Lean loading (mol_{CO_2}/mol_{MEA})	0.3145
Rich loading (mol_{CO_2}/mol_{MEA})	0.4803
Absorber stages	6
Stripper stages	10
Absorber pressure (bar)	1.01325
Stripper pressure (bar)	2

Table 3.16: Results of the capture unit model

As expected, the unit is able to capture $1\,t_{CO_2}/h$, which is the targeted amount. The reboiler heat duty reaches $3.6396\,GJ/t_{CO_2}$.

3.5 Submodel 3: thermodynamic cycle

The Rankine cycle is the last submodel to complete the modelling of the facility. The purpose of this submodel is to assess the penalty of the carbon capture unit on the existing CHP plant. For this reason, it is not relevant to strive for a perfectly-fitting model.

The cycle is a closed loop and does not receive any material stream as an input. However, it receives a heat stream from the biomass furnace submodel. It represents the thermal transfer between the hot flue gas and the water in the Rankine cycle.

3.5.1 Thermodynamic properties model

As steam is the only component in this model, the selected property model is the *IAPWS-95 Formulation for Thermodynamic Properties of Water and Steam* (IAPWS-95). It is currently the best available property model for water and steam. [AspenTech 2019]

It is important to note that the IAPWS-95 model can only handle pure water. For this reason, the set of equilibrium equations defined for the model of the CO_2 capture unit (Table 3.9) must be dismissed. Indeed, it includes water hydrolysis and the ions (*i.e.* OH^- and H_3O^+) can provoke solver issues.

3.5.2 Modelling

The flowsheet of the Rankine cycle submodel is depicted in Figure 3.7. As the cycle was thoroughly described in Chapter 1, this section only addresses the chosen parameters and the underlying assumptions.

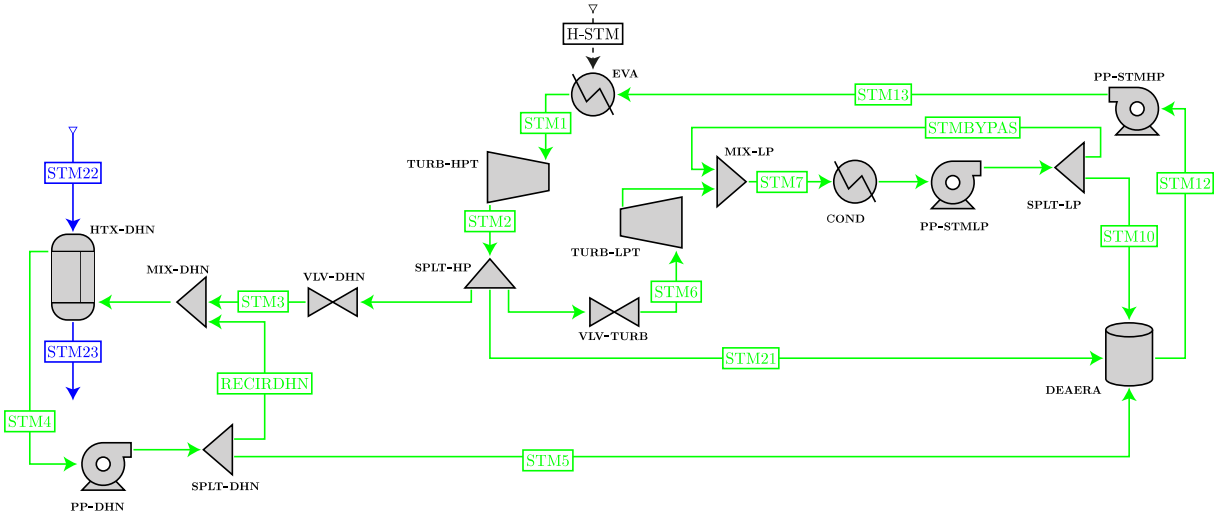

Figure 3.7: Flowsheet of the Rankine cycle

The EES model developed by P. Dewallef and K. Sartor helped identify many equipment parameters (partially compiled in Tables 3.17 and 3.18). These results are used directly in the Aspen Plus block models.

As explained before, the heat exchanger network is simplified into a single heat exchanger (EVA-STM) that receives the heat stream (H-STM) from the biomass furnace. This heat transfer is the interface between the two submodels.

The two turbines (TURB-HPT and TURB-LPT) are modelled after isentropic turbines with the parameters indicated in Table 3.17. Valves and turbines can presumably be seen as choked nozzles. The mass flow rate, the pressure and the temperature can thus be connected by the following expression:

$$p = \frac{\dot{m}\sqrt{T}}{K} \tag{3.9}$$

with p in kPa, T in K, $\dot{m}$ in kg/h and K in $\mathrm{kg\,h^{-1}\,K^{0.5}\,kPa^{-1}}$. The value of K was identified in the parent model (501,7 for the DHN regulation valve and 532,7 for the LPT).

Regarding the DHN heat exchanger (HTX-DHN), two additional assumptions are made. First, the return water (STM22) is set at 120 °C and 1200 kPa. And second, the condensing steam is assumed to reach liquid saturation at the outlet of the heat exchanger.

As a final hypothesis, the cycle is perfectly sealed and steam losses can therefore be neglected. Consequently, no water make-up stream is modelled and that suppresses the consideration for dissolved gases. For this reason, the deaerator can be seen as a simple tank collecting the condensed streams in addition to the extracted steam from the intermediate pressure level (STM21). To specify the downstream conditions (115 °C and 200 kPa), it is

convenient to use the HEATER block. However, as the tank is not really a heat exchanger, it is important to ensure that no external heat duty is injected into the block model. For that purpose, the flow rate of the extracted steam is manipulated by a *Design Spec*. The necessary energy to reach the specified downstream state is therefore entirely supplied by the extracted steam.

	HPT	LPT
Isentropic efficiency (%)	69.42	70
Mechanical efficiency (%)	90	90
Discharge pressure (kPa)	550	8.2

Table 3.17: Turbines parameters

	PP-DHN	PP-STMLP	PP-STMHP
Efficiency (%)	52,78	40,22	59,12
Discharge pressure (kPa)	890	847	7641

Table 3.18: Pumps parameters

3.5.3 Validation

To validate the Aspen Plus model, simulation results from the EES model can be used as a comparison basis. Table 3.19 contrasts values obtained from both simulations with the same amount of heat supplied from the boiler.

One of the compared metrics is the cogeneration efficiency. It is defined as the sum of the thermal efficiency and the electrical efficiency:

$$\eta_{chp} = \eta_{el} + \eta_{th} = \frac{\dot{Q}_{DHN}}{\dot{m}_{comb} LHV} + \frac{\dot{W}_{el,net}}{\dot{m}_{comb} LHV} \tag{3.10}$$

Although the fan is included in the biomass furnace submodel, it is important to note that its electricity consumption should be taken into account to calculate the electrical efficiency. This is done by reporting directly the value obtained in the aforementioned submodel.

A severe bias must be reported: because the EES model served as a basis for the present model, validating it only ensures that subsequent calculations were done properly.

To further validate the model, the results of the Aspen Plus model are challenged by the following linear regression, which is based on experimental results:

$$\dot{W}_{el,net} = 2213.19 - 0.17547\ \dot{Q}_{DHN} \tag{3.11}$$

with $\dot{Q}_{DHN}$ the thermal power transferred to the DHN (from $0\,\mathrm{kW_{th}}$ to $7000\,\mathrm{kW_{th}}$) and $\dot{W}_{el,net}$ the net electricity generation (in $\mathrm{kW_e}$).

	EES model	Aspen Model
Gross power (kW)	1429.8	1403.33
Auxiliary power (kW)	413.3	354.97
Net power (kW)	1015.4	1048.35
Power to DHN (kW)	7000	6885.52
η_{th} (%)	59.83	58.85
η_{el} (%)	8.68	8.96
η_{chp} (%)	68.51	67.81

Table 3.19: Validation of the thermodynamic cycle

This comparison is plotted in Figure 3.8. The Aspen Plus model appears to fit satisfyingly the experimental results and its forthcoming utilisation as an assessment tool for the energy penalty is justified. However, it is important to keep in mind that it remains an approximation and is certainly not sufficient to study the Rankine cycle in depth.

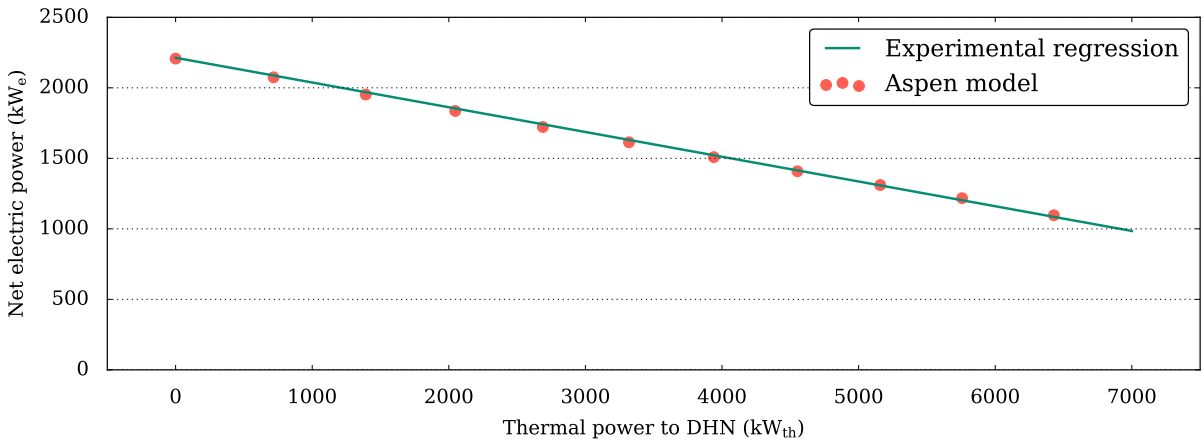

Figure 3.8: Comparison between the experimental correlation and the simulation results

3.6 Combined model

In the previous sections, three submodels have been developed for each of the three main systems that constitute the studied facility. As they have been validated, they can be interconnected according to the modelling approach described in Figure 3.1.

Figure 3.9 illustrates the complete flowsheet. This combined model can also be used to gauge the behaviour of the CO_2 capture unit given a change in operating conditions (*e.g.* a different biomass composition, a change in ambient conditions and so on).

As a concluding evaluation, it is relevant to calculate how much CO_2 is effectively captured. The combined model predicts the emission of 3134.63 kg_{CO_2}/h and the capture of 1000.08 kg_{CO_2}/h. The reduction of emissions therefore amounts to 24%, which is in line with the value calculated at the end of Section 3.3.

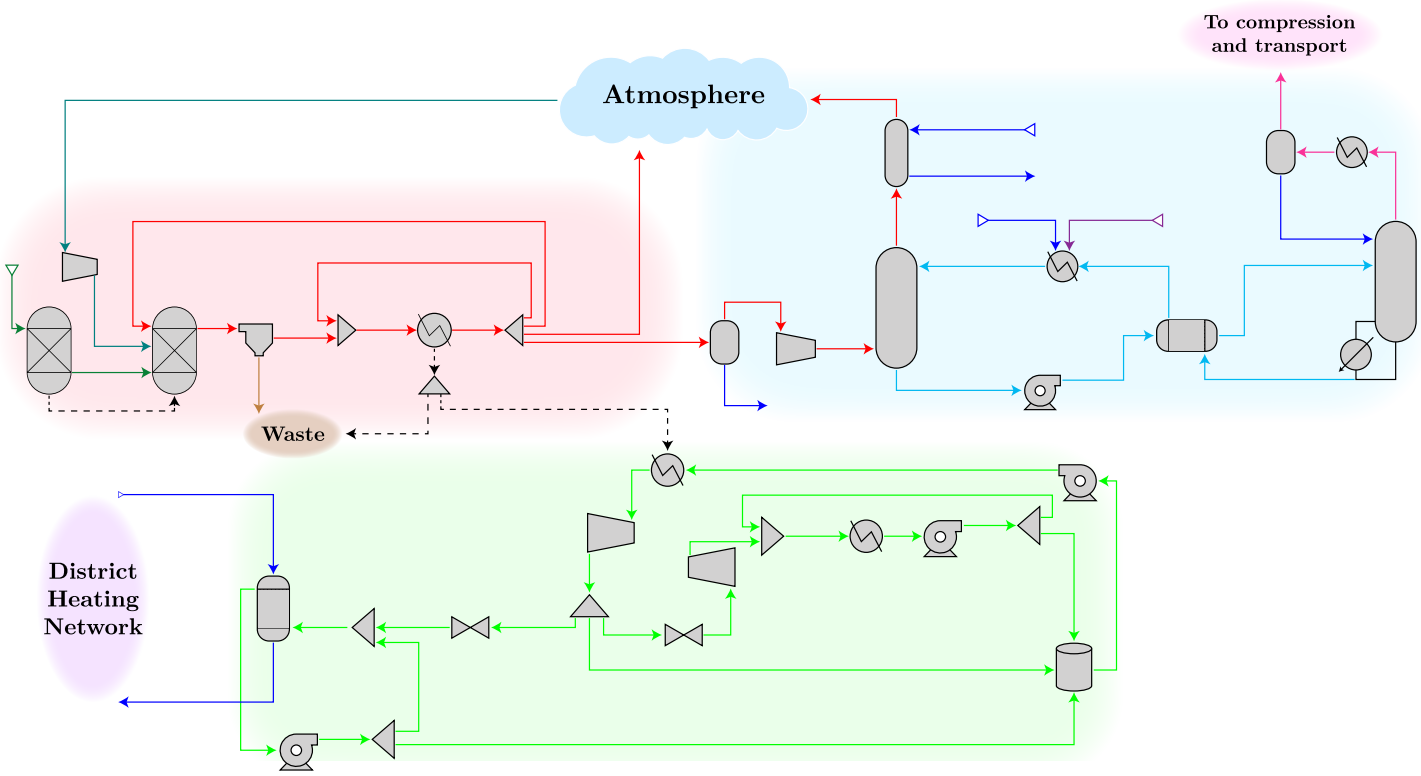

Figure 3.9: Flowsheet of the combined model

CHAPTER 4

Sizing of the pilot

In the previous chapter (Chapter 3), the desired performance of the studied capture unit was translated into operating conditions by means of simulations. In this chapter, the design of the facility is brought to its next step: the equipment sizing. It allows to bridge the gap between simulations and reality and it paves the way to a preliminary economic evaluation (Chapter 6).

4.1 Methodology

The accent is put on the larger pieces of equipment, *i.e.* the two columns and the lean-rich heat exchanger. Their complexity and their size motivate the particular attention that they receive. As several possible configurations exist for each of them, a complete design optimisation could be performed but it is not within the scope of this master's thesis. Instead, realistic assumptions are made. The other pieces of equipment are not neglected and are also roughly sized.

4.2 Sizing of the columns

4.2.1 The case for rate-based modelling

The most straightforward approach to column sizing is to apply the Height Equivalent to a Theoretical Plate (HETP) to the simulation results obtained in Chapter 3. The HETP is the required column length to reach equilibrium between the liquid and the gas phases [Perry and Green 2008]. In Chapter 3, the number of equilibrium stages was chosen so as to reach a satisfying separation. The total height of a column could therefore be calculated by multiplying this number of stages by an expected HETP value.

However, this approach deserves to be questioned. As equilibrium stages are an idealised representation of the separation process, the calculated column height could be an underestimation of the required tower dimension.

A deeper understanding of the functioning of a column is required. In Chapter 2, it was explained that, while flowing downwards, the liquid solvent preferentially reacts with CO_2, which flows upwards within the vapour phase. This is the principle of chemical absorption (also known as reactive absorption): a chemical reaction between the liquid phase and the target substance dictates the absorption process. In such processes, mass transport kinetics are usually the driving force of reactive absorption. [Yildirim et al. 2012]

Equilibrium models neglect the heat and mass transfer limitations. This approximation makes them physically incompatible with reality. As rate-based models include actual rates of mass transfer, heat transfer and chemical reactions directly, it stands out that their use is prefered. Authors have highlighted the superiority of the rate-based approach over the equilibrium one, in particular for CO_2 absorption [Ghaemi et al. 2021; Léonard 2013; Yildirim et al. 2012; Zhang and C.-C. Chen 2013; Zhang, H. Chen, et al. 2009].

The equilibrium model developed in Chapter 3 must therefore be converted to a rate-based model, *i.e.* a model in which the columns are switched to rate-based calculations.

Aspen Plus uses its own rate-based model, named *RateSep*, which is available in the RADFRAC block model. It assumes that the absorption occurs at the gas-liquid interface and uses the two-film theory in addition to the Maxwell-Stefan equations to calculate the mass transfer rates. [Zhang, H. Chen, et al. 2009]

This calculation mode requires the definition of the column internals, of which the selection belongs to the sizing process and is addressed in the next section.

4.2.2 Sizing procedure

As absorption occurs by mass transfer coupled with chemical reactions between the liquid phase and the vapour phase, intimate contact between the phases favours the process. Columns are filled with specific internal structures with extensive contact areas to promote absorption. Available internals can be broadly divided into two categories:

- trays: a stack of discrete perforated plates, oriented horizontally, that retain a liquid volume at each stage while the gas phase rises through cuts in the plate floor. Tray internals come in three types: sieve trays, which are simple perforated plates, fixed valve trays, which have covers over the perforations and an elevated section of the floor, and moving valve trays, for which the covers are displaced proportionally to the rising gas phase velocity.
- packing: a continuous structure filling the entire height of the column. The subcategories are:
  - random packing: packing elements, such as rings or saddles, filling randomly the tower.
  - structured packing: material shaped in specifically-designed, regular patterns.

Figure 4.1 illustrates the different types of internals. Each one of them has its own strengths. For instance, packed towers offer lower pressure drops and are suitable for corrosive applications, with random packing being available at low cost and structured

packing operating at a higher efficiency. Tray towers offer more residence time for slow processes. The selection process of the best-suited column internal is not discussed in this work. [Perry and Green 2008]

(a) (b) (c)

Figure 4.1: Examples of trays (a), random packing (b) and structured packing (c). All images are from the Sulzer website [Sulzer 2020].

Aspen Plus includes extensive data from different manufacturers so real column internals can be simulated directly in rate-based calculation mode. In this work, it has been decided to select the structured packing type *Mellapak 250Y*, from the manufacturer Sulzer [Sulzer 2020]. It is one of the most common packing types used for absorption [Choi et al. 2019; B.-H. Li et al. 2016; Zhang and C.-C. Chen 2013]. It is also well documented in literature as a high-performance packing type [Lassauce et al. 2014]. Its contact area amounts to $250\,\mathrm{m}^2/\mathrm{m}^3$, hence its name.

To determine its size, the absorber is isolated in the Aspen Plus flowsheet (Figure 4.2). The flue gas composition is constant and the solvent conditions are assumed optimised (Chapter 3). Because all inputs are known and constant, isolating the absorber appears to be a valid approach.

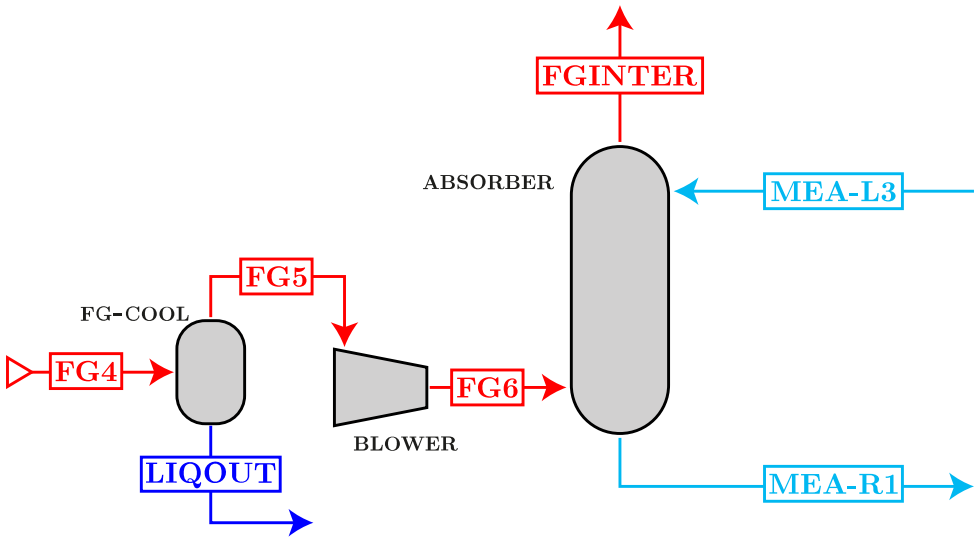

Figure 4.2: Flowsheet of the isolated absorber model

To run rate-based simulations, the dimensions of the column (*i.e.* the height and the diameter) have to be specified in addition to the packing type. As sizing the column is the objective of this procedure, several runs are performed and the results are analysed in order to determine if they meet the targeted performance. The corresponding metric is the capture rate, which should reach 90%. In other words, from the standalone absorber model with known input streams, the dimensions of the column must be calculated so as to capture 90% of the inlet CO_2.

A first estimation of the dimensions can be obtained from the results of the equilibrium model in conjunction with data from the manufacturer. Indeed, as explained in Section 4.2.1, the height of the column is proportional to the number of equilibrium stages. The proportionality constant is the aforementioned HETP, which is given in the product datasheet as a function of the F-factor (Figure 4.3, solid curves).

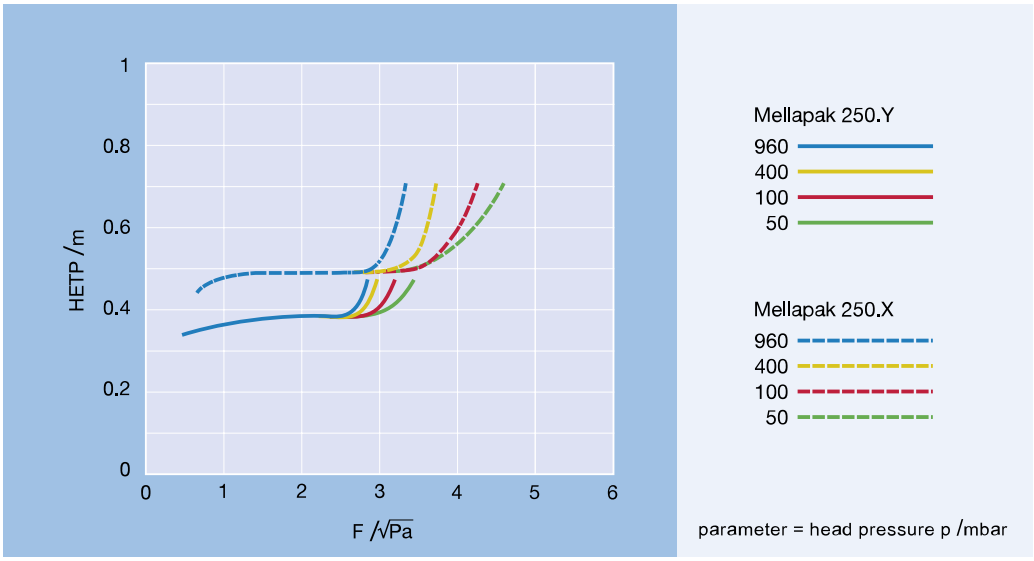

Figure 4.3: HETP as a function of the F-factor for Mellapak 250 series [Sulzer 2020]

The F-factor is the square root of the gas density ρ_{vapour} (kg/m^3) multiplied by its superficial velocity $V_{S,vapour}$ (m/s) [Lassauce et al. 2014; Zhang and C.-C. Chen 2013]. It is therefore expressed in Pa$^{0.5}$:

$$F = \sqrt{\rho_{vapour}} \cdot V_{S,vapour} \tag{4.1}$$

Developing the superficial velocity with the volume flow rate Q and the column cross-section A, the equation can be rewritten to include the column diameter D:

$$F = \sqrt{\rho_{vapour}} \cdot \frac{Q_{vapour}}{A_{column}} = \sqrt{\rho_{vapour}} \cdot \frac{\dot{m}_{vapour}}{\rho_{vapour}} \cdot \frac{1}{\frac{\pi}{4} D_{column}^2} \tag{4.2}$$

The gas density and mass flow rate are deduced from the hydraulic results of the equilibrium simulation (Table 4.1) and are averaged over all stages.

Using these results, the F-factor is plotted against the column diameter in Figure 4.4. As the HETP is only given for a limited range of F-factors (0.5 Pa$^{0.5}$ to 3 Pa$^{0.5}$, Figure 4.3), the possible diameter is restricted to these bounds, *i.e.* it can only vary from 0.8 m to 2 m.

Stage	Mass flow rate (kg/s)	Density (kg/m^3)
1	1,7131	0,97932
2	1,7887	1,0046
3	1,7803	1,0282
4	1,7564	1,0548
5	1,7253	1,0906
6	1,6816	1,1551
Average	1,7409	1,0521

Table 4.1: Hydraulic results from the equilibrium simulation, 1 being the top stage

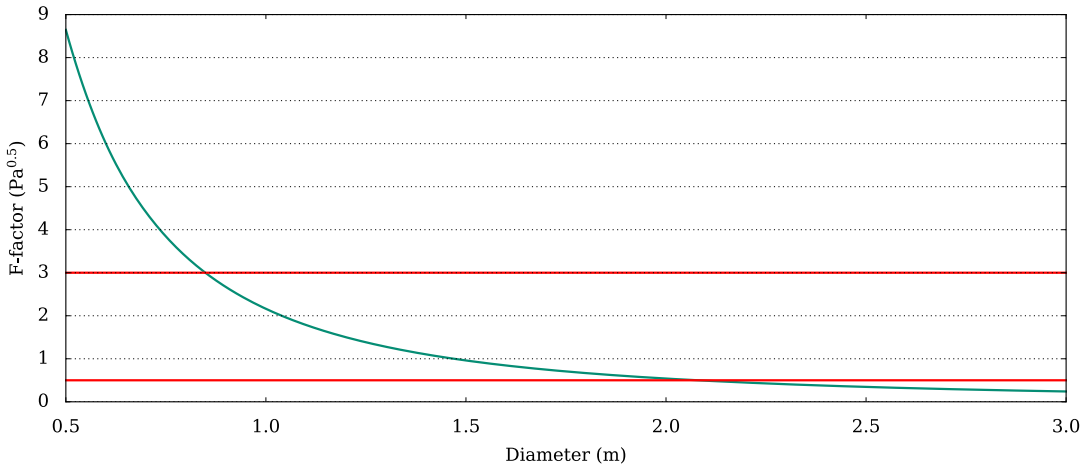

Figure 4.4: F-factor as a function of the column diameter (Equation (4.2))

As a first guess, the diameter is set to 1 m, which is equivalent to setting the F-factor to 2.1 $Pa^{0.5}$. The corresponding HETP is 0.38 m. From the observation of the packing datasheet (Figure 4.3), it emerges that the HETP is fairly constant around the chosen value. Another diameter would therefore yield a similar HETP value.

Having identified the HETP for the selected packing and remembering that 6 equilibrium stages are sufficient for the targeted performance (see Section 3.4.5), it is possible to calculate the first estimation of the absorber height: 2.28 m.

Running the isolated absorber model with rate-based calculations and this guessed height yields a mediocre, off-target capture rate: 79.70%. As expected, the performance of the column falls short of the objective when the equilibrium model is naively switched to rate-based calculation mode. This observation confirms the inaccuracy of equilibrium models.

Therefore, it is crucial to increase the height of the column until a satisfying performance (*i.e.* a 90% capture rate) is attained.

To sustain the comparison with the equilibrium approach, it is relevant to increase the height by small increments of 0.38 m, which is the HETP marketed by the manufacturer.

To do so, the packed height per stage is set to the aforementioned HETP value and the number of stages is gradually increased until the desired capture rate is reached. This is illustrated in Figure 4.5.

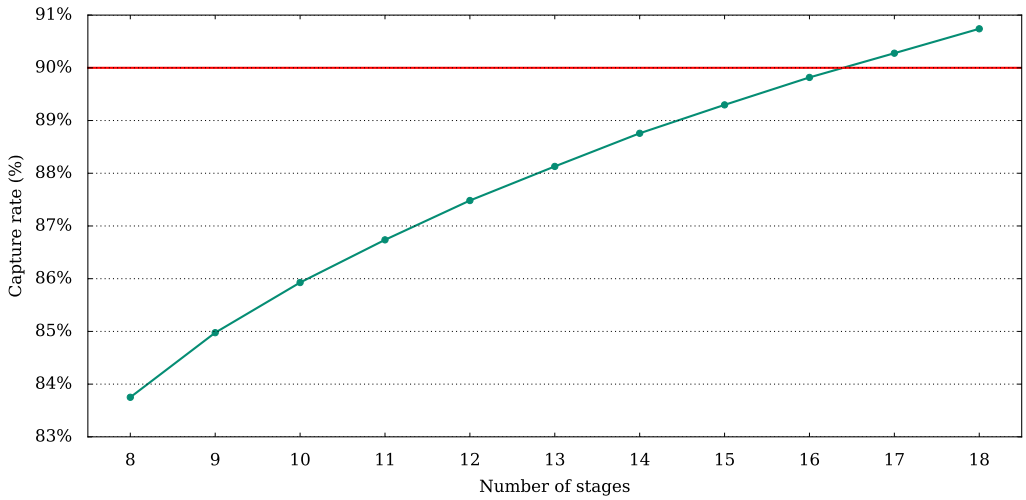

Figure 4.5: Capture rate as a function of the number of stages in the rate-based simulation

As it allows the capture rate to reach 90 %, the number of stages is set to 17. The corresponding column height amounts to 6.46 m. When increasing the number of stages, the diameter must be slightly increased to 1.1 m in order to keep the flooding under 80 % of the capacity, which is a typical design choice [Perry and Green 2008].

In rate-based calculation mode, stages do not correspond to equilibrium stages. Instead, they represent discretisation points within the numerical resolution of the column. Usually, a sufficient number of stages is set to enable a realistic numerical resolution and the height is specified independently to reach the desired performance of the column. However, in the chosen approach, the packing height *per stage* is specified so a relationship is established between the number of stages and the height. The underlying assumption is that the number of discretisation points (*i.e.* the number of stages) is always sufficient for a realistic resolution of the column. To support this assumption, the sizing of the column can be performed again using the conventional method. For that purpose, the isolated absorber is simulated with 20 stages (which is a conventional number of discretisation points for pilot plants [Zhang and C.-C. Chen 2013]) and the height is varied independently. It is illustrated in Figure A3, which can be found in the Appendix. The targeted capture rate is also reached for a similar height and the approach is therefore valid.

The developed approach enables to reflect on the marketed HETP value: using realistic, rate-based calculations, 17 equilibrium stages are necessary while only 6 are necessary with equilibrium equations. Thus, the HETP value seems optimistic and should be used with care.

The washing section of the absorber is modelled separately in Aspen Plus. As its functioning does not involve chemical absorption, sticking to the equilibrium model is assumed sufficient. An additional height of 2 m is estimated on top of the previously-sized absorber main body. A summary is provided in Table 4.2.

Regarding the stripper, the same column internal is selected (Mellapak 250Y). To size it, the entire flowsheet must be run in rate-based mode. Indeed, the two columns form a loop and interactions could be neglected by isolating the submodels.

The diameter is chosen based on the available F-factors (Figure 4.3) and the packing height per stage is also set at 0.38 m. The initial number of stages is sufficient to reach a satisfying rich loading and it is kept as such. The integrated washer tolerates a narrower diameter because of the difference in liquid flow rates between the two sections. The results are presented in Table 4.2.

	Absorber		Stripper	
	Main body	Washer	Main body	Washer
Packing type	Mellapak 250Y		Mellapak 250Y	
Diameter (m)	1.1	1.1	0.6	0.4
Height (m)	6.46	2	2.66	0.76

Table 4.2: Dimensions of the columns

To validate the results, it is relevant to reflect on the assumed diameters. Indeed, they are the basis of the subsequent calculations and a guess was chosen for each column at the beginning of the procedure.

The rate-based solver in Aspen Plus recalculates the optimal diameter of each tower, based on the height and on the user-defined flooding (*i.e.* 80%). The calculated values are put in perspective with respect to the assumed values in Table 4.3. For both columns, the chosen value is close to the recalculated one. This observation supports the results.

	Absorber	Stripper	
		Main body	Washer
Assumed diameter (m)	1.1000	0.6000	0.4000
Calculated diameter (m)	1.0083	0,5336	0,3398

Table 4.3: Comparison of assumed and calculated diameters

4.2.3 Results of the rate-based simulation

The simulation results presented in Chapter 3 ought to be updated as the simulation model was upgraded to a rate-based model. They are compiled in Table 4.4.

It emerges that the reboiler heat duty increases but this observation is logical. Indeed, the mass transfer limitations deteriorate the efficiency of the absorption and stripping processes. To compensate for this phenomenon, more heat must be supplied to the reboiler.

	Equilibrium model	Rate-based model
Captured CO_2 (kg/h)	1000.11	1000.03
CO_2 purity (wt-%)	98.28	98.28
Reboiler heat duty (kW)	1011.12	1020.30
Reboiler heat duty (GJ/t_{CO_2})	3.6396	3,6730
Capture rate (%)	90.02	90.00
Solvent flow rate (kg/s)	7.75	7.75
MEA concentration (wt-%)	29.99	30.02
Lean loading (mol_{CO_2}/mol_{MEA})	0.3145	0.3154
Rich loading (mol_{CO_2}/mol_{MEA})	0.4803	0.4812
Absorber stages	6	17
Stripper stages	10	10
Absorber pressure (bar)	1.01325	1.01325
Stripper pressure (bar)	2	2

Table 4.4: Summary of the results from the rate-based model

The methodology applied for the sizing of the columns assumed that the optimal solvent operating conditions identified in Chapter 3 are equally valid for the rate-based model. To validate this assumption, a similar parametric optimisation can be performed with the upgraded model. As can be seen in Figure 4.6, the minimum reboiler duty is also attained for a lean loading of 0.31 mol_{CO_2}/mol_{MEA}, effectively validating the assumption.

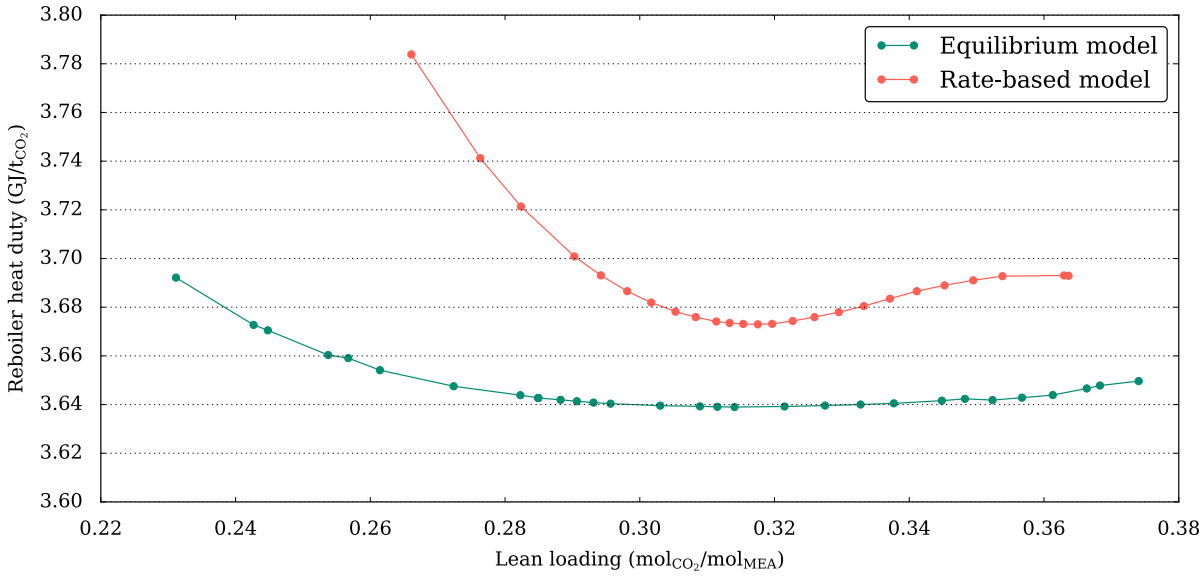

Figure 4.6: Comparison between the equilibrium model and the rate-based model regarding the optimal solvent lean loading

The simulated reboiler heat duty amounts to 3.6730 GJ/t_{CO_2}. This result appears to be coherent. Indeed, it is possible to compare it to the experimental value measured at the Esbjerg pilot plant. During the operation of this carbon capture facility described in Chapter 2, the reboiler heat duty was equal to 3.7 GJ/t_{CO_2}.

4.3 Sizing of the lean-rich heat exchanger

Sizing the major heat exchanger is done with Aspen Exchanger Rating and Design (Aspen EDR). Based on the flowsheet results and on user-defined constraints, the software evaluates numerous configurations and selects the most economical possibility.

The heat exchanger is assumed to be a counter-current shell and tubes heat exchanger. These heat exchangers are often divided into categories defined by the Tubular Exchanger Manufacturers Association [TEMA 2022]. In this work, the selected type is the BEM heat exchanger (depicted in Figure 4.7). It is sealed by a bonnet on one side (B), has a single pass shell (E) and has a fixed tubesheet with a bonnet on the other side (M). Other assumptions are gathered in Table 4.5.

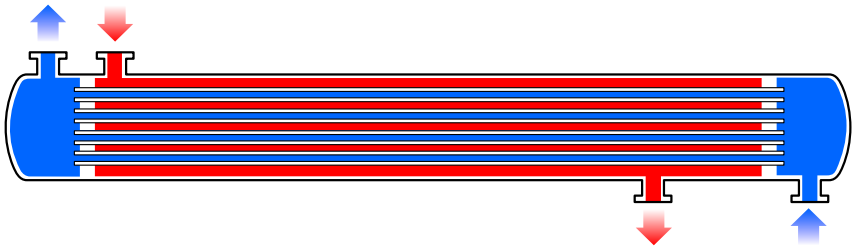

Figure 4.7: Illustration of a BEM shell and tubes heat exchanger [Wikipedia 2022c]

Exchanger type	BEM
Tube outside diameter (cm)	1.905
Baffle type	Single segmental
Baffle cut orientation	Horizontal

Table 4.5: Additional assumptions for the sizing of the lean-rich heat exchanger

According to Aspen EDR, the optimal configuration is a combination of four 6m-long shells placed in series. The complete description is available in Table 4.6. This selected design permits the operating conditions as there were identified in the modelling work (Chapter 3) but the heat exchanger is bulky.

The minimum approach temperature, which reflects the efficiency of the heat exchanger, was set to 5 K. This demanding assumption implies the selection of a large, costly heat exchanger. To nuance the choice, the flowsheet is simulated using a new minimum temperature approach of 10 K. The repercussion of this performance softening is the reduction of the exchanger size (top half of Table 4.6) at the expense of increased reboiler heat duty and solvent cooling duty (bottom half of Table 4.6).

Temperature approach (K)	5	10
Shells in series	4	2
Shell outside diameter (m)	0.864	0.789
Tube length (m)	6	6
Hot side pressure drop (kPa)	6.439	4.287
Cold side pressure drop (kPa)	7.585	4.108
Hot side outlet temperature (°C)	56.95	61.69
Cold side outlet temperature (°C)	112.5	107.85
Lean-rich heat exchanger duty (kW)	1638,57	1508,56
Reboiler heat duty (kW)	1020.34	1107,31
Reboiler heat duty (GJ/t_{CO_2})	3,6730	3,9863
Lean solvent cooling duty (kW)	444.07	576,81
Captured CO_2 cooling duty (kW)	350,64	305,68

Table 4.6: Comparison between the two heat exchanger designs

4.4 Sizing of the other pieces of equipment

Alongside the columns and the lean-rich heat exchanger, the other pieces of equipment can also be roughly sized. They include the precooler, the blower, the solvent pump and the coolers (one in the solvent loop and another one to condensate the water out of the CO_2 stream).

The blower and the pump are compact and can be simply described in terms of power consumption (Table 4.7). Similarly, the coolers are best described by their cooling duties (Table 4.8). It is relevant to note that the simulation model neglects some other compact pieces of equipment such as pumps in the washing sections. They are also neglected in this chapter.

Equipment	Consumption (kW_e)
Blower	1.8
Solvent pump	1.9
Total	3.7

Table 4.7: Electricity consumption

Equipment	Consumption (kW_{th})
COOL-MEA	444.07
COOL-CO2	350,64
Total	794.71

Table 4.8: Cooling duties

What remains to be sized is the direct contact cooler (DCC) and the condenser at the outlet of the stripper. Both of them can be seen as cylindrical vessels and they can be sized according to the gas flow rate. Assuming a diameter and a retention time allows for a first estimation of the dimensions (Table 4.9). An arbitrary safety factor is added to account for the approximate nature of these assumptions.

	Condenser	DCC
Vapour flow rate (m^3/h)	305,31	7775,30
Vapour flow rate (m^3/min)	5.09	129,59
Retention time (min)	0.25	0.25
Safety factor (-)	1.2	1.2
Required volume (m^3)	1.57	38.88
Assumed height/diameter ratio (-)	4	4
Calculated diameter (m)	0.79	2.31
Calculated height (m)	3.17	9.25

Table 4.9: Dimensions of the vessels

CHAPTER 5

Heat integration

In addition to the beneficial reduction of CO_2 emissions, retrofitting a capture unit also causes adverse effects on the power plant. Indeed, the existing facility must cater for the energetic needs of the capture unit by sacrificing a part of its own production, therefore undergoing an energy penalty.

This chapter addresses the energetic integration of the CO_2 capture unit (modelled in Chapter 3 and sized in Chapter 4) into the CHP plant. Integration strategies are investigated and the corresponding repercussions are quantified.

5.1 Methodology

5.1.1 Breakdown of the studied interactions

The energy consumption of the capture unit can be divided into four categories, illustrated in Figure 5.1 and listed hereunder:

1. the ancillary power
2. the compression power
3. the cooling duties
4. the reboiler heat duty

The first category engulfs the consumption of the blower and the pumps, but also lighting, data acquisition equipment, control devices and so on. The integration of this consumption is straightforward, as it is purely electrical.

Since the CO_2 compression train is not modelled in this work, the second category is not thoroughly investigated. However, as it is an energy-intensive process, it is not totally neglected and estimates from the literature are considered.

Cooling is achieved by cold water circulating in dedicated piping. The CHP plant itself requires cooling and the capture unit adds on top of that. This increase in utility consumption is however a financial consequence and not so much of an energy penalty. It has been cited in terms of cooling power in Table 4.8.

Finally, the reboiler heat duty is the most important category as it represents the largest consumption. Different sources of heat are considered and investigated in the following sections, as shown in Figure 5.1.

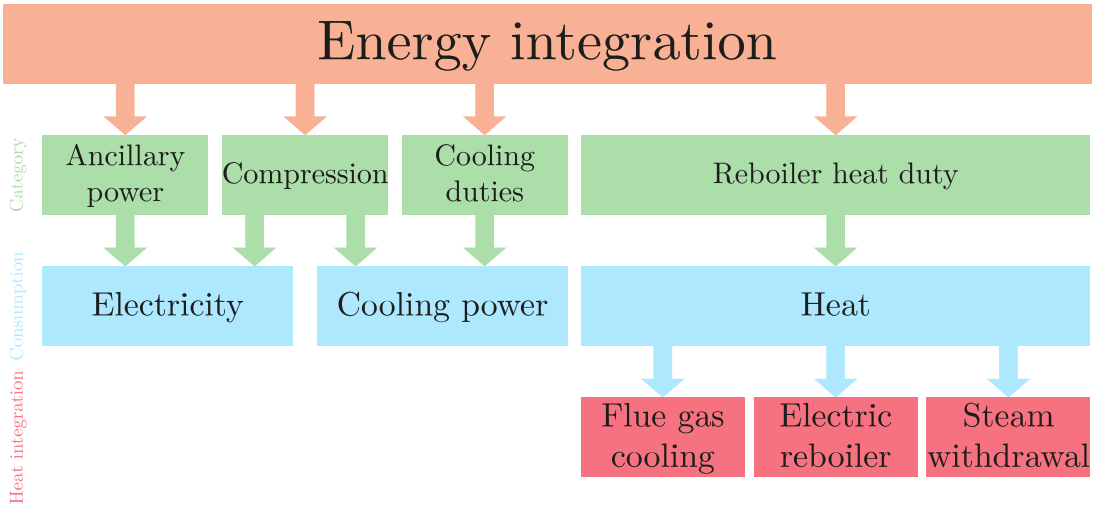

Figure 5.1: Studied heat integration stategies (not to scale)

5.1.2 Metrics used for quantification

To measure the impact of integrating the capture unit into the CHP plant, two distinct metrics are used:

1. the efficiency loss, noted $\Delta\eta_{chp}$, expressed in percentage points
2. the electricity output penalty, noted EOP, expressed in $\mathrm{kWh_e/t_{CO_2}}$

The latter expresses the shortfall of electricity production caused by the CO_2 capture unit divided by the mass flow rate of captured CO_2 [Lucquiaud and Gibbins 2011]:

$$EOP = \frac{E_{reboiler} + E_{comp} + E_a}{\dot{m}_{\mathrm{CO_2}}} \tag{5.1}$$

with:

- EOP: the electricity output penalty ($\mathrm{kWh_e/t_{CO_2}}$)
- $E_{reboiler}$: the loss of generator output due to the reboiler heat duty (kW)
- E_{comp}: the compression power (kW)
- E_a: the ancillary power (kW)
- $\dot{m}_{\mathrm{CO_2}}$: the mass flow of captured CO_2 ($\mathrm{t_{CO_2}/h}$)

It is used to assess the energy penalty of carbon capture on power plants. As the priority is given to heat generation in the studied CHP plant, the integration must be done in order not to affect it. The disrupted product is therefore the electricity generation and the EOP metric is relevant.

The EOP is convenient to compare several capture units as it expresses the penalty as a function of the captured CO_2, while the efficiency is more suited to assess the direct impact on the CHP plant itself.

It should be noted that the efficiency is sometimes inadequate to describe the operation of a CHP plant. As defined in Equation (3.10), the overall efficiency of a CHP plant is the sum of two efficiencies: the electrical efficiency and the thermal efficiency. These two forms of energy are actually not equivalent: producing heat from electricity is straightforward but the production of electricity from heat requires a whole energetic system and is penalized by transformation losses. One of the ways to account for this difference is to express energy as exergy (*i.e.* the ability to produce work), effectively taking into account the quality of the considered energy. By convention, the thermal exergy is the product of the thermal energy and the Carnot efficiency, while the electrical exergy is equivalent to the electrical energy. In this work, the focus is not placed upon the performance of fuel conversion but rather on the loss of performance caused by an additional load. For this reason, the aforementioned summed efficiency is kept as a metric.

As an order-of-magnitude estimate, the power consumption of the compression train is set at $0.33\,\mathrm{MJ/kg_{CO_2}}$, according to values found in the literature [Dutta et al. 2017; Luo et al. 2015; Metz et al. 2005]. The simulation model developed in Chapter 3 and enhanced in Chapter 4 yielded a captured flow rate of $1000.03\,\mathrm{kg_{CO_2}/h}$. The compression power therefore amounts to 91.67 kW. The ancillary consumption of the capture unit has been computed from the simulation (Chapter 4). It is rounded up to account for the consumption of secondary pumps and other electrical equipment. Both figures are summarised in Table 5.1.

Compression power (kW)	91.67
Ancillary power consumption (kW)	4
Sum (kW)	95.67

Table 5.1: Summary of the constant consumption of the capture unit

Those two values are constant for all investigated integration strategies and the focus is placed on providing the required heat to the reboiler.

5.1.3 Reboiler description

The reboiler is located at the bottom of a distillation column and provides the necessary energy to generate the required vapour flow. Several configurations of reboilers exist [Hewitt 2011], but the selected one is the kettle reboiler.

A kettle boiler resembles a shell and tubes heat exchanger: a cold fluid in a vessel is vaporised by the latent heat of steam condensing in U-tubes. It is illustrated in Figure 5.2.

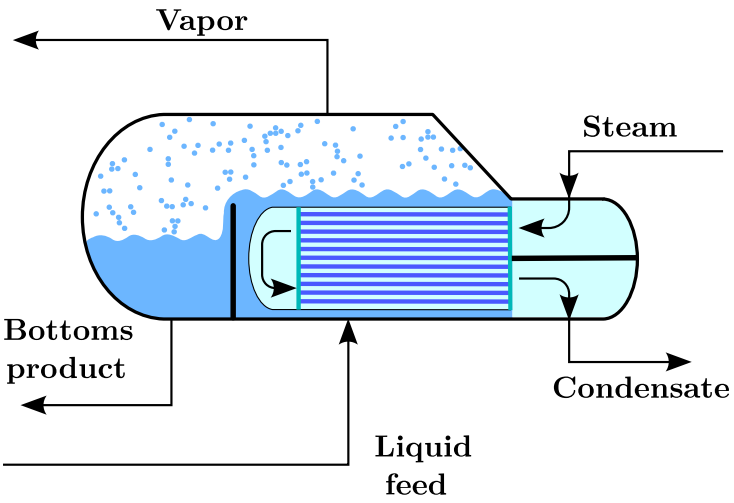

Figure 5.2: Schematic of a kettle reboiler. Adapted from [Wikipedia 2022c]

The bottoms liquid of the column is collected in the vessel of the reboiler. Steam is injected into the U-tubes and condensates, effectively transferring its latent heat to the liquid in the vessel. A fraction of the liquid product is vaporised and reinjected in the column, while the other fraction remains liquid and is disposed of as the liquid product of the distillation process.

5.2 Flue gas cooling

So as to minimize the consumption of valuable energetic products to power the capture unit, it appears most appealing to exploit any wasted heat from the operation of the CHP plant.

The most obvious source of such wasted heat is the remaining sensible heat of the flue gas. Indeed, as calculated in Chapter 3, the biomass boiler emits approximately 23 000 kg/h of flue gas at 170 °C.

The treated fraction of this flue gas undergoes cooling down to 40 °C before entering the absorber. The simulation predicts that 346 kW_{th} are released in this precooler. Oversizing this heat exchanger in order to cool down the entire flue gas volume may seem interesting, as the simulation shows that the extracted heat goes up to 1523 kW_{th}. However, this potential must be seriously tempered for several reasons.

First of all, the operating temperature of the stripper sits around 120 °C. Cooling the flue gas down to 40 °C releases unusable, low-grade heat. Unless a heat pump is used to increase the temperature level, the naively-predicted 1523 kW_{th} is mostly irrelevant.

Secondly, special care must be taken with respect to the risk of corrosion. Biomass is a solid fuel that contains sulphur. During combustion, sulphur is oxidised to form SO_2 and a limited fraction of it is further oxidised to SO_3. Several generation pathways can be

identified [Zuo et al. 2020], but the general idea can be summarised as follows:

$$SO_2 + \frac{1}{2} O_2 \longrightarrow SO_3 \tag{5.2}$$

Sulphur trioxide tends to react with water when the temperature drops below 425 °C [Zuo et al. 2020], producing sulphuric acid, *i.e.* H_2SO_4, which can cause corrosion damage:

$$SO_3 + H_2O \longrightarrow H_2SO_4 \tag{5.3}$$

Making the heat exchanger corrosion-proof would resort to the use of stainless steel, effectively requiring extensive capital investments. To avoid such expenditures, a limitation on the cooling temperature can be set. The corresponding threshold is the acid dew point, *i.e.* the temperature from which the gaseous sulphuric acid begins to condensate. Staying above this limit should ensure limited corrosion.

The acid dew point can be difficult to identify. Several models exist [Zuo et al. 2020], and most of them involve the partial pressure of H_2O and SO_3 within the flue gas. In previous works involving the Sart Tilman CHP plant, the acid dew point for biomass boilers was identified as 150 °C [Sartor, Quoilin, et al. 2014].

Cooling the entire flue gas volume down to this temperature would lead to a realistic heat recovery of 164 kW_{th}.

Finally, this result must be put in perspective. The identified heat recovery potential only represents 16 % of the required reboiler heat duty and would require a threefold oversizing of the precooler in order to admit the entire flue gas volume rather than the treated fraction. For these reasons, this integration route is not encouraged.

5.3 Electric reboiler

Replacing the kettle reboiler by an electric boiler appears to be an easy-to-implement approach. A heating element could indeed be immersed in the reboiler vessel and provide the necessary heat by the Joule effect. This integration strategy has been deployed in some pilot plants (*e.g.* the CSIRO CO_2 capture pilot plant at the Tarong Power Station in Queensland, Australia [Cousins et al. 2016]).

Neglecting any transmission loss, the required electrical power is strictly equal to the previously-identified reboiler duty (*i.e.* 1020.3 kW). Combining it with the identified constant consumption (Table 5.1), the electrical consumption of the capture unit amounts to 1115.97 kW_e.

Considering that the electricity production of the CHP plant varies between 1 MW_e and 2.4 MW_e, it is concerning to realise that this predicted consumption represents a colossal share of the electricity production.

The penalty can be quantified by using the two metrics defined in Section 5.1.2. The results are presented in Table 5.2.

Different power distributions between thermal power (supplied to the DHN) and electrical power are plotted in Figure 5.3. It emerges that there is a range of operating conditions for which the capture unit could not operate at full capacity. Indeed, whenever the heat demand of the district heating network (DHN) is superior to 6400 kW_{th}, the available electrical power is insufficient.

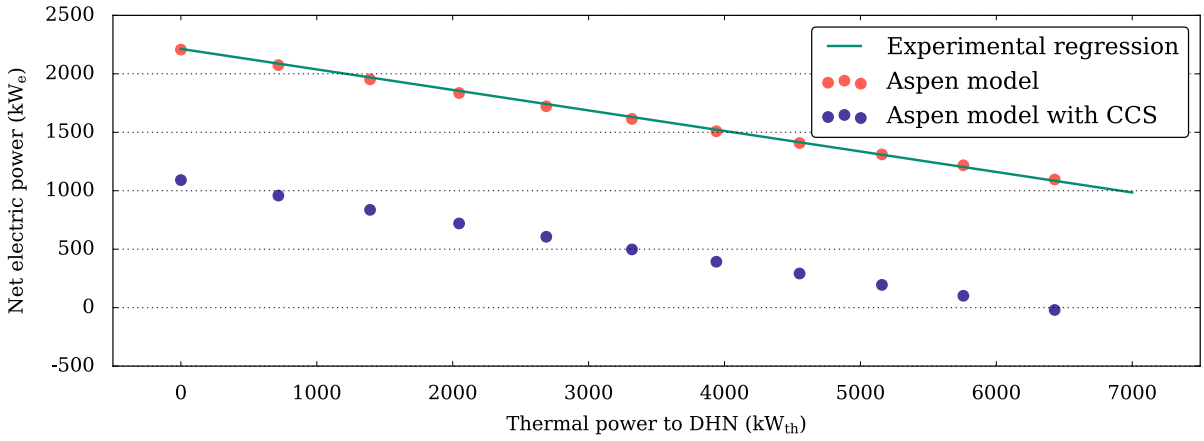

Figure 5.3: Distribution between thermal power and electricity generation with the addition of the capture unit

In this range, two possibilities are conceivable:

1. the missing fraction of power can be drawn from the grid.
2. the capture rate of the capture unit can be partially decreased.

The first suggestion permits the operation of the capture unit at its design point at the expense of an increased cost of operation. The second one requires flexibility from the capture unit.

Sticking with the second possibility, it is interesting to estimate the concession in the worst-case scenario. This case corresponds to a power distribution that entirely favours the DHN, *i.e.* when 7000 kW_{th} are supplied to the DHN. Assuming that the entire electricity production is dedicated to the reboiler, the captured amount of CO_2 (and therefore the capture rate) can be calculated. Indeed, a linear regression between the reboiler heat duty and the captured CO_2 flow rate can be obtained by successive simulations. Adding the specific power consumption of compression and the ancillary consumption into the equation, it can be estimated that consuming the entire net power at this point would only permit the capture of 817 kg_{CO_2}/h, reducing the capture rate down to 73.48 %.

Loss of cogeneration efficiency $\Delta\eta_{chp}$ (%)	9.54
Electricity output penalty (kWh_e/t_{CO_2})	1116
Inoperable range at full capacity (kW_{th})	6400-7000
Worst-case capture rate (%)	73.48

Table 5.2: Summary of the heat integration using an electric reboiler

5.4 Steam extraction from the Rankine cycle

The most common and efficient integration strategy is to withdraw steam from the thermodynamic cycle, to condensate it directly in the reboiler and to reinject it in the condenser of the plant. [Cousins et al. 2016; Lucquiaud and Gibbins 2011]

The critical constraint is the degradation limit of the solvent to be regenerated. As reported in Chapter 2, thermal degradation of MEA begins from 120 °C onwards. Heating the solvent above this threshold should be avoided in order to reduce losses.

Assuming an approach temperature of 10 K in the kettle reboiler, it implies that the supplied steam must not exceed 130 °C [1]. Moreover, it is desirable to supply heat at a constant temperature [Pfaff et al. 2010]. It is therefore relevant to operate at the corresponding saturation pressure, *i.e.* 270.3 kPa.

In the design phase of new power plants, it is possible to account for these requirements. However, when retrofitting a capture unit to an existing facility, perfect integration would only be coincidental [Duan et al. 2012] and, most of the time, the extracted steam must undergo conditioning steps, which are explained after the determination of the steam flow rate.

The required steam flow rate can be calculated thanks to the EES software and its integrated thermodynamic properties. The flow rate can be deduced from an energy balance:

$$\dot{Q}_{reboiler} = \dot{m}_{steam}(h_{in} - h_{out}) \tag{5.4}$$

with h_{in} the specific enthalpy of saturated steam at 130 °C, h_{out} the specific enthalpy of saturated water at 130 °C and $\dot{Q}_{reboiler}$ the required reboiler duty (1020.3 kW).

This calculation can be validated in Aspen Plus. The kettle reboiler is modelled by a shell and tubes heat exchanger in series with a flash tank separator. This configuration is shown in Figure 5.4. The built-in RADFRAC model comes with a tool, named *Reboiler Wizard*, that allows linkage between the column and the two-block reboiler model, effectively making sure that the steam flow rate is sufficient to meet the required duty.

Equation (5.4) and the Aspen Plus simulation both yield the same extracted steam flow rate: 1529 kg/h.

In the Sart Tilman CHP plant, the best location to withdraw steam is between the two turbines, at the intermediate pressure level (550 kPa). To reach 270.3 kPa, steam can either be laminated in a valve or expanded in an additional turbine in order to take profit from the pressure differential. The use of this supplementary turbine, called a *letdown steam turbine generator* (LSTG), has been suggested extensively in the literature [Duan et al. 2012; Goto et al. 2013; Pfaff et al. 2010].

In both options, the steam temperature after the pressure changer is still too elevated. In order to bring it to saturation, it has to be attemperated. For economical reasons, it is

[1] The temperature approach could be larger and it is also possible to operate at temperatures that are slightly beyond the degradation limit. For these reasons, a more flexible temperature constraint can be expected in reality. In this work, it is however kept at 130 °C to avoid additional assumptions.

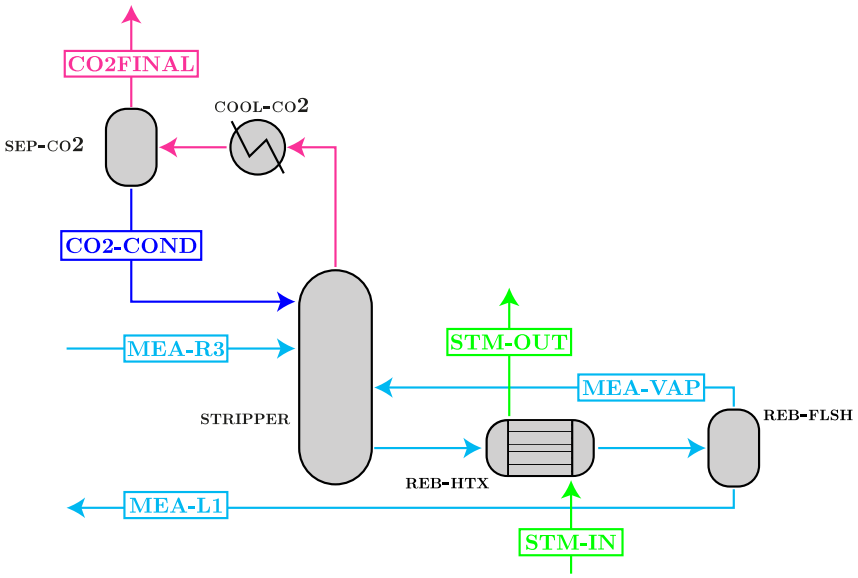

Figure 5.4: Flowsheet of the kettle reboiler

reasonable to abstain from investing in another heat exchanger. Instead, a fraction of the condensate, *i.e.* saturated water exiting the reboiler, can be recycled. At the outlet of the pressure changer, liquid droplets of water are injected into the steam stream and get evaporated, effectively consuming the sensible heat of the superheated steam. The flow rate of this recycling loop must be set correctly to reach saturation.

To assess the two options (*i.e.* using a valve or an LSTG), a model of the steam conditioning unit is modelled in Aspen Plus. The flowsheet is shown in Figure 5.5. In both cases, the recirculation rate of the condensate is controlled by a *Design Spec* that ensures an exact temperature of 130 °C at the inlet of the reboiler.

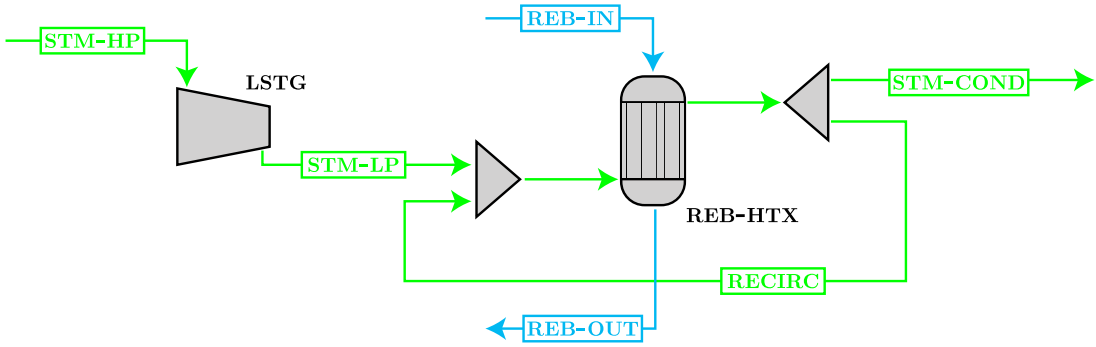

Figure 5.5: Flowsheet of the steam conditioning unit

In the first case, the valve is modelled after an adiabatic pressure changer (not illustrated). In the second one, the parameters of the turbine are taken as identical to the two other turbines of the CHP plant (Table 3.17): the isentropic efficiency is set to 70 % and the mechanical efficiency to 90 %. The results of both simulations are presented in Table 5.3. Albeit it requires a larger flow rate, the addition of an LSTG is temporarily the preferred option as the additional power generation helps minimise the energy penalty.

	With a valve	With an LSTG
Steam flow rate (kg/h)	1529	1565
Additional power generation (kW_e)	–	41.55
Temperature after the pressure changer (°C)	237.2	182.8
Required recirculation flow rate kg/h	160.4	78.67

Table 5.3: Comparison between the two options for the heat integration using withdrawn steam

An additional constraint inherent to the case study must be considered. The low-pressure turbine accepts a flow rate between 3000 kg/h and 13 000 kg/h [Sartor 2018]. The lower bound limits the operation of the steam withdrawal integration strategy. Steam extraction should be suspended when the heat demand of the district heating network requires such a steam flow rate that the remaining steam is just sufficient to reach the lower bound.

Using the simulation model of the Rankine developed in Chapter 3, the threshold can be identified at 5800 kW_{th}. Above this limit, the extracted steam flow rate would be gradually decreased, declining de facto the capture rate, until it could not operate at all due to the lack of available steam. The capture unit would then be brought to a stop.

The comparison metrics are calculated for both cases using the aforementioned simulation model and the constant electricity consumption identified in Table 5.1. The results are gathered in Table 5.4.

	With a valve	With an LSTG
Loss of cogeneration efficiency $\Delta\eta_{chp}$ (%)	2.44	2.13
Electricity output penalty (kWh_e/t_{CO_2})	382	344
Inoperable range at full capacity (kW_{th})	5800-7000	5800-7000
Worst-case capture rate (%)	0	0

Table 5.4: Summary of the heat integration using steam withdrawal

5.5 Conclusion

Three different heat integration strategies have been investigated. The results are summarised in Table 5.5 and a discussion leading to a preferred integration route is provided in this final section.

First, cooling the flue gas should be discarded as a standalone option because it could not cater for the entire energy consumption of the capture unit. Indeed, it must be combined with another source of energy. Extensive investment is also expected for the heat exchanger.

Second, using an electric reboiler stands out as the most flexible alternative because, at any time, there would be the availability of electricity from the grid if the electricity

generated by the CHP plant would fall short of the needs of the capture unit. It is also relevant to note that, alongside the grid availability, this route could take advantage of the on-site renewable electricity production as photovoltaic panels are installed on the campus. However, for this integration option, the energy penalty on the CHP plant is a serious concern.

And finally, the less invasive integration strategy (performance-wise) seems to be the withdrawal of steam from the intermediate pressure level with the addition of an LSTG. Using a valve can also be recommended if the budgetary constraints prevail. The main drawback of this choice would be the suspended operation whenever the district heating network would require full thermal power. This penalty should be tempered by putting it in perspective with the number of hours spent in this adverse operating range, which is known to be away from the average operating point.

	Electric reboiler	Steam withdrawal	
		Valve	LSTG
Loss of cogeneration efficiency $\Delta\eta_{chp}$ (%)	9.54	2.44	2.13
Electricity output penalty (kWh_e/t_{CO_2})	1116	382	344
Inoperable range at full capacity (kW_{th})	6400-7000	5800-7000	5800-7000
Worst-case capture rate (%)	73.48	0	0

Table 5.5: Summary of the heat integration strategies

CHAPTER 6

Economic evaluation of the pilot

One of the most crucial steps in the decision-making process of any project is the economic evaluation. Pilot plants do not escape budgetary constraints and the present chapter proposes a first estimation of the cost.

6.1 Methodology

At this stage, design choices, simulation results and the subsequent sizing are certainly not definitive. Some pieces of equipment and physical phenomena have been neglected throughout the preliminary design developed in this master's thesis. Moreover, the required time investment is correlated with the preciseness of any economic evaluation. For these reasons, an order-of-magnitude estimate is sufficient.

The chosen method for this cost estimation is the bare module cost method, which is generally accepted as the best for preliminary estimations. The capital expenditures (CAPEX) and operational expenditures (OPEX) are assessed independently and then combined in a single discussion to study the impact of some assumptions. Unless specified, the methodology and the associated data come from [Turton et al. 2018]. Case-specific considerations and assumptions are also included and motivated.

As the pilot plant is intended to be retrofitted to the existing Sart Tilman CHP plant, the expenditures of the CHP plant are not taken into account. However, any deviation from the current OPEX of the existing plant that is provoked by the addition of the capture unit must be taken into account.

6.2 Estimating capital expenditures (CAPEX)

Capital expenditures encompass all costs that precede the operation of the plant. Without being exhaustive, they include the purchase costs of equipment, the budget allocated to the design, the installation costs and so on.

6.2.1 Methodology

The bare module cost method is used to calculate the individual purchase cost of each piece of equipment. It can be summarised as follows:

1. Based on a correlation (Equation (6.1)) and on tabulated data, the purchase cost for each individual piece of equipment is estimated. This correlation assumes a base case for the studied unit: made of carbon steel and stress-free operating pressure (*i.e.* at near-atmospheric pressure).

$$log_{10}(C_p^0) = K_1 + K_2\, log_{10}(A) + K_3\, (log_{10}(A))^2 \tag{6.1}$$

   where

   - C_p^0 is the purchase cost of the equipment. The zero indicates the base case.
   - K_1, K_2 and K_3 are equipment-specific empirical constants.
   - A is the capacity factor, which represents the parameter of the evaluated equipment that is expected to dictate the cost, *e.g.* the exchange area for heat exchangers, the flow rate for fans and so on.

2. As the correlations are given for a certain validity range, any equipment with an out-of-bounds capacity cannot be directly evaluated. To bypass this issue, the correlation is first applied to the nearest bound to obtain the limit price C_{lim} and then scaled with the famous *six-tenths rule* to obtain the purchase cost C_p^0 :

$$C_p^0 = C_{\text{lim}} \left(\frac{A_{\text{actual}}}{A_{\text{lim}}} \right)^{0.6} \tag{6.2}$$

3. To account for potential deviations from the base case (*i.e.* the use of another material or the operation at another pressure level), a correction factor F_{BM} can be applied to calculate the bare module cost C_{BM}, which is therefore the purchase cost of the standalone piece of equipment:

$$C_{BM} = C_p^0\, F_{BM} \tag{6.3}$$

   The determination of its value depends on the type of equipment:

   - For blowers and tower packing, F_{BM} is found in tabulated data.
   - For heat exchangers, process vessels (*e.g.* reactors, towers) and pumps:

$$F_{BM} = B_1 + B_2 F_M F_P \tag{6.4}$$

     B_1 and B_2 are again equipment-specific empirical constants, F_M is a correction factor to account for the use of a different material than carbon steel and F_P is a correction factor accounting for the operation at another pressure level. The latter is given by one of the following formulas:

     – For process vessels:

$$F_P = \frac{\frac{(P+1)D}{2[850-0.6(P+1)]} + 0.00315}{0.0063} \tag{6.5}$$

       where P is the pressure level (in bar_g) and D is the diameter (in m).

– For others:

$$log_{10}(F_P) = C_1 + C_2\, log_{10}(P) + C_3\, [(log_{10}(P)]^2 \tag{6.6}$$

where P is the pressure level (in bar_g) and C_1, C_1 and C_1 are equipment-specific empirical constants.

4. The bare module costs of the n pieces of equipment are summed to obtain the total purchase cost of the equipment:

$$C_{BM,total} = \sum_{i=1}^{n} C_{BM,i} \tag{6.7}$$

This methodology is used with the results of the sizing detailed in Chapter 4. In addition, amongst the integration strategies investigated in Chapter 5, the selected route is the use of an LSTG with recirculation of the condensate. The chosen lean-rich heat exchanger has a minimum approach temperature of 5 K.

6.2.2 Results

The different pieces of equipment included in the cost estimation are listed in Table 6.1, alongside their type and the corresponding empirical factors for Equation (6.1).

Equipment	Type	Factors		
		K_1	K_2	K_3
DCC	Vertical process vessel	3,4974	0,4485	0,1074
Blower	Centrifugal fan	3,5391	-0,3533	0,4477
Absorber casing	Packed tower	3,4974	0,4485	0,1074
Absorber packing	Packing	2,4493	0,9744	0,0055
Solvent pump	Centrifugal	3,3892	0,0536	0,1538
L-R exchanger	Shell and tubes (fixed tubes)	4,3247	-0,303	0,1634
Stripper casing	Packed tower	3,4974	0,4485	0,1074
Stripper packing	Packing	2,4493	0,9744	0,0055
Reboiler	Kettle reboiler	4,4646	-0,5277	0,3955
LSTG	Axial turbine	2,7051	1,4398	-0,1776
CO_2 cooler	Shell and tubes (fixed tubes)	4,3247	-0,303	0,1634
Flash tank	Vertical process vessel	3,4974	0,4485	0,1074
Solvent cooler	Shell and tubes (fixed tubes)	4,3247	-0,303	0,1634

Table 6.1: Considered pieces of equipment and associated empirical factors

For most of them, the sizing results from Chapter 4 can be directly applied. However, the reboiler exchange area and the LSTG fluid power are out-of-bounds of their respective correlation. The maximum exchanger area for kettle reboilers is 100 m^2 (versus 110.37 m^2 in the case study) and the minimum fluid power for axial turbines is 100 kW (versus 41.55 kW in the case study). The purchase cost of these two pieces is rescaled using the six-tenth rule, described by Equation (6.2). This approach is valid as the actual capacities

are close to the bounds of the correlations. Less favourable values could discredit the use of the six-tenth rule.

The exchange area of the coolers is estimated by assuming that cooling water enters the cooler at 20 °C and exits at 25 °C ($\Delta T = 5$K). This allows the calculation of the logarithmic mean temperature difference:

$$\Delta T_{LM} = \frac{\Delta T_A - \Delta T_B}{\ln \frac{\Delta T_A}{\Delta T_B}} \tag{6.8}$$

Assuming an overall heat transfer coefficient U of $0.85\,\mathrm{kW\,m^{-2}\,K^{-1}}$, the exchange area A can be deduced from:

$$\dot{Q} = U\ A\ \Delta T_{LM} \tag{6.9}$$

With these additional considerations, the results are summarised in Table 6.2.

Equipment	Capacity	C_p^0	Rescaled ?
DCC	$38.88\,\mathrm{m^3}$	30 323.94 $	No
Blower	$100\,\mathrm{m^3/s}$	3111.43 $	No
Absorber casing	$8.04\,\mathrm{m^3}$	9804.23 $	No
Absorber packing	$8.04\,\mathrm{m^3}$	2167.10 $	No
Solvent pump	1.93 kW	2611.69 $	No
L-R exchanger	$379.33\,\mathrm{m^2}$	42 666.19 $	No
Stripper casing	$0.97\,\mathrm{m^3}$	3096.59 $	No
Stripper packing	$0.97\,\mathrm{m^3}$	272.33 $	No
Reboiler	$110.37\,\mathrm{m^2}$	103 971.62 $	Yes
LSTG	41.55 kW	44 204.19 $	Yes
CO_2 cooler	$10.39\,\mathrm{m^2}$	15 329.79 $	No
Flash tank	$1.57\,\mathrm{m^3}$	3890.77 $	No
Solvent cooler	$21.44\,\mathrm{m^2}$	16 252.11 $	No

Table 6.2: Equipment capacities and the corresponding purchase costs in the base case

From the basic purchase costs, the bare module costs C_{BM} can be calculated using the correction factor F_{BM} (Equation (6.3)). Indeed, in order to protect equipment from corrosion, stainless steel (SS) is used instead of carbon steel (CS). Stainless steel being more expensive than carbon steel, a scaling factor is applied through F_{BM}. The results are reported in Table 6.3.

Some equipment also operates at a pressure level that is superior to ambient conditions. However, the calculated pressure factors F_P are all inferior to unity. They are therefore set to the default value of one. For this reason, they are not reported in Table 6.3.

These calculated bare module costs are not only off-the-shelf prices but also account for fireproofing, freight, insurance and any other expense linked to installation. However, to account for unforeseen expenses, a safety factor of 1.18 is applied. This yields the total module cost:

$$C_{TM} = 1.18\ C_{BM,total} \tag{6.10}$$

Equipment	C_p^0	Material	B_1	B_2	F_M	F_{BM}	C_{BM}
DCC	30 323.94 $	SS	2,25	1,82	1	4.07	123 418.42 $
Blower	3111.43 $	CS	-	-	-	2.8	8712.00 $
Absorber casing	9804.23 $	SS	2,25	1,82	3.1	7,89	77 375.02 $
Absorber packing	2167.10 $	SS	-	-	-	7,1	15 386.39 $
Solvent pump	2611.69 $	SS	1,89	1,35	2,3	5.00	13 045.41 $
L-R exchanger	42 666.19 $	SS	1,63	1,66	2,7	6.11	260 775.75 $
Stripper casing	3096.59 $	SS	2,25	1,82	3,1	7.89	24 438.25 $
Stripper packing	272.33 $	SS	-	-	-	7,1	1933.53 $
Reboiler	103 971.62 $	SS	1,63	1,66	2,7	6.11	635 474.54 $
LSTG	44 204.19 $	CS	-	-	-	6,1	269 645.58 $
CO_2 cooler	15 329.79 $	CS	1,63	1,66	1	3,29	50 435.00 $
Flash tank	3890.77 $	CS	2,25	1,82	1	4.07	15 835.45 $
Solvent cooler	16 252.11 $	SS	1,63	1,66	2.7	6.11	99 332.87 $
Total $C_{BM,total}$							1 595 808.22 $

Table 6.3: Bare module cost calculation using the factor F_{BM}

The resulting total module cost amounts to 1 883 053.70 $.

6.2.3 Scaling the costs for today

The tabulated data used in the previous section are average values from different manufacturers calculated for the year 2001. To take inflation (and other price changes over time) into account, the index technique is used (Equation (6.11)). This linear relationship permits the conversion of an amount in a reference year to a target year by using indexes, which are reference values calculated for each year.

$$C_t = C_{ref}\left(\frac{I_t}{I_{ref}}\right) \tag{6.11}$$

The index technique is one of the most common cost evolution models.

For chemical plants, the recommended index is the Chemical Engineering Plant Cost Index (CEPCI), which is a compound index published every month in *Chemical Engineering* (ISSN: 0009-2460).

Equation (6.11) can be rewritten as:

$$C_{2022} = C_{2001}\left(\frac{\text{CEPCI}_{2022}}{\text{CEPCI}_{2001}}\right) = C_{2001}\left(\frac{797.6}{397}\right) \tag{6.12}$$

The updated total module cost amounts to 3 783 182.95 $.

6.2.4 Scaling the cost for the location

The calculated total cost is valid for a capture unit erected in the United States. As the studied facility is located in Belgium, currency conversion can be applied based on current

exchange rates (1.0358 \$/€). [ECB 2022]

A final correction factor could be applied to take into account the potential difference between the American petrochemical sector and the local availability of suppliers [Towler and Sinnott 2013]. It is however assumed that the prevalence of petrochemistry in Belgium suffices to neglect this contribution.

The final value of the CAPEX is 3 642 930.14 €.

6.3 Estimating operating expenditures (OPEX)

Operating expenditures are the annual costs for the operation of the plant. In opposition to CAPEX, they do not represent the initial investment but the required expenses to run the plant on a day-to-day basis.

6.3.1 Methodology and assumptions

Three items of expenditure are considered:

- the cost of operating labour C_{OL}, *i.e.* the salaries of the actual operators and, therefore, not including the payrolls of design engineers.
- the cost of utilities C_{UT}, including cooling water, electricity and steam.
- the cost of raw materials C_{RM} that are consumed during the operation of the plant.

In addition, it is relevant to account for the reduction in OPEX for the CHP plant. As it emits less CO_2 into the atmosphere, fewer carbon allowances must be purchased. This can be seen as a virtual revenue R_{EUA} attributed to the capture unit.

These contributions can be gathered in a single equation in which the different terms are weighted to account for maintenance, administrative costs, and other expenses:

$$\text{OPEX} = 0.18\,\text{CAPEX} + 2.73\,C_{OL} + 1.23\,(C_{UT} + C_{RM}) - R_{\text{EUA}} \tag{6.13}$$

Finally, it is assumed that the plant operates for 5200 h/year [Sartor, Quoilin, et al. 2014]. As the capture rate is $1\,\text{t}_{\text{CO}_2}$/h, the annual volume of captured CO_2 comes to $5200\,\text{t}_{\text{CO}_2}$/year.

6.3.2 Cost of raw materials

As the plant operates in a closed loop, it does not consume any constant stream of raw materials. However, there are solvent losses (either by atmospheric emission or by degradation) that must be compensated to keep operating at the design point.

The simulation model estimated the losses by emissions to be equal to 1.84×10^{-14} kg/h, which is negligible. This extremely low value reflects the efficiency of the washing section.

As degradation is not integrated into the simulation model, degradation losses can only be considered by taking reference values from the literature. In this work, the degradation

rate is set at 1.5 $\mathrm{kg_{MEA}/t_{CO_2}}$ [Abu Zahra 2009; Cousins et al. 2016] and the annual MEA consumption becomes 7800 $\mathrm{kg_{MEA}}$/year.

It is worth noting that the selected degradation rate was also observed during the operation of the Esbjerg pilot plant that was introduced in Chapter 2. [Knudsen et al. 2009]

Considering 1.8 €/$\mathrm{kg_{MEA}}$ [Jilvero et al. 2014], the annual cost of MEA make-up is 14 040 €/year.

6.3.3 Cost of labour

The number of full-time operators dictates the cost of labour. From the previously-defined annual operation length and assuming a typical shift duration of 8h, 650 shifts must be staffed over the course of a year.

For a single shift, the number of working positions depends on the number of large pieces of equipment, such as compressors, towers, reactors, heaters and heat exchangers:

$$N_{\text{working positions}} = (6.29 + 0.23 N_{np})^{0.5} \tag{6.14}$$

In this case study, N_{np} is equal to 6. In other words, there is work for 2.77 operators during a single shift. Per se, this decimal figure does not make a lot of sense but it is used as a basis for the subsequent calculations.

A single operator works 5 shifts per week and 46 weeks per year (*i.e.* he/she is entitled to 6 weeks of annual vacation). Therefore, he/she is able to do 230 shifts per year.

By combining previous results, it stands out that 2.83 operators are needed for each working position. In total, 7.83 (rounded up to 8) full-time operators must thus be hired.

The gross salary of an operator is assumed to be 3500 €/month or, equivalently, 42 000 €/year. The annual cost of labour thus amounts to 336 000 €/year.

6.3.4 Cost of utilities

The utility consumption includes cooling water in the cooling heat exchangers, electricity to power the pumps and steam to supply the reboiler.

6.3.4.1 Cooling water

The cooling duties are reported in Table 4.8. In total, they amount to 794.71 kW, or 794.71 kJ/s, which makes 25 061.97 GJ/year.

Assuming the price of cooling water to be 0.354 $/GJ, the annual expense is equal to 8871.94 $/year, or 8543.03 €/year (using the same exchange rate as for the CAPEX calculation).

6.3.4.2 Electricity and steam

The capture unit consumes both electricity and steam that are supplied by the CHP plant. In turn, the energetic products cannot cater for the electricity consumption of the University. To compensate, a larger volume of electricity must be purchased from the grid. The additional volume corresponds to the sum of the electricity consumption of the capture unit and the potential electricity that could have been produced by the withdrawn steam. Both contributions are included in the Electricity Output Penalty (EOP) metric, which has been calculated in Chapter 5.

Considering an EOP of $344\,\mathrm{kWh_e/t_{CO_2}}$ and assuming a purchase price of $0.1218\,€/\mathrm{kWh_e}$ [Statista 2022], the combined cost of electricity and steam amounts to $217\,875.84\,€$/year.

6.3.5 Virtual revenue because of the reduction in emissions

Compared to the current operation of the CHP plant, the combined facility with a retrofitted capture unit emits less CO_2 into the atmosphere. Therefore, fewer carbon credits must be purchased and net savings are made. They are taken into account in this economic evaluation as a virtual revenue that decreases the annual OPEX.

The EU ETS system, introduced in Chapter 1, is used as a basis for the assumption on the carbon price. The EUA price is set at $80\,€/\mathrm{t_{CO_2}}$.

Over the course of a year, the CO_2 capture unit generates a saving on EU allowances that amounts to $416\,000\,€$/year.

It should be noted that this saving could be overshadowed by uncertainty. Indeed, the fate of the captured CO_2 could condition the saving made on EU allowances. The calculated saving is therefore a best-case estimate.

6.3.6 Results

Using Equation (6.13) and the intermediate results from the previous sections, the total OPEX is calculated and it amounts to $1\,452\,771.96\,€$/year.

6.4 Discussion and results

6.4.1 Net present value

In order to gather both CAPEX and OPEX into a single metric, the *net present value* (NPV) is calculated. The NPV is the present worth of the project. To calculate it, all future cash flows are discounted to the current time by applying an expected discounting rate. This rate represents the expected return on investment that could be attained if the money were invested in another project.

Assuming a discount rate of 10% and a project duration of 20 years, the calculated NPV amounts to $-16\,011\,197.47\,€$. This negative value is expected as the OPEX is negative, which means that the annual income never surpasses the annual expenses and the initial

investment is therefore never recovered.

In the private sector, the NPV is used to assess the profitability of a studied project. A positive NPV indicates a profitable investment because it implies that the present worth of the cash inflows outweighs the present worth of the cash outflows. In the public sector, it is important to account for externalities, *i.e.* non-monetary benefits that affect society as a whole. In the present case study, an externality would be the reduction of CO_2 emissions, which benefits society as it mitigates the contribution of the plant to climate change. Another example is the quality of education for engineering students because of the pedagogical potential of deploying a pilot plant of an emerging technology. Externalities are often difficult to estimate, and the NPV figure is less reliable than for private projects. However, it is still relevant for two reasons:

- As all preliminary projects have room for improvement, it is important to identify the critical parameters that can have a significant influence on profitability.
- Assumptions can be tempered and the effect of a deviation can be calculated.

This is addressed in the next section.

6.4.2 Reflection on some assumptions

First of all, the general assumptions (*i.e.* the project duration and the discounting rate) depend on many factors and the selected values are arbitrary. Figure 6.1 illustrates the evolution of the NPV for a change in either of these.

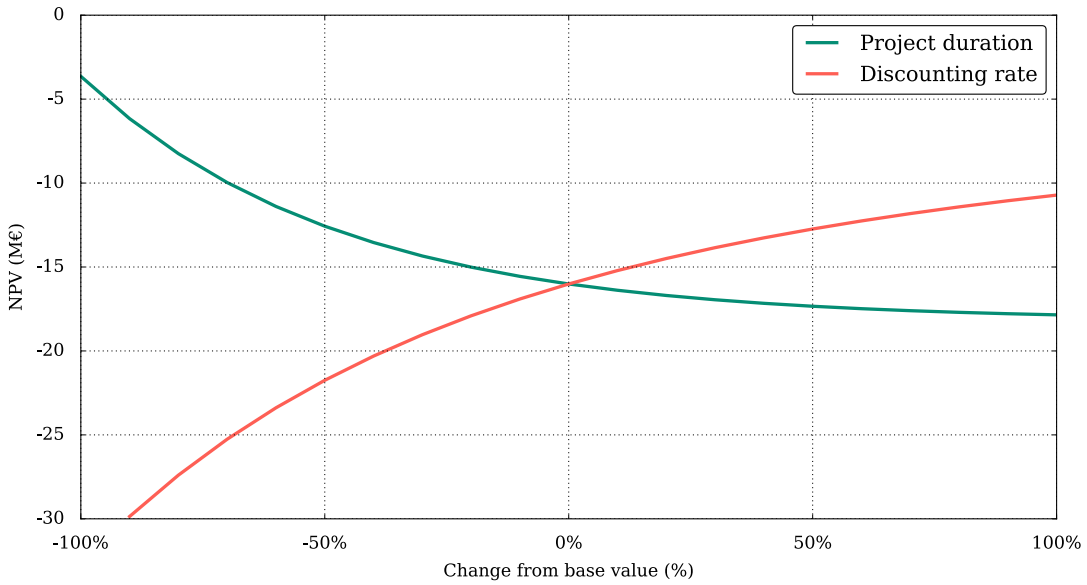

Figure 6.1: Influence of the base project assumptions

As the OPEX is negative, it is logical to observe that the NPV keeps decreasing with an increase in the duration. However, the discounting rate acts as a damping factor and limits this evolution for higher numbers of operating years. This trend can also be deduced by the observation of the second curve.

Regarding the expected cost of labour, the applied methodology is best-suited for the operation of a *large-scale* greenfield facility. In the present case study, the studied installation is a pilot that is integrated into an existing (and staffed) plant. For this reason, it is reasonable to expect that fewer additional operators have to be hired. Figure 6.2 highlights the extensive influence of this parameter on the NPV. In the best base (*i.e.* the current operators of the CHP plant are able to take care of the pilot plant), the NPV is even halved compared to the base case.

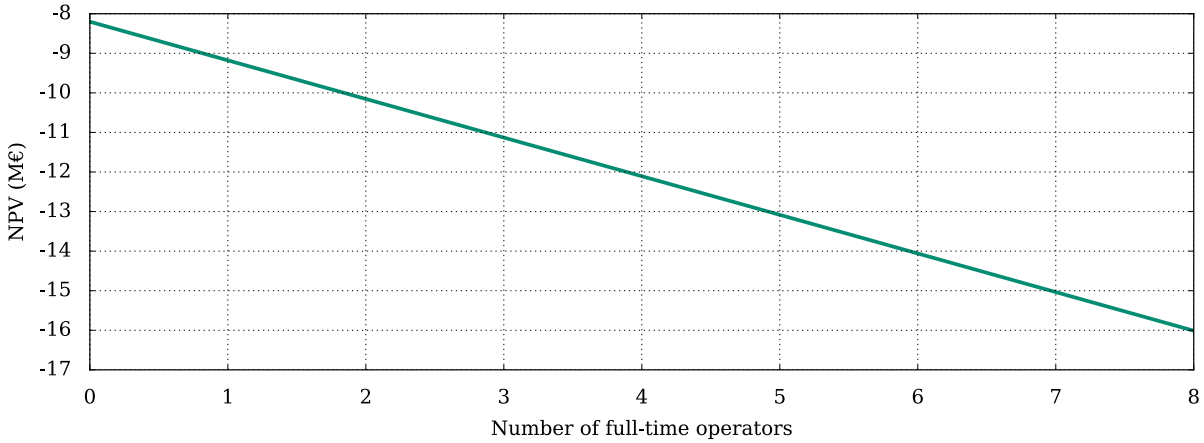

Figure 6.2: Influence of the labour cost

Estimating utility costs can be delicate. In particular, the cost of cooling water was calculated from a tabulated value, which could potentially be far away from reality. In addition, the prices of MEA and electricity were sourced but changes over time can be expected. Their influence is depicted in Figure 6.3, alongside the impact of the carbon price (from the EU ETS system).

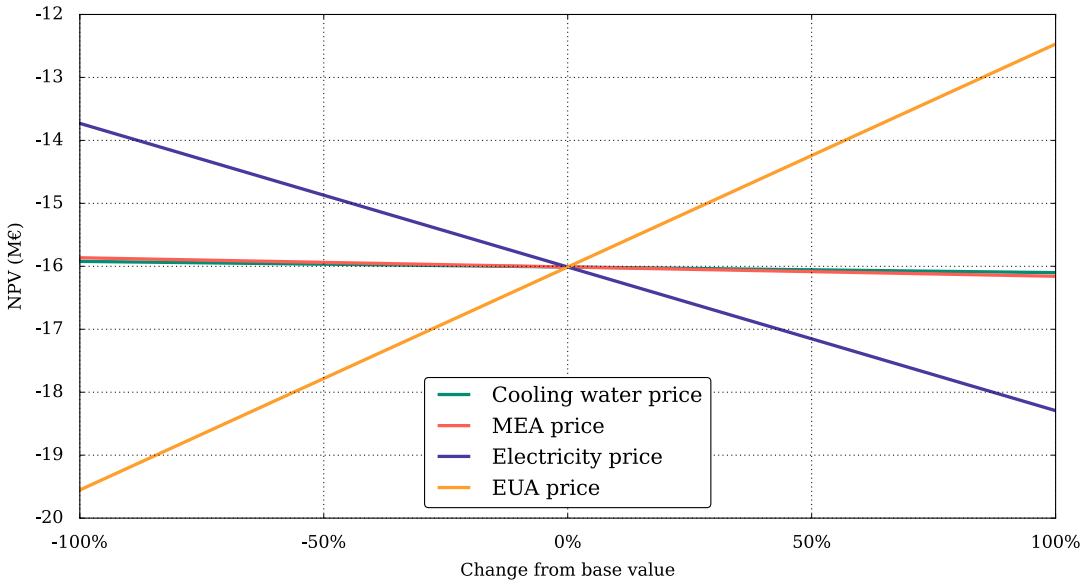

Figure 6.3: Influence of the costs of utilities and raw materials

It stands out that the cooling water and MEA prices make a marginal contribution to the final profitability of the project. Assuming an inaccurate value for any of them is thus not

critical. It is worth noting that the degradation rate of MEA is expected to have the same limited influence on the project as it is involved in a linear relationship alongside the cost of MEA.

The most impacting parameters are therefore the EUA price, which is the only income of the project, and the electricity price, which reflects the energy consumption of the capture unit. Depending on the future energy mix of Europe, both figures could vary substantially.

From this sensitivity analysis, it emerges that a single parameter cannot enable the profitability of the project. However, under a certain combination of conditions, the deployment of the capture unit could be profitable, even by neglecting the externalities. This optimism should nonetheless be nuanced by the quality of the economic values: the CAPEX and OPEX remain order-of-magnitude estimates and caution must be used when drawing conclusions from them. In conclusion, better knowledge of the economic parameters is necessary to refine the economic evaluation but the key parameters are already identified.

CHAPTER 7

Conclusion

The objective of this master's thesis was to lay the basis for the installation of an MEA-based, post-combustion pilot plant coupled to the biomass-fired Sart Tilman CHP plant.

At first, a literature review was conducted to delineate the state of the art of Carbon Capture, Utilisation and Storage with emphasis on amine-based, post-combustion capture. The review included, notably, an overview of current efforts to deploy CCUS facilities in the world. Preliminary design choices that pertain to the studied pilot plant, such as the selected technology and the targeted capture rate, were made based on the literature review.

With additional, motivated design choices, a simulation model of the CO_2 capture pilot plant was developed in Aspen Plus, based on a parent model validated in previous studies. The model was simulated with the equilibrium calculation mode as a robust approach to numerical resolution. Moreover, the expected nominal operating conditions were identified by optimising some of the key parameters that were not set upfront. Amongst others, the solvent loading and the corresponding flow rate can be cited.

The existing CHP plant could operate under different conditions (*e.g.* a different biomass composition or a change in ambient atmospheric conditions). A submodel of the biomass furnace was developed and validated in Aspen Plus to allow for the impact assessment of such a change in operating conditions. Moreover, in preparation for the integration of the pilot plant into the host CHP plant, an Aspen Plus submodel of the Rankine cycle was also built and validated, based on a previously-validated model.

The three submodels, *i.e.* the biomass furnace, the Rankine cycle and the CO_2 capture unit, were then merged into a single model. This combined model is certainly proving to be an asset because it enables the understanding of the system's behaviour as a whole in addition to the assessment of the respective interactions between the different subsystems.

To anchor the simulation results of the CO_2 capture unit in reality, they were translated into a preliminary design by sizing the most important pieces of equipment. For this purpose, the previously-developed equilibrium model was revamped into a rate-based

model, which came with improved accuracy. Therefore, the expected performance of the pilot plant was updated and put in perspective with the initial approach.

Furthermore, strategies to integrate the capture unit into the existing CHP plant were investigated and compared. The three studied options were the flue gas cooling, the electric reboiler and the steam withdrawal. For each of them, the induced energy penalty was calculated.

At last, an order-of-magnitude cost estimation was performed so as to contrast the ambitions with realistic expectations. The CAPEX and OPEX were evaluated individually and then combined into an economic study. From the latter, the key economic and operational parameters were identified.

The results of the present work form the first evaluation to support the decision making of the project. They also pave the way for future perspectives.

First of all, the developed model of the facility could be overhauled by including additional components. For instance, the heat exchanger network could be implemented to strengthen the connection between the biomass furnace and the Rankine cycle submodels. More importantly, the selected heat integration strategy, be it an electric reboiler or a steam withdrawal process, could also be added to assess directly the system's response to a change in operating conditions. With these upgrades, the combined model would become more faithful.

In the continuity of the previous perspective, solvent degradation mechanisms could also be added to the model, as they remain one of the main concerns for the long-term operation of a carbon capture unit. In addition, the simulation model could be used to predict the degradation due to SO_x and NO_x, which are pollutants of particular importance in biomass-fired boilers. The need for a pretreatment unit would then be justified or discarded.

Regarding the project itself, the ambitions could be adapted based on the economic evaluation and the energetic requirements of the pilot plant. Both are results of this master's thesis. More choices could also be made upfront, which would help to refine the evaluation. For instance, a preferred heat integration approach could be selected and the fate of the captured CO_2 could be specified. From there, a new iteration of the preliminary design could be performed and, in turn, a more precise economic evaluation could be executed.

Depending on the demand for energetic products, it was demonstrated that inoperable conditions are possible. In practice, the capture could thus be paused and then restarted several times. Developing a dynamic model of the facility would allow for the study of these transient regimes. A better understanding of the day-to-day operation of the facility would be obtained.

Finally, novel solvents could be considered as a replacement for MEA. Recent studies highlighted the increased performance of alternatives and switching to one of those could ease the integration of the capture unit into the CHP plant. In particular, an amine blend of amino-methyl-propanol and piperazine (AMP + PZ) appears to be a promising candidate as it has supplanted MEA as the benchmark solvent.

As a concluding statement, beyond the economic and technical challenges that lie ahead, it is important to highlight the beneficial outcomes of the project. The reduction in CO_2 emissions stands out as the most obvious one. Moreover, taking advantage of the specific energetic systems that are available on the University campus and complementing them with a pilot plant of an emerging technology would certainly strengthen the position of the University as an institution that invests in research towards climate change mitigation. And finally, alongside research opportunities, it would engender pedagogical points of interest for aspiring engineers and stimulate interest in solutions to address what is expected to be the problem of the century.

References

Abu Zahra, Mohammad R. M (2009). "Carbon dioxide capture from flue gas: development and evaluation of existing and novel process concepts". PhD thesis.

AspenTech (2013). *Getting Started Modeling Processes with Solids*. Version 8.4.

– (2019). *Aspen Plus User Guide*. Version 11.

Baburao, Barath et al. (2014). "Advanced Amine Process Technology Operations and Results from Demonstration Facility at EDF Le Havre". In: *Energy Procedia* 63, pp. 6173–6187. DOI: 10.1016/j.egypro.2014.11.649.

Beiron, Johanna, Fredrik Normann, and Filip Johnsson (2021). "A case study of the potential for CCS in Swedish combined heat and power plants". In: 15th International Conference on Greenhouse Gas Control Technologies. URL: https://ssrn.com/abstract=3811373.

Bonanno, Riccardo (2020). "Small-scale CO_2 capture". MA thesis.

Boot-Handford, Matthew E. et al. (2014). "Carbon capture and storage update". In: *Energy & Environmental Science* 7.1, pp. 130–189. DOI: 10.1039/C3EE42350F.

Bui, Mai et al. (2018). "Carbon capture and storage (CCS): the way forward". In: *Energy & Environmental Science* 11.5, pp. 1062–1176. DOI: 10.1039/C7EE02342A.

Canepa, Roberto and Meihong Wang (2015). "Techno-economic analysis of a CO_2 capture plant integrated with a commercial scale combined cycle gas turbine (CCGT) power plant". In: *Applied Thermal Engineering*. 6th International Conference on Clean Coal Technologies CCT2013 74, pp. 10–19. DOI: 10.1016/j.applthermaleng.2014.01.014.

Choi, Jaeuk et al. (2019). "Process design and optimization of MEA-based CO_2 capture processes for non-power industries". In: *Energy* 185. DOI: 10.1016/j.energy.2019.07.092.

CORDIS (2011). *CO_2, from Capture to Storage (CASTOR)*. URL: https://cordis.europa.eu/project/id/502586/reporting.

Cousins, A., L. Wardhaugh, and A. Cottrell (2016). "26 - Pilot plant operation for liquid-absorption-based post-combustion CO_2 capture". In: *Absorption-Based Post-combustion Capture of Carbon Dioxide*. Ed. by Paul H. M. Feron. Woodhead Publishing. ISBN: 978-0-08-100514-9. DOI: 10.1016/B978-0-08-100514-9.00026-3.

Drax (2020). *BECCS and negative emissions*. URL: https://www.drax.com/about-us/our-projects/bioenergy-carbon-capture-use-and-storage-beccs/.

Duan, Liqiang, Mingde Zhao, and Yongping Yang (2012). "Integration and optimization study on the coal-fired power plant with CO_2 capture using MEA". In: *Energy*. The 24th International Conference on Efficiency, Cost, Optimization, Simulation and Environmental Impact of Energy, ECOS 2011 45.1, pp. 107–116. DOI: 10.1016/j.energy.2011.12.014.

Dutta, Rohan, Lars O. Nord, and Olav Bolland (2017). "Selection and design of post-combustion CO_2 capture process for 600 MW natural gas fueled thermal power plant based on operability". In: *Energy* 121, pp. 643–656. DOI: 10.1016/j.energy.2017.01.053.

ECB (2022). *Euro foreign exchange reference rates*. URL: https://www.ecb.europa.eu/stats/policy_and_exchange_rates/euro_reference_exchange_rates/html/index.en.html.

ECN (2022). *Phyllis2 database*. URL: https://phyllis.nl/.

EEA (2016). *Efficiency of conventional thermal electricity and heat production in Europe*. URL: https://www.eea.europa.eu/data-and-maps/indicators/efficiency-of-conventional-thermal-electricity-generation-4/assessment-2.

EIA (2020). *Average Operating Heat Rate for Selected Energy Sources*. URL: https://www.eia.gov/electricity/annual/html/epa_08_01.html.

Ember (2022). *Carbon pricing*. URL: https://ember-climate.org/data/data-tools/carbon-price-viewer/.

European Commission (2022a). *EU Emissions Trading System (EU ETS)*. URL: https://ec.europa.eu/clima/eu-action/eu-emissions-trading-system-eu-ets_en.

– (2022b). *Paris Agreement*. URL: https://ec.europa.eu/clima/eu-action/international-action-climate-change/climate-negotiations/paris-agreement_en.

Feron, Paul H. M. et al. (2020). "An update of the benchmark post-combustion CO_2-capture technology". In: *Fuel* 273, p. 117776. DOI: 10.1016/j.fuel.2020.117776.

Fuss, Sabine et al. (Oct. 2014). "Betting on negative emissions". In: *Nature Climate Change* 4.10, pp. 850–853. DOI: 10.1038/nclimate2392.

Ghaemi, Ahad, Alireza Hemmati, and Hossein Mashhadimoslem (2021). "Non-equilibrium modeling of CO_2 reactive-absorption process using sodium hydroxide–ammonia–water solution in a packed bed column". In: *Journal of the Iranian Chemical Society* 18.9, pp. 2303–2314. DOI: 10.1007/s13738-021-02190-3.

Global CCS Institute (2019). *Bioenergy and Carbon Capture and Storage*. URL: https://www.globalccsinstitute.com/resources/publications-reports-research/bioenergy-and-carbon-capture-and-storage/.

– (2022). *CO2RE database of CCS facilities*. URL: https://co2re.co/.

Goto, Kazuya, Katsunori Yogo, and Takayuki Higashii (2013). "A review of efficiency penalty in a coal-fired power plant with post-combustion CO_2 capture". In: *Applied Energy* 111, pp. 710–720. DOI: 10.1016/j.apenergy.2013.05.020.

Hewitt, Geoffrey (2011). *Reboilers*. In: *Thermopedia*. DOI: https://dx.doi.org/10.1615/AtoZ.r.reboilers.

Idem, Raphael et al. (2015). "Practical Experience in Post-Combustion CO_2 Capture Using Reactive Solvents in Large Pilot and Demonstration Plants". In: *International Journal of Greenhouse Gas Control*. Special Issue Commemorating the 10th Year Anniversary of the Publication of the Intergovernmental Panel on Climate Change Special Report on CO2 Capture and Storage 40, pp. 6–25. DOI: 10.1016/j.ijggc.2015.06.005.

IEA (2019). *Putting CO_2 to Use - Creating value from emissions*. URL: https://www.iea.org/reports/putting-co2-to-use.

– (2020a). *European Union 2020 - Energy Policy Review*. URL: https://www.iea.org/reports/european-union-2020.

– (2020b). *The role of CCUS in low-carbon power systems*. URL: https://www.iea.org/reports/the-role-of-ccus-in-low-carbon-power-systems.

– (2021). *About CCUS*. URL: https://www.iea.org/reports/about-ccus.

– (2022). *Direct Air Capture: A Key Technology for Net Zero*. OECD. ISBN: 978-92-64-58587-4. DOI: 10.1787/bbd20707-en.

IEAGHG (2019). *Further Assessment of Emerging CO_2 Capture Technologies for the Power Sector and Their Potential to Reduce Costs*. URL: https://www.ieaghg.org/publications/technical-reports/reports-list/9-technical-reports/944-2019-09-further-assessment-of-emerging-co2-capture-technologies-for-the-power-sector-and-their-potential-to-reduce-costs.

IPCC (2018). *Special Report: Global Warming of 1.5°C*. URL: https://www.ipcc.ch/sr15/.

– (2021). *Climate Change 2021: The Physical Science Basis. Contribution of Working Group I to the Sixth Assessment Report of the Intergovernmental Panel on Climate Change*. Vol. In Press. Cambridge, United Kingdom and New York, NY, USA: Cambridge University Press. DOI: 10.1017/9781009157896.

Jana, Kuntal and Sudipta De (2014). "Biomass Integrated Combined Power Plant with Post Combustion CO_2 Capture – Performance Study by Aspen Plus". In: *Energy Procedia*. 4th International Conference on Advances in Energy Research (ICAER 2013) 54, pp. 166–176. DOI: 10.1016/j.egypro.2014.07.260.

Jilvero, Henrik et al. (2014). "Techno-Economic Analysis of Carbon Capture at an Aluminum Production Plant – Comparison of Post-combustion Capture Using MEA and Ammonia". In: *Energy Procedia*. 12th International Conference on Greenhouse Gas Control Technologies, GHGT-12 63, pp. 6590–6601. DOI: 10.1016/j.egypro.2014.11.695.

Knudsen, Jacob N. et al. (2009). "Experience with CO_2 Capture from Coal Flue Gas in Pilot-Scale: Testing of Different Amine Solvents". In: *Energy Procedia*. Greenhouse Gas Control Technologies 9 1.1, pp. 783–790. DOI: 10.1016/j.egypro.2009.01.104.

Krzemień, Alicja et al. (2013). "Risk Assessment of a Post-Combustion and Amine-Based CO_2 Capture Ready Process". In: *Journal of Sustainable Mining* 12.4, pp. 18–23. DOI: 10.7424/jsm130404.

Kuramochi, Takeshi et al. (2012). "Comparative Assessment of CO_2 Capture Technologies for Carbon-Intensive Industrial Processes". In: *Progress in Energy and Combustion Science* 38.1, pp. 87–112. DOI: 10.1016/j.pecs.2011.05.001.

Lassauce, A. et al. (2014). "Pressure Drop, Capacity and Mass Transfer Area Requirements for Post-Combustion Carbon Capture by Solvents". In: *Oil & Gas Science and Technology – Revue d'IFP Energies nouvelles* 69.6, pp. 1021–1034. DOI: 10.2516/ogst/2013154.

LEILAC (2020). *Low Emissions Intensity Lime & Cement - LEILAC*. URL: https://www.project-leilac.eu/leilac-pilot-plant.

Léonard, Grégoire (2013). "Optimal design of a CO_2 capture unit with assessment of solvent degradation". PhD thesis.

Levihn, Fabian et al. (2019). "Introducing BECCS through HPC to the research agenda: The case of combined heat and power in Stockholm". In: *Energy Reports* 5, pp. 1381–1389. DOI: 10.1016/j.egyr.2019.09.018.

Li, Bao-Hong, Nan Zhang, and Robin Smith (2016). "Simulation and analysis of CO_2 capture process with aqueous monoethanolamine solution". In: *Applied Energy* 161, pp. 707–717. DOI: 10.1016/j.apenergy.2015.07.010.

Li, Kangkang et al. (2016). "Systematic Study of Aqueous Monoethanolamine (MEA)-Based CO_2 Capture Process: Techno-economic Assessment of the MEA Process and Its Improvements". In: *Applied Energy* 165, pp. 648–659. DOI: 10.1016/j.apenergy.2015.12.109.

Lucquiaud, Mathieu and Jon Gibbins (2011). "On the integration of CO_2 capture with coal-fired power plants: A methodology to assess and optimise solvent-based post-combustion capture systems". In: *Chemical Engineering Research and Design*. Special Issue on Carbon Capture & Storage 89.9, pp. 1553–1571. DOI: 10.1016/j.cherd.2011.03.003.

Luis, Patricia (2016). "Use of Monoethanolamine (MEA) for CO_2 Capture in a Global Scenario: Consequences and Alternatives". In: *Desalination* 380, pp. 93–99. DOI: 10.1016/j.desal.2015.08.004.

Luo, Xiaobo, Meihong Wang, and Jian Chen (2015). "Heat integration of natural gas combined cycle power plant integrated with post-combustion CO_2 capture and compression". In: *Fuel* 151, pp. 110–117. DOI: 10.1016/j.fuel.2015.01.030.

Lv, Bihong et al. (2015). "Mechanisms of CO_2 Capture into Monoethanolamine Solution with Different CO_2 Loading during the Absorption/Desorption Processes". In: *Environmental Science & Technology* 49.17. Publisher: American Chemical Society, pp. 10728–10735. DOI: 10.1021/acs.est.5b02356.

Madejski, Paweł et al. (2022). "Methods and Techniques for CO_2 Capture: Review of Potential Solutions and Applications in Modern Energy Technologies". In: *Energies* 15.3, p. 887. DOI: 10.3390/en15030887.

Metz, Bert et al. (2005). *Special Report on Carbon Dioxide Capture and Storage*. URL: https://www.ipcc.ch/report/carbon-dioxide-capture-and-storage/.

Minx, Jan C. et al. (May 2018). "Negative emissions—Part 1: Research landscape and synthesis". In: *Environmental Research Letters* 13.6, p. 063001. DOI: 10.1088/1748-9326/aabf9b.

Mumford, Kathryn A. et al. (2012). "Post-Combustion Capture of CO_2: Results from the Solvent Absorption Capture Plant at Hazelwood Power Station Using Potassium Carbonate Solvent". In: *Energy & Fuels* 26.1, pp. 138–146. DOI: 10.1021/ef201192n.

NASA (2022). *Global Climate Change*. URL: https://climate.nasa.gov/.

Ortega, Emmanuel (2019). *What is Aspen Plus?* DOI: 10.13140/RG.2.2.32424.11522.

Peeters, Thomas (2021). "Design of a mobile post-combustion CO_2 capture test unit". MA thesis.

Perry, Robert H and Don W Green (2008). *Perry's Chemical Engineers' Handbook*. 8th ed.

Pfaff, I., J. Oexmann, and A. Kather (2010). "Optimised integration of post-combustion CO_2 capture process in greenfield power plants". In: *Energy* 35.10, pp. 4030–4041. DOI: 10.1016/j.energy.2010.06.004.

Pour, Nasim (2019). "Chapter 5 - Status of bioenergy with carbon capture and storage—potential and challenges". In: *Bioenergy with Carbon Capture and Storage*. Academic Press, pp. 85–107. ISBN: 978-0-12-816229-3. DOI: https://doi.org/10.1016/B978-0-12-816229-3.00005-3.

Reynolds, A.J., T.V. Verheyen, and E. Meuleman (2016). "Degradation of Amine-Based Solvents". In: *Absorption-Based Post-combustion Capture of Carbon Dioxide*. Elsevier, pp. 399–423. ISBN: 978-0-08-100514-9. DOI: 10.1016/B978-0-08-100514-9.00016-0.

Sai Bhargava Reddy, M. et al. (2021). "Carbon dioxide adsorption based on porous materials". In: *RSC Advances* 11 (21), pp. 12658–12681. DOI: 10.1039/D0RA10902A.

Salomón, Marianne et al. (2011). "Small-scale biomass CHP plants in Sweden and Finland". In: *Renewable and Sustainable Energy Reviews* 15.9, pp. 4451–4465. DOI: 10.1016/j.rser.2011.07.106.

Sartor, Kevin (2018). "Développement d'un outil de simulation et d'analyse technico-économique et environnementale d'un réseau de chaleur". PhD thesis.

Sartor, Kevin and Pierre Dewallef (Feb. 2018). "Integration of heat storage system into district heating networks fed by a biomass CHP plant". In: *Journal of Energy Storage* 15, pp. 350–358. DOI: 10.1016/j.est.2017.12.010.

Sartor, Kevin, Sylvain Quoilin, and Pierre Dewallef (2014). "Simulation and optimization of a CHP biomass plant and district heating network". In: *Applied Energy* 130, pp. 474–483. DOI: 10.1016/j.apenergy.2014.01.097.

Statista (2022). *Prices of electricity for industry in Belgium from 2008 to 2021*. URL: https://www.statista.com/statistics/595775/electricity-industry-price-belgium/.

Sulzer (2020). *Structured Packings*. URL: https://www.sulzer.com/-/media/files/products/separation-technology/distillation-and-absorption/brochures/structured_packings.pdf.

TEMA (2022). *TEMA Standards*. URL: https://tema.org/.

Towler, Gavin and Ray Sinnott (2013). "Chapter 7 - Capital Cost Estimating". In: *Chemical Engineering Design*. Ed. by Gavin Towler and Ray Sinnott. 2nd ed. Butterworth-Heinemann, pp. 307–354. ISBN: 978-0-08-096659-5. DOI: https://doi.org/10.1016/B978-0-08-096659-5.00007-9.

Turton, Richard et al. (2018). *Analysis, Synthesis and Design of Chemical Processes*. 5th ed. Pearson Education.

Wang, Jiawei et al. (2019). "Flexibility of combined heat and power plants: A review of technologies and operation strategies". In: *Applied Energy* 252, p. 113445. DOI: 10.1016/j.apenergy.2019.113445.

Wang, M. et al. (2011). "Post-combustion CO_2 capture with chemical absorption: A state-of-the-art review". In: *Chemical Engineering Research and Design* 89.9. Special

Issue on Carbon Capture & Storage, pp. 1609–1624. ISSN: 0263-8762. DOI: https://doi.org/10.1016/j.cherd.2010.11.005.

Wikipedia (2022a). *Cogeneration*. URL: https://en.wikipedia.org/wiki/Cogeneration.

– (2022b). *Ethanolamine*. URL: https://en.wikipedia.org/wiki/Ethanolamine.

– (2022c). *Heat exchanger*. URL: https://en.wikipedia.org/wiki/Heat_exchanger.

Yildirim, Ömer et al. (2012). "Reactive absorption in chemical process industry: A review on current activities". In: *Chemical Engineering Journal* 213, pp. 371–391. DOI: 10.1016/j.cej.2012.09.121.

Zhang, Ying and Chau-Chyun Chen (2013). "Modeling CO_2 Absorption and Desorption by Aqueous Monoethanolamine Solution with Aspen Rate-based Model". In: *Energy Procedia* 37, pp. 1584–1596. DOI: 10.1016/j.egypro.2013.06.034.

Zhang, Ying, Hern Chen, et al. (2009). "Rate-Based Process Modeling Study of CO_2 Capture with Aqueous Monoethanolamine Solution". In: *Industrial & Engineering Chemistry Research* 48.20, pp. 9233–9246. DOI: 10.1021/ie900068k.

Zuo, Wujun, Xiaoyu Zhang, and Yuzhong Li (2020). "Review of flue gas acid dew-point and related low temperature corrosion". In: *Journal of the Energy Institute* 93.4, pp. 1666–1677. DOI: 10.1016/j.joei.2020.02.004.

Appendix

	Actual pellet	Sample from [ECN 2022]
Moisture content (wt-%)	7.20	7.30
Lower Heating Value ($MJ\,kg^{-1}$)	17.258	17.54
Higher Heating Value ($MJ\,kg^{-1}$)	20.034	20.39

Table A1: Compared values between the actual wood pellets and the chosen sample from the *Phyllis2* database

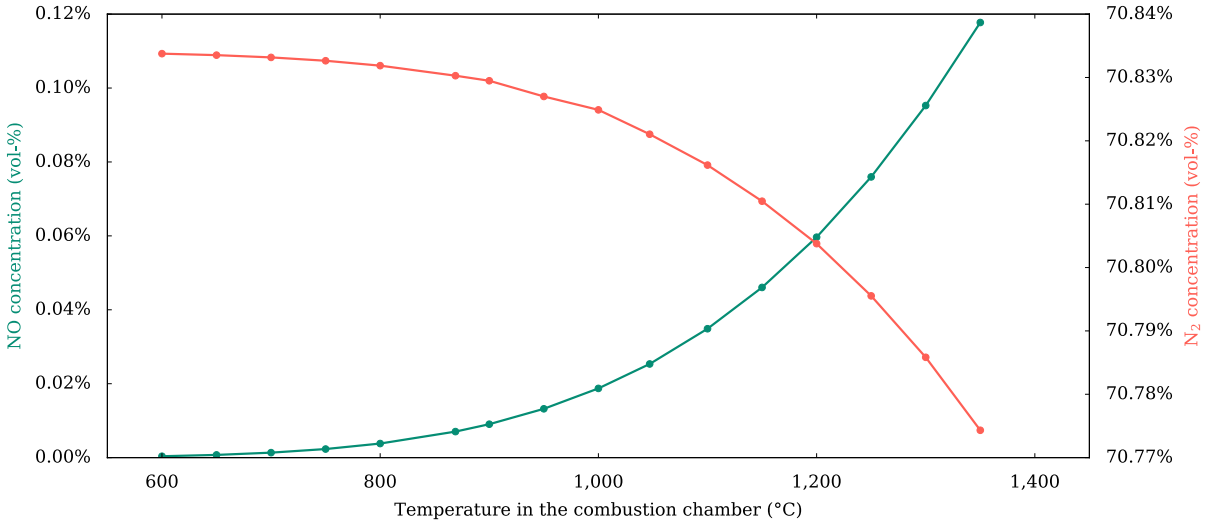

Figure A1: Evolution of the NO and N_2 concentrations with the combustion chamber temperature

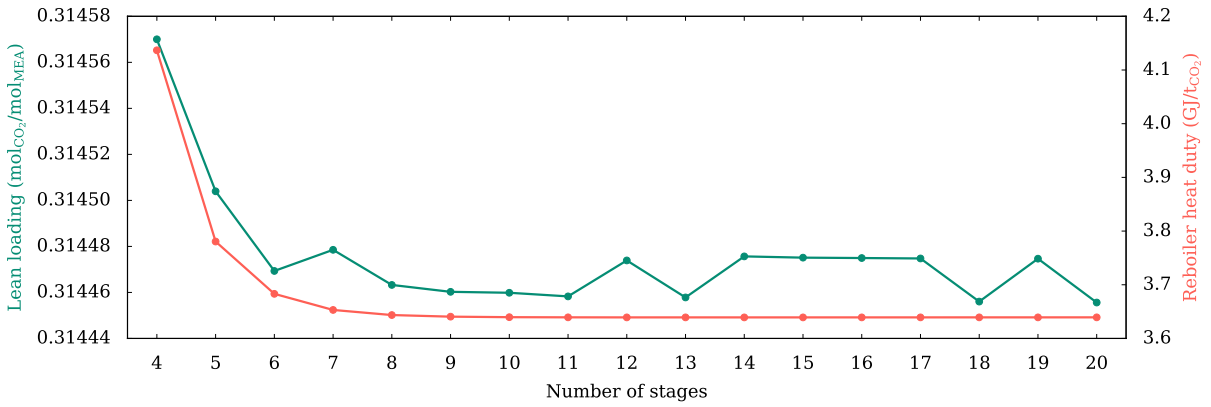

Figure A2: Evolution of the lean loading and the reboiler heat duty as a function of the number of equilibrium stages in the stripper

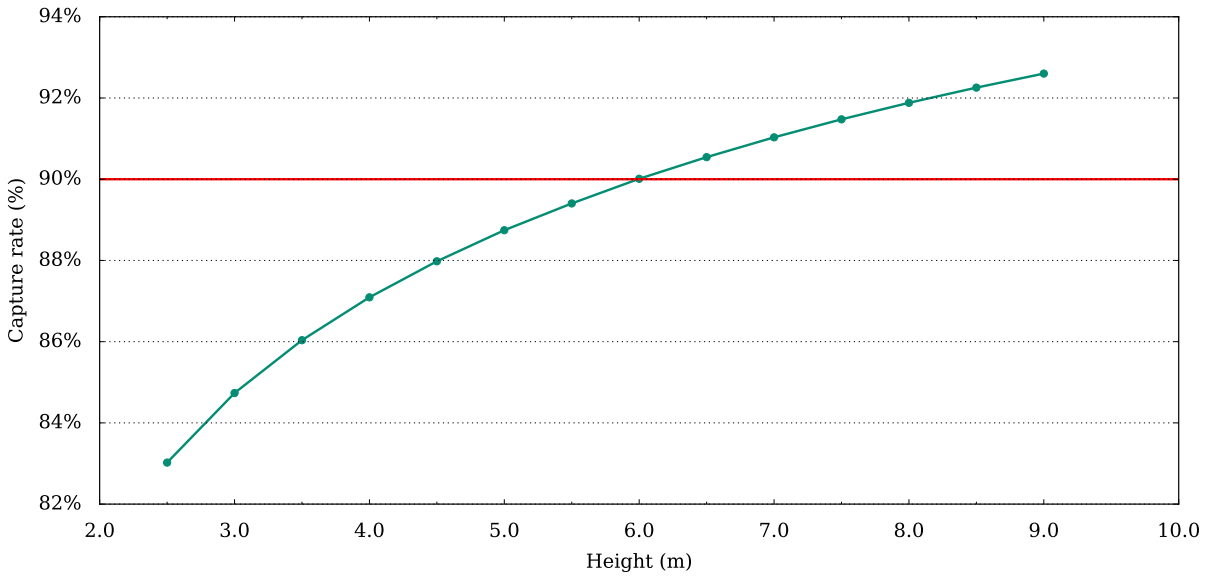

Figure A3: Capture rate computed for different absorber heights with rate-based calculations based on 20 stages